# Genomic Evaluation of Models of Human Disease:

# The $Fech^{m1PAS}$ Model of Erythropoietic Protoporphyria.

By

Colin Barker

MRC Toxicology Unit

University of Leicester

Thesis submitted for the degree of

Doctor of Philosophy (PhD)

2006

UMI Number: U217438

All rights reserved

INFORMATION TO ALL USERS
The quality of this reproduction is dependent upon the quality of the copy submitted.

In the unlikely event that the author did not send a complete manuscript
and there are missing pages, these will be noted. Also, if material had to be removed,
a note will indicate the deletion.


UMI U217438
Published by ProQuest LLC 2013. Copyright in the Dissertation held by the Author.
Microform Edition © ProQuest LLC.
All rights reserved. This work is protected against
unauthorized copying under Title 17, United States Code.


ProQuest LLC
789 East Eisenhower Parkway
P.O. Box 1346
Ann Arbor, MI 48106-1346

## Abstract

Genomic Evaluation of Models of Human Disease: The Fech$^{m1PAS}$ Model of Erythropoietic Protoporphyria.

Colin R Barker, MRC Toxicology Unit, University of Leicester.

Erythropoietic protoporphyria (EPP) is a member of the prophyria disease class and is caused by abnormal function of the enzyme ferrochelatase (Fech).

Here I have investigated the nature of the progression of EPP using the Fech$^{m1PAS}$ mouse. This mouse contains a point mutation in the *fech* gene resulting in reduced Fech activity to <7% of wild type, with resultant loss of haem, anaemia and hepatic cholestasis. The phenotypic progression of Fech$^{m1PAS/m1PAS}$ mice was established using pathology and clinical biochemistry from 18 days gestation to 32 weeks of age. Pathological changes were found from 4 weeks with biochemical and differential gene expression (DGE) analysis showing intrahepatic cholestasis from birth. Genomic data from cDNA microarrays was derived and analysed by phenotypic anchoring.

DGE was observed in processes responsible for cell protection and epigenetic regulation. DGE analysis have led me to the hypothesise that the porphyria leads to a chronic attack by reactive oxygen species (ROS), causing DNA damage, eventually leading to hepatocarcinoma. This was indicated by changes in the GSH, cytochrome P450, circadian rhythm and methylation pathways. DGE in these processes included downregulation of DNA methyltransferases (*Dnmt1, Dnmt6a* and *Dnmt6b*), and upregulation of cytochrome oxidase (*Cox* and *Por*) and GSH metabolism transcription factors (*Gclc* and *Gclm*).

The findings made here contribute to the understanding of EPP progression and the relationship between phenotype and DGE.

## Acknowledgements

It's hard to convey my gratitude to all the people who have made this thesis possible. I'd like to start by thanking the MRC for funding me and my supervisors Tim Gant and Andy Smith for their long suffering patience, understanding and the occasional kick up the ass where required.

I owe a debt to everyone in the MRC Toxicology Unit. From day one I have been shown both help and friendship. In particular I have to say a huge thank you to those who have helped me the most, the people I have spent time with everyday. I would like to thank Martina, Gemma, Sue, Bruce, Tanya, Jin-Li, Shu Dong, Reginald (whose raw garlic lunches will always bring a tear to my eyes), Angelique (who helped us stay abreast of the latest fashions) and Kate for not just their scientific help but their friendship as well. You have all supported me through thick and thin and trying to thank you is near impossible.

One person at the MRC has had a massive role in my reaching this point. Joan Riley is one of the most fantastic people I have ever had the honour to meet. Always up for a laugh (but only enjoying alcohol in a responsible manner), if I needed something she'd have it or know who to "borrow" it from. She is and always will be a cherished friend.

I'd also like to thank all the other people at the University of Leicester who have really made a difference to me, all the porters and security staff I've shared a joke with (the jokes continually get worse) especially Andy and John. I'd also like to say a big thank you to Lorraine Holland whose cheerful greeting and smile sets me up for the day.

Annette Cashmore has been a good friend from my BSc days. She always told me that the hardest thing about a PhD was sticking the distance. Without her support I probably wouldn't have. Annette's friendship and the support of everyone else in the Genetics department has made a real difference to me and I will always be grateful.

Life didn't stop outside of work. This would not have happened without my friends and family. They have stood at my side supportive to the end both financially (mums and dads are fab) and emotionally. Their love and encouragement has always had an impact on my life and it helped turn this thesis into reality.

Last but by no means least I want to thank Lucy, my partner in crime and my wife. She has put up with a lot and I must thank her friends including Lyn for looking after her whilst I've been writing this. My long nights at work, my stubbornness that she is in a bad mood despite it being me; she's rode above it all showing me love and understanding. Words simply cannot express my love and gratitude and so I dedicate this thesis to you and our life together.

## Contents

# Chapter 1) Introduction

## 1.1 Introduction to Erythropoietic Protoporphyria

Erythropoietic protoporphyria (EPP) is a member of the class of diseases called porphyrias and is caused by abnormal function of the enzyme ferrochelatase. The reduced ferrochelatase (Fech) activity leads to a deficiency in the amount of reduced iron collated with protoporphyrin IX. The result is a net lowering of haem synthesis.

EPP was defined in 1961 by Professor Ian Magnus describing the symptoms of photosensitivity and protoporphyrin accumulation (Magnus, Jarett et al. 1961). Since then the full symptoms have been defined as well as the genetic basis. The prevalence of the disease in the human population is difficult to estimate, but reports vary from 1 in 75,000 to 1 in 130,000.

### *1.1.1 Genetic basis of EPP and its inheritance patterns.*

Ferrochelatase is located in the human genome at cytological position 18q21.3 with a pseudogene also present on chromosome 3 at cytological position 3p23. In the mouse the *Fech* gene is found on chromosome 18 at cytological position 18E1 39.0cM. Unlike the human there is no pseudogene known to be present in the mouse. A pseudogene is a nucleotide sequence similar to the actual gene that lacks the ability to be transcribed (i.e the promoter and regulatory elements are absent). They can arise through several mechanisms including deactivation of a complete gene, aberrant cell division and spontaneous reverse transcription (RT) of mRNA; if they have no selective disadvantage they persist in the population. With the lack of a pseudogene in the

mouse the human pseudo gene is most likely the result of the spontaneous RT or aberrant cell division.

EPP has a complex inheritance with both recessive and dominant variants of the disease with very variable penetrance. There are at least 70 published alleles in ferrochelatase of which the majority are null mutants and the rest are missense mutations that will reduce function of the enzyme (Human Gene Mutation Database: http://www.hgmd.org). It is the coinheritance of a defective allele with a wild-type low-expressed allele which is most commonly involved in the clinical presentation of EPP(Gouya, Puy et al. 2004)

Any combination of the missense mutations and null alleles can occur leading to hugely variable phenotypes which cannot be easily predicted. However it is very unlikely that two null mutant alleles will be inherited as there is an absolute requirement for basal FECH activity to provide a basal haem level.

The combination of different alleles has great effect on the inheritance patterns of the disease. Autosomal recessive inheritance can occur if two reduced activity alleles are co-inherited as the presence of a single wild type allele is enough to raise FECH activity above the critical point where individuals remain asymptomatic which is believed to be 35% of wild type.(Nordmann, Amram et al. 1990) As a result of the asymptomatic nature, the low expression allele persists in the population as it does not have a significantly disadvantageous phenotype. The most common low expression allele is a cytosine variant of SNP;IVS3-48C/T in intron 3 which shows this persistence by its presence in about 11% of the white French and UK population(Gouya, Puy et al. 2002;

Whatley, Mason et al. 2004). This mutation modulates the use of an alternate splice acceptor site leading to a mutated mRNA. The prevalence of autosomal recessive inheritance is 3% of EPP cases in the UK.(Whatley, Mason et al. 2004)

The most common mode of inheritance in EPP is autosomal dominant. There are two major variants of genotype. The first is the inheritance of a null allele with a missense allele. The penetrance of the condition then relies on the nature of the missense allele. If FECH activity is maintained above 35% of normal, protoporphyrin will not accumulate in tissues to a critical point where the patient will experience photosensitivity, however, liver damage may still occur.

The second variant is the co-inheritance of a low-expression allele *in trans* to a severe mutation in *FECH*. This combination covers the majority of clinical expression in EPP families. Although inherited in a dominant fashion, the penetrance is variable as the presence of the low expression allele allows the influence of other environmental factors. The effect of these other factors is to modulate the penetrance of the wild type allele giving a mechanism for the high variability in clinical presentation.

The penetrance and its effect on the symptoms presented can be attributed to mutations in several regions of the gene. These can have several mechanisms for impairing the activity of the enzyme. The most obvious is mutation at the enzyme active site, this can cause either a conformational change preventing one of the substrates from entering the active site or mutation of the catalytic region of the enzyme preventing or hindering the enzyme from inserting the iron into the protoporphyrin ring. The second region of interest relies on FECH acting as a dimer. If

the mutation occurs in the region of the protein-protein binding domain responsible for dimerisation it can cause instability in the dimer formation and maintenance. Instability in dimer maintenance then introduces another means by which the penetrance can be modulated as other variables controlling the intracellular environment can affect the efficiency of dimer stability and hence FECH activity.

Another factor that could contribute to the presentation of the clinical symptoms is the theory that EPP has a series of genetic determinants from several genes as opposed to a single locus. This hypothesis was put forward by Sheng Zhou *et al.*(Zhou, Zong et al. 2005) who noted that mice containing ABCG2 null mutants have been shown to accumulate protoporphyrin IX and in over expression of ABCG2 intracellular porotoporphyrin was significantly lowered. ABCG2 is a member of the ATP Binding Cassette family of genes and functions in xenobiotic excretion from the hepatocytes(Krishnamurthy, Ross et al. 2004) and as Zhou demonstrated may also play a supporting role in protoporphyrin excretion.

### *1.1.2 Clinical Presentation of EPP*

EPP in its full form is a very disabling disease with complex and severe symptoms. The symptoms can be divided into categories based on their anatomical location.

The most common and earliest diagnosed symptoms are those affecting the skin. Patients with EPP present with a severe photosensitivity early in childhood resulting in burning pain on exposure to sunlight. This pain can persist for days and is followed by

development of oedema. If exposure continues this may then lead to extravasation of the skin in the affected area resulting in local scarring most often of the face and hands. This effect is exacerbated by subsequent exposures due to a priming effect from the initial insult. Over time, chronic effects are observed of hyperkeratosis and skin thickening in the areas most commonly exposed. Of all the symptoms associated with EPP, the effects on the skin carry with them the greatest psychological trauma due to impairment of social interaction. The cause of the light sensitivity is due to light activation leading to free radical production from the accumulated protoporphyrin.

The most aggressive symptoms are seen in the liver. Protoporphyrin is highly hyrdrophobic and as a result crystallises and accumulates in erythroid and non-erythroid tissue, in particular the liver and blood plasma. This modulates hepatic bile formation and flow as well as impairing the function of mitochondria in the hepatocytes resulting in cholestatic liver disease. In addition to cholestasis approximately 5-20% of patients will develop cirrhosis and jaundice, with a smaller percentage leading to hepatic failure and requiring a liver transplant.

Once hepatic symptoms have arisen a vicious cycle is initiated whereby the further accumulation of protoporphyrin further exacerbates the cholestatic disease and obstructive jaundice. In addition to extrahepatic cholestatic injury as a result of bile duct occlusion it is also possible that intrahepatic cholestasis occurs through disturbance of the regulatory systems associated with bile transport.

## 1.2 The Fech$^{m1PAS}$ model of EPP

The *Fech*$^{m1PAS}$ mouse is a model of inherited EPP. The mouse contains a viable structural mutant of the ferrochelatase gene that was induced by chemical mutagenesis with ethylnitrosourea (ENU) showing autosomal recessive inheritance(Tutois, Montagutelli et al. 1991).

### *1.2.1. The Fech$^{m1PAS}$ mutation*

Ethylnitrosourea is an ethylating agent which when given in a controlled manner will induce point mutations in DNA. A chemical mutagenesis experiment was carried out in BALB/c mice by Tutois *et al.* resulting in an inbred strain exhibiting a murine form of EPP(Tutois, Montagutelli et al. 1991). The cloning of the full-length mouse ferrochelatase cDNA in 1990 (Taketani, Nakahashi et al. 1990)then allowed the characterisation of the *Fech*$^{m1PAS}$ mutation.

The *Fech*$^{m1PAS}$ mutation is a thymine (T) to adenosine (A) transversion at nucleotide 293 of the 2.9kb *Fech* mRNA (Figure 1.1). This results in an amino acid substitution of methionine to lysine at residue 98(Boulechfar, Lamoril et al. 1993).

**Figure 1.1**

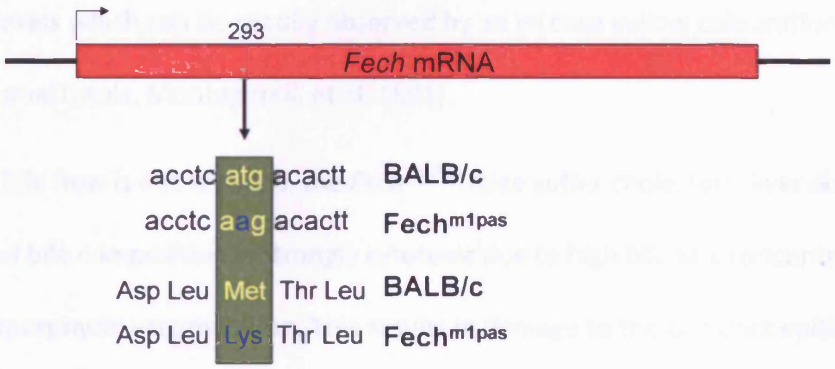


Figure 1.1) **Graphic showing the T→A transversion in the Fech$^{m1PAS}$ allele**

Mice homozygous for the *Fech$^{m1PAS}$* allele have a reduction in ferrochelatase activity maintaining a basal activity of <7% of normal. This basal level is enough to maintain viability of the strain. Heterozygotes are asymptomatic and maintain Fech activity of 45-65% of wild type. These data affirm the conclusion that in humans a reduction of 35% or less Fech activity is required for clinical symptoms.

### *1.2.2. Symptoms in the Fech$^{m1PAS}$ mouse*

The homozygous *Fech$^{m1PAS}$* mouse presents with symptoms very similar to severe human EPP. Photosensitivity can be demonstrated with a 20 minute exposure to a mercury vapour lamp resulting in ulceration of the skin. This can be attributed to local Fech enzyme deficiency as introduction of wild type Fech to the dermis is sufficient to

prevent photosensitivity(Pawliuk, Tighe et al. 2005). In addition to photosensitivity, Jaundice is also observed in the skin and is caused by a 45 fold increase in plasma bilirubin levels which can be readily observed by an intense yellow colouration of the blood plasma(Tutois, Montagutelli et al. 1991).

Although bile flow is not reduced, the *Fech*$^{m1PAS}$ mice suffer cholestatic liver disease as the altered bile composition is strongly cytotoxic due to high bile salt concentration and protoporphyrin accumulation. This results in damage to the bile duct epithelium resulting in biliary fibrosis and also impairment to bile formation (Meerman, Koopen et al. 1999). This is demonstrated by the histopathology which shows classic signs of cholestatic injury(Libbrecht, Meerman et al. 2003).

Analysis of blood plasma also shows a marked increase in cholesterol levels due to the presence of lipoprotein-X, composed of bile lipids.

## 1.3 Porphyrins and Haem Metabolism

In higher eukaryotes, haem is essential to life as it is involved in many important biological processes. It has an essential role in the active site of cytochrome P450's which are crucial enzymes in the metabolism of xenobiotics (Lowe 2000). More essentially haem is the central component of haemoglobin; the key to the evolution of higher eukaryotes, allowing efficient gaseous transport to and from the tissues.

Haem consists of a tetrapyrrolic macrocycle or porphyrin with a reduced Iron ($Fe^{2+}$) atom covalently bound to the centre (figure 1.2). The tetrapyrrolic ring in haem is

protoporphyrin IX, a porphyrin with 2 vinyl, 4 methyl and 2 propionic acid groups (2,4-divinyl-1,3,5,8-tetramethylporphin-6,7-dipropionic acid)

By holding the iron atom within the porphyrin ring and surrounding the haem group in proteins the redox potential of the iron can be modulated. This allows the chemistry of the haem group to alter to its role; In haemoglobin, the α and β globins modify conditions such that Fe(II) won't undergo oxidation to Fe(III). This allows it to reversibly bind oxygen. In cytochrome *c* the iron atom cycles through 2+ and 3+ states as part of the electron transfer chain in respiration.(Milgrom 1997)

**Figure 1.2**

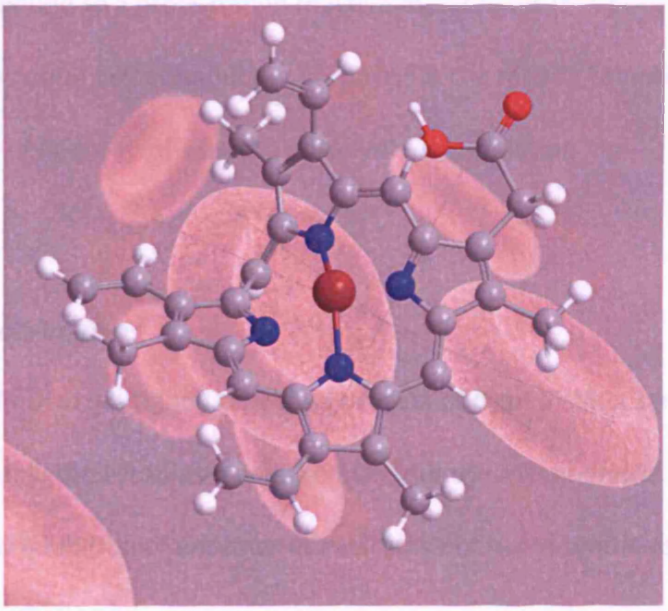

Figure 1.2) **Structure of haem.** The central Iron atom (maroon) is covalenly bonded to two nitrogens (blue) that sit in opposite pyrrole rings.

The highly reactive nature of haem that makes it so useful is also the same chemical characteristic that makes it so dangerous when things go wrong. As the reactive nature of the porphyrins are kept in control by their surrounding proteins, mutations in these proteins may cause severe disorders. In the case of haem, mutations in the surrounding proteins lead to haemoglobinopathies . Examples of these are the thalassaemias, where a whole protein subunit is absent due to mutation and sickle cell anaemia where a mutated form of the β-globin subunit causes erythrocytes to deform reducing blood flow.

The above conditions relate to the proteins surrounding haem. If things go wrong before haem is bound to a protein then reactive metabolites (the porphyrins produced as precursors to haem) will accumulate. Porphyria is the result of the accumulation of the break down of haem synthesis and porphyrin accumulation.

### *1.3.1. Haem Metabolism*

The synthesis of haem is a tightly regulated process of eight distinct synthesis steps which occur both in the cytoplasm and the matrix of the mitochondria. Table 1.1 summarises how inhibition of enzymes at each stage of haem synthesis will result in different porphyrias.

**Table 1.1**

| Enzyme | Condition |
|---|---|
| α-Aminolevulinic Acid Dehydratase | ALAD Porphyria |
| Porphobilogen Deaminase | Acute Intermittent Porphyia |
| Uroporphyrinogen III Cosynthase | Congenital Erythropoietic Porphyria |
| Uroporphyrinogen Decarboxylase | Porphyria Cutanea Tarda<br>Hepatoerythropoietic Porphyria |
| Coproporphyrinogen Oxidase | Heriditary Coproporphyria |
| Protoporphyrinogen Oxidase | Variegate Porphyria |
| Ferrochelatase | Erythropoietic Protoporphyria (EPP) |

Table 1.1) **Table showing the enzymes responsible for haem metabolism and their associated porphyrias.**

Haem synthesis starts in the mitochondria with the enzyme δ-aminolevulinic Acid Synthase (ALAS), which requires vitamin B-6 as a cofactor. ALA synthase condenses succinyl CoA and glycine to form an enzyme bound α-amino-β-ketoadipate. This is then decarboxylated to form δ-aminolevulinate. This is the rate limiting step in haem synthesis.

The δ-aminolevulinate is transported to the cytosol and undergoes a condensation reaction catalysed by the enzyme ALA Dehydratase (ALAD) to form porphobilogen. Porphobilogen is the pyrrole precursor, the next steps join four porphobiligen molecules together to form the porphyrin ring.

Hydroxymethyl Bilane Synthase (HMBS) removes the amino groups from porhobilogen allowing the linear tetrapyrrole hydroxymethylbilane to form containing alternate acetic and propionic acid groups. This tetrapyrrole is made cyclic by the action of Uroporphryrinogen III Synthase (UROS) creating the substrate for the next stage, uroporphyrinogen III.

The next stage replaces the acetic acid groups on Uroporphyrinogen III with methyl groups and then shuttles the resultant coproporphyrinogen III into the mitochondria. This step is catalysed by Uroporphyrinogen decarboxylase (UROD).

Once in the mitochondria, coproporphyrinogen III oxidase (CPOX) converts two of the propionic groups to vinyl groups forming protoporphyrinogen IX. The protoporphyrinogen IX is stabilized by the conversion of the methylene bridges between the pyrrole rings to methenyl bridges by Protoporphyrinogen IX oxidase (PPOX) forming protoporhyrin IX. The protoporphyrin IX is then passed on to Ferrochelatase (FECH), the last step of haem synthesis which adds reduced iron to the ring resulting in haem (Figure 1.3).

**Figure 1.3**

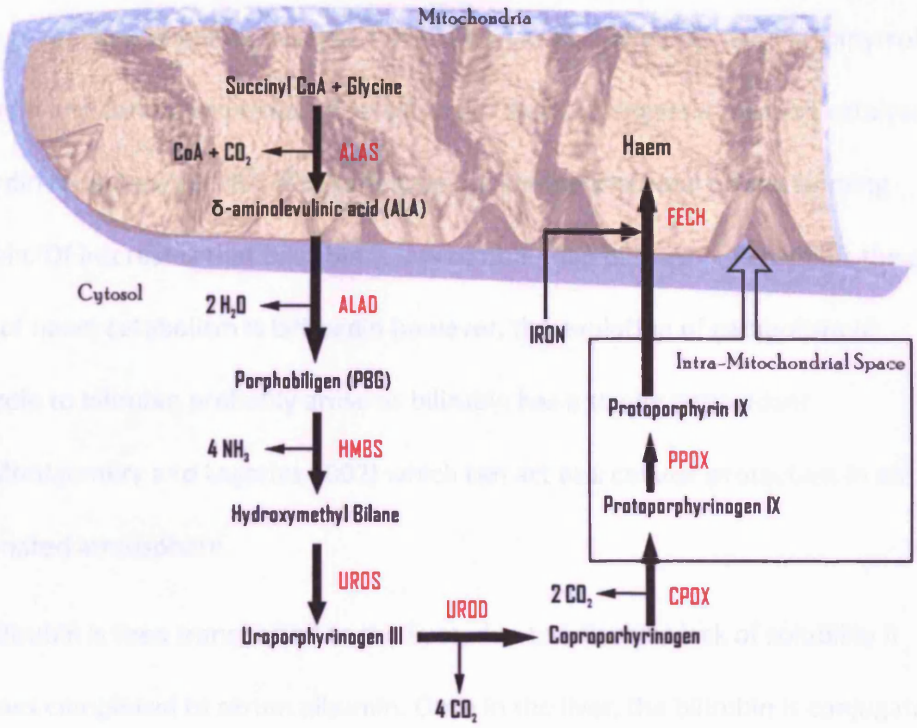


Figure 1.3) **Haem Synthesis.** The eight steps of haem synthesis. The enzymes responsible for each step are shown by their symbols in red.

### *1.3.2. Haem Catabolism*

When released from old erythrocytes, haem is broken down to a non reactive state and excreted from the body as bile pigments. The first step in haem catabolism is to linearise the tetrapyrrole ring. This is achieved in the spleen by cleavage of the α-

methane bridge by heme oxygenase (HMOX1 & 2, a member of the P450 family). Haem oxygenase uses the iron within the haem group itself to reduce NADPH for the cleavage reaction resulting in release of the iron as $Fe^{3+}$, the linearised tetrapyrrol biliverdin and carbon monoxide. The biliverdin then undergoes a reaction catalysed by biliverdin reductase (BLVRA & B) to reduce the central methane bridge forming bilirubin. Of interest is that bilirubin is less soluble than biliverdin. In reptiles the end point of haem catabolism is biliverdin however, the evolution of catabolism of biliverdin to bilirubin probably arose as bilirubin has a strong antioxidant role(Montgomery and Lagarias 2002) which can act as a cellular protectant in an oxygenated atmosphere.

The bilirubin is then transported to the liver; due to bilirubins lack of solubility it becomes complexed to serum albumin. Once in the liver, the bilirubin is conjugated to glucuronic acid by the action of UDP glucuronosyltransferases (UGT) at the caniliculi membrane(Wolkoff 1978); the attachment of the glucuronate residues to the propionic groups solubilises the bilirubin to a point where it is be excreted into the bile caniliculi as bile pigment. Figure 1.4 summarises the catabolism of haem.

**Figure 1.4**

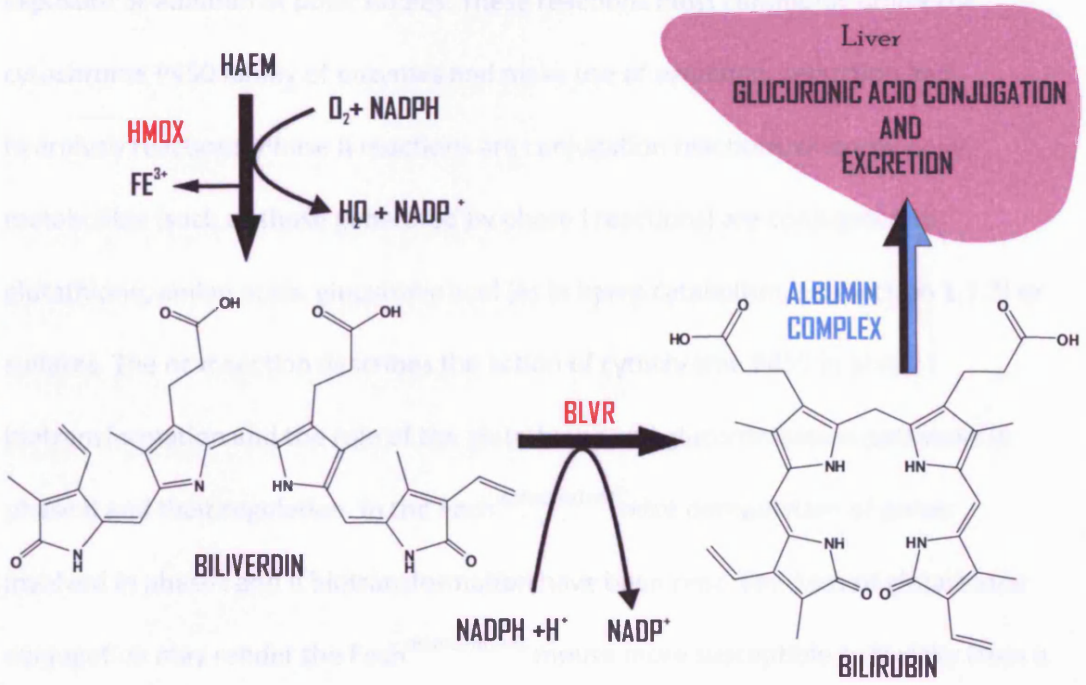


Figure 1.4) **Graphic showing an overview of haem catabolism.** The enzymes responsible for each step are shown by their symbols in red.

## 1.4 Role of Haem in the Biotransformation and Excretion of Toxins

The liver plays a central role in the detoxification and removal of metabolites and xenobiotics within the body. Biotransformation involves toxic lipophillic compounds being made more polar such that they become more water soluble prior to excretion in hydrophilic systems such as urine and faeces (Meeks, Harrison et al. 1991). This process is known as biotransformation or drug metabolism.

Biotransformation is split into two phases. Phase I reactions are responsible for the exposure or addition of polar bodies. These reactions most commonly utilise the cytochrome P450 family of enzymes and make use of oxidation, reduction and hydrolysis reactions. Phase II reactions are conjugation reactions whereby polar metabolites (such as those generated by phase I reactions) are conjugated to glutathione, amino acids, glucuronic acid (as in haem catabolism, see section 1.1.2) or sulfates. The next section describes the action of cytochrome P450 in phase I biotransformation and the role of the glutathione and glucuronidation pathways in phase II and their regulation. In the $Fech^{m1PAS/m1PAS}$ mice deregulation of genes involved in phase I and II biotransformation have been reported. Loss of glutathione conjugation may render the $Fech^{m1PAS/m1PAS}$ mouse more susceptible to toxicity from a variety of xenobiotics that require conjugation with glutathione for detoxification and excretion.

### *1.4.1 Phase I: The Role of Cytochrome P450*

Cytochrome P450 is not a single enzyme but a superfamily consisting of 57 putatively functional genes and 58 pseudogenes in humans and nearly double the number in the mouse (Nelson). The genes are separated into 10 families and are all named *CYP* followed by their unique identifier.

In addition to their role in phase I biotransformation, the *CYP* enzymes are also involved in bile acid, cholesterol and vitamin D synthesis as well as steroid metabolism

and catabolism. Table 1.2 shows an overview of the cytochrome P450 families and their substrates

The cytochrome P450 enzymes are found at the highest concentration in the liver where they make up about 2.5% of the hepatic microsomal protein. They are proteins bound to a prosthetic haem group allowing the haem group to transport electrons in oxidation and hydrolysis reactions. In order to carry out oxidation reactions a coenzyme, cytochrome P450 reductase (*POR*) is required as a transducer to provide electrons into the P450 enzyme complex one at a time (figure 1.5).

**Table 1.2**

| *CYP* Family | Number of genes | Substrates and functions |
|---|---|---|
| CYP1 | 3 | Xenobiotics, arachidonic acid, eicosanoids |
| CYP2 | 16 | Xenobiotics, arachidonic acid, eicosanoids |
| CYP3 | 4 | Xenobiotics, arachidonic acid, eicosanoids |
| CYP4 | 12 | Fatty acids, arachidonic acid, eicosanoids |
| CYP5 | 1 | Thromboxane $A_2$ synthase |
| CYP7 | 2 | Cholesterol, bile acid synthesis |
| CYP8 | 2 | Prostacyclin synthase, bile acid synthesis |
| CYP11 | 3 | Steroidogenesis |
| CYP17 | 1 | Steroid 17 $\alpha$–hydroxylase, 17/20-lyase |
| CYP19 | 1 | Aromatase to form oestrogen |
| CYP20 | 1 | Unknown |
| CYP21 | 1 | Steroid 21-hydroxylase |
| CYP24 | 1 | Vitamin $D_3$ 24-hydroxylase |
| CYP26 | 3 | Retinoic acid hydroxylation |
| CYP27 | 3 | Bile-acid biosynthesis, Vitamin $D_3$ hydroxylations |
| CYP39 | 1 | 24-hydroxycholesterol 7$\alpha$-hydroxylase |
| CYP46 | 1 | Cholesterol 24-hydroxylase |
| CYP51 | 1 | Lanosterol 14$\alpha$-desmethylase |

Table 1.2) **Table showing some of the human *CYP* gene families and their substrates.** (Nebert and Russell 2002)

**Figure 1.5**

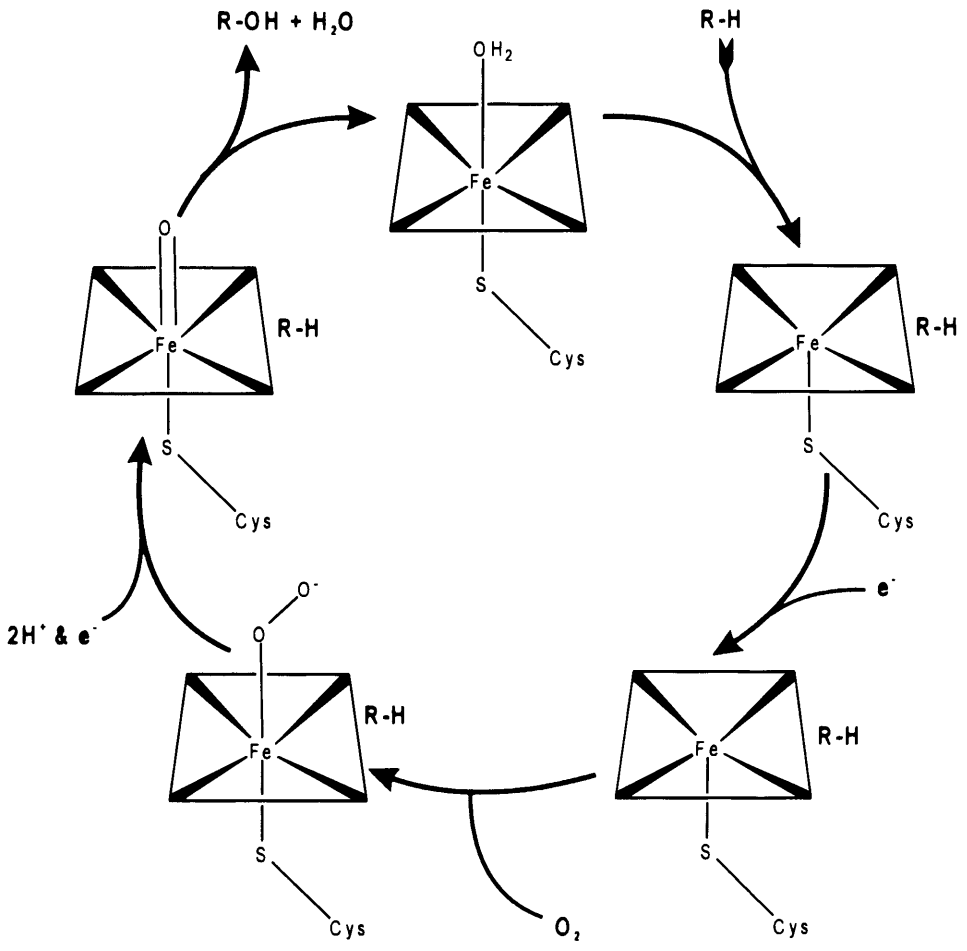


Figure 1.5) **Graphical representation of cyclic oxidation reactions mediated by cytochrome P450**. R is the substrate which can be taken as highly lipophillic and therefore insoluble in its parental form.

Oxidised P450 ($Fe^{3+}$) binds the lipophillic substrate and then becomes reduced ($Fe^{3+} \rightarrow Fe^{2+}$) by the addition of an electron from NADPH through the action of *POR*. The iron in the reduced P450-substrate complex then binds molecular oxygen, accepts another electron from *POR* and two hydrogens causing the reduced P450-Substrate-Oxygen complex to rearrange and release hydroxylated substrate, water and oxidised P450.

In addition to their oxidation reactions, P450s are also capable of peroxidation in the form:

$$RH + R'OOH \rightarrow ROH + R'OH$$

where R is the substrate and R' the peroxy-substrate acting as an oxygen donor and reduction reactions in regions of low oxygen tension.

The net product of these reactions is a substrate that is now soluble and so may be transported and excreted either directly or by conjugation and then excretion by the phase II pathways(Stryer 1995).

However, the polarisation of some compounds does not render them safe but activates them forming highly genotoxic compounds that can lead to tumourgenesis. A classic example of this is the bioactivation of aflatoxin $B_1$ ($AFB_1$), a mycotoxin produced by the *Aspergillus* family of fungi. $AFB_1$ is ingested and transported to the liver where it enters the cytochrome P450 biotransformation pathway. Through the action of several cytochrome P450s the $AFB_1$ is oxidised to $AFM_1$, $AFQ_1$ and $AFB_1$-8,9-epoxide (AFBO). The latter, in its $AFB_1$-8,9-exo-epoxide stereoisomer, is highly genotoxic and has been known to be a cause of hepatocellular carcinoma(Kamdem, Meineke et al. 2006).

### *1.4.2 Phase II: Glucuronidation and Glutathione Mediated Detoxification*

Glucuronidation and the glutathione pathway both utilise conjugation reactions. Glucuronidation, the process forming the end point of haem catabolism, is a relatively high capacity system whereas the glutathione (GSH) is a low capacity system but is vital for the detoxification of highly reactive metabolites from phase I.

#### *1.4.2.1 Glucuronidation*

Glucuronidation forms one of the largest phase II detoxification pathways as the conjugate, UDP-glucuronic acid is readily available at levels that prevent depletion, unlike the GSH pathways(Plant 2003); glucuronic acid is conjugated to the substrate from UDP-glucuronic acid to increase solubility and allow excretion. These reactions are catalysed by the UDP glucuronosyltransferases (UGT) of which many different isoenzymes are known, allowing handling of a broad, chemically diverse range of metabolites and xenobiotics(Meeks, Harrison et al. 1991). The UGT genes are split into four phylogenetic families, UGT1, 2, 3 and 8.

As with the P450 reactions of phase I, the primary aim of the process is detoxification; conjugation normally terminates biological activity, however, bioactivation resulting in toxic compounds formation can occur leading to carcinogenesis and in the case of xenobiotics adverse drug reactions. With the genetic regulation of different isoenzymes determining the body's ability to handle different xenobiotic and metabolic substrates, a cascading toxic affect can occur when bioactivated products damage DNA. The genetic regulation of the detoxification pathways is interconnected

(see section 1.2.2.2). Attack by reactive oxygen species (ROS) can unbalance this regulation affecting the expression level of other UGT isoenzymes. The modulation of UGT isoenzymes would lead to a further reduction in the body's ability to handle other xenobiotics and metabolites.

*1.4.2.2 Glutathione Pathways*

The tri-peptide glutathione (GSH) consists of glutamate, cysteine and γ-glyciene. Its detoxicant role acts through several mechanisms allowing a large range of substrates. It can hydrolyse peroxide groups through the oxidation of glutathione or it can be conjugated to substrates with electrophillic atoms such as epoxides. As described in section 1.2, the glutathione pathway has a relatively low capacity in comparison to the glucuronidation pathway with the availability of glutathione being the rate limiting step. Glutathione can be obtained via two channels; synthesis of new glutathione or reduction of oxidised glutathione (GSSG) by glutathione reductase (GSHR)(Figure 1.6b).

Glutathione is synthesised in a two step process from γ-glutamate, cysteine and glycine catalysed by glutamate-cysteine ligase (GCLM) and glutathione synthetase (GS)(Figure 1.6a). Synthesis is regulated by the abundance of glutathione via non-allosteric negative feedback inhibition of GCLM(Njalssson and Norgren 2005). When cellular GSH levels decrease inhibition of GCLM is removed and GSH synthesis increases.

**Figure 1.6**

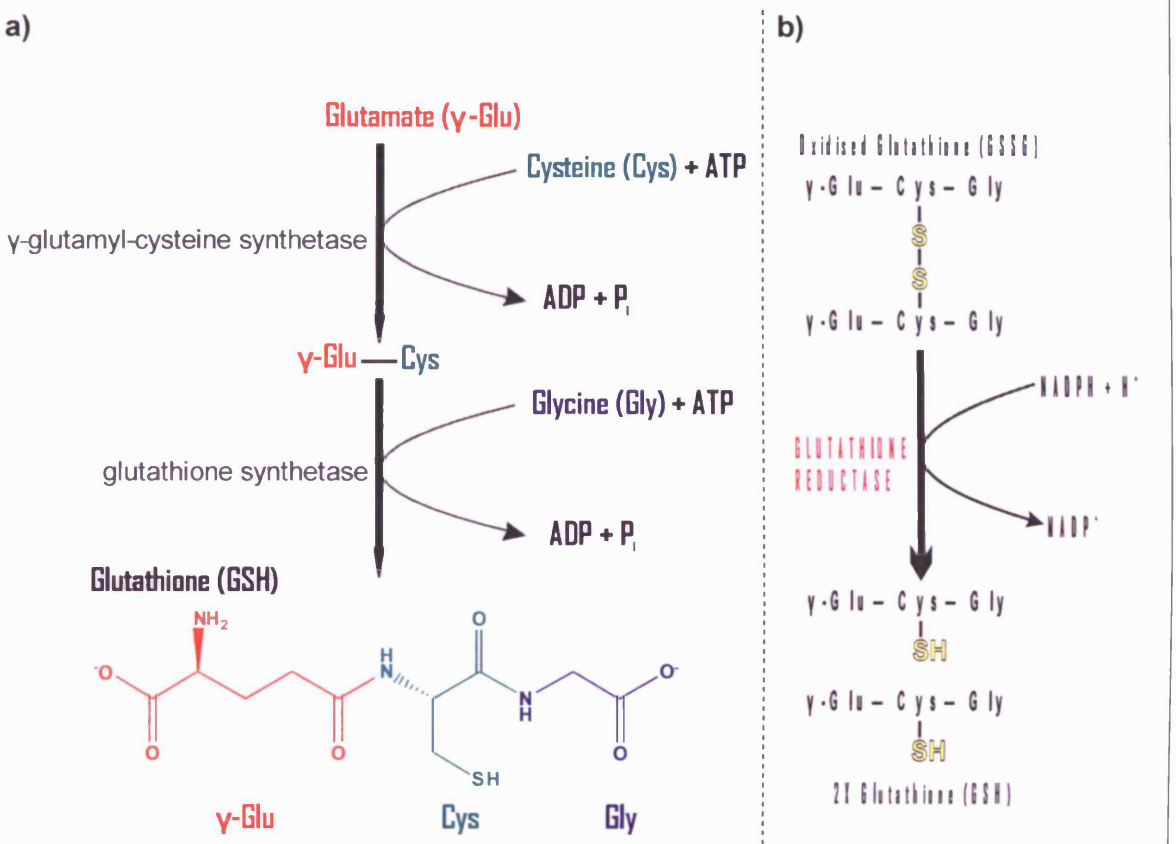


Figure 1.6) a) **Graphical representation of GSH Synthesis**. Adapted from Stryer(Stryer 1995) b) **Graphical representation of reduction of GSSG by glutathione reductase (GSHR) to GSH.**

The glutathione peroxidases (GPX) are a family of enzymes containing the selenium analogue of cysteine at the active site which undergo successive oxidations and

reductions through the catalytic cycle(Arthur 2000). The selenolate form of GPX reacts with the substrate reducing the peroxide group, oxidising the GPX. Two molecules of GSH then regenerate the active form of GPX by the formation of a selenosulfide adduct before leaving as oxidised GSSG(Stryer 1995) (see figure 1.7) The reduced substrate is passed onto other mechanisms for either direct excretion or further biotransformation; the oxidised GSSG is reduced back to GSH for further use as per figure 1.6b.

Because of the high usage of GSH as a sulfhydryl buffer in the above reaction activity of the GPXs must be tightly regulated. GPX-1, the first described glutathione peroxidase (Mills 1957), has been shown to have tight post-transcriptional regulation determined by levels of selenium. GPX-1 mRNA contains a selenocysteine insertion sequence (SECIS) motif in the 3' untranslated region (UTR) which allows insertion of the selenocysteine. In a deficiency of selenium, selenocysteine cannot be integrated and translation does not occur(Weiss and Sunde 1997). An increase in cellular selenium increases translation and GPX activity. This mechanism provides a level of control of the GPX pathway preventing unnecessary protein synthesis but it does not prevent the possibility of glutathione depletion. However, if dietary selenium is increased to a point where it is no longer rate limiting (3-4nmol $L^{-1}$), GPX-1 activity does not increase exponentially but plateaus. This is due to a secondary level of regulation limiting the activity of the glutathione peroxidises, acting as a mechanism against glutathione depletion (Arthur 2000).

**Figure 1.7**

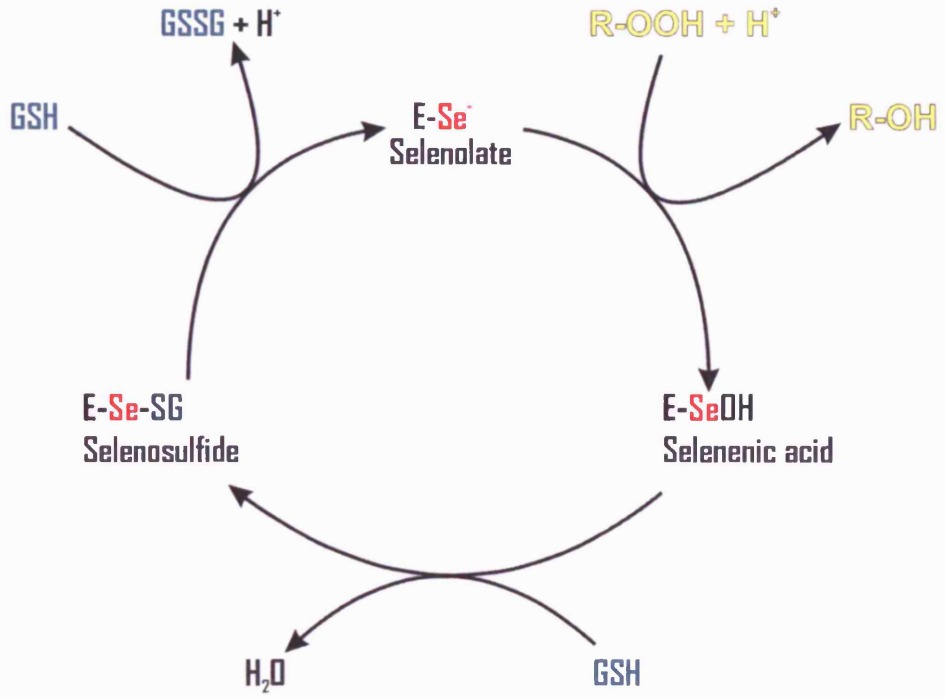


Figure 1.7) **Graphical representation of the Mechanism of GPX mediated Reduction**

Glutathione conjugation is targeted towards highly reactive substrates. Through either non-enzymatic means or the action of glutathione S-transferases (GST), *N*-acetlycysteine derivatives of xenobiotics are formed by nucleophillc attack of glutathione on electrophillic atoms of carbon, oxygen, nitrogen or sulphur in the substrate. Glutathione is present in the hepatocyte at very high concentrations (10mM) allowing non-enzymatic conjugation to occur when substrates are sufficiently

electrophillic. However, the majority of the reactions are catalysed by the action of GST's.

GSTs form two superfamilies based upon their subcellular localisation to either the microsomal or cytosolic with the largest group being the latter. The cytosolic GSTs are further split into classes (α, μ, π, τ and ξ) and a unique identifier. The functional GST forms as a dimer (both homo- and hetero-dimers) with the name of the functional enzyme reflecting the composition of the dimmer (i.e. GSTM1-1 is a homodimer of GSTμ1)(Plant 2003). Once dimerised, GST is active and capable of GSH conjugation with the general stoichiometry:

$$\text{R–epoxide} + \text{GSH} \rightarrow \text{R–GSH}$$

Once conjugated the substrate can either be excreted in the bile or transported to the kidney where they are cleaved to mercapturic acids for excretion in urine(Casarett, Klaassen et al. 2003)(Figure 1.8).

As with all the detoxification pathways discussed above GSH conjugation can mediate toxicity by the bioactivation of xenobiotics. An example of bioactivation is the renal failure in rats as a result of exposure to the widespread solvent Trichloroethylene. Lock and Reed (Lock and Reed 2006) reported that chronic exposure led to depletion of GSH levels and higher incidence of renal adenoma and carcinoma as a result of a chloromethyl radical being produced on conjugation with GSH. This evidence supports the thinking that activated xenobiotics can be highly genotoxic causing disruption to normal regulation; this may cause liver damage as a down regulation of GST leaves the

body vunerable to reactive oxygen species (ROS) attack whereas over expression will encourage GSH depletion with the same end result.

GSTs provide two functions, in addition to their role in detoxification, GSTs also act as stores to a number of compounds that would not normally be substrates for GSH conjugation. An example of this is the storage of bilirubin. GST has a very high affinity for bilirubin. Bilirubin that is not subject to glucuronidation is bound by GST and held in the cytoplasm (Wolkoff 1978). It is possible that the intrahepatocytic storage by GST may allow a reservoir of bilirubin to be retained so that its antioxidant role may be utilised during severe ROS attack.

**Figure 1.8)**

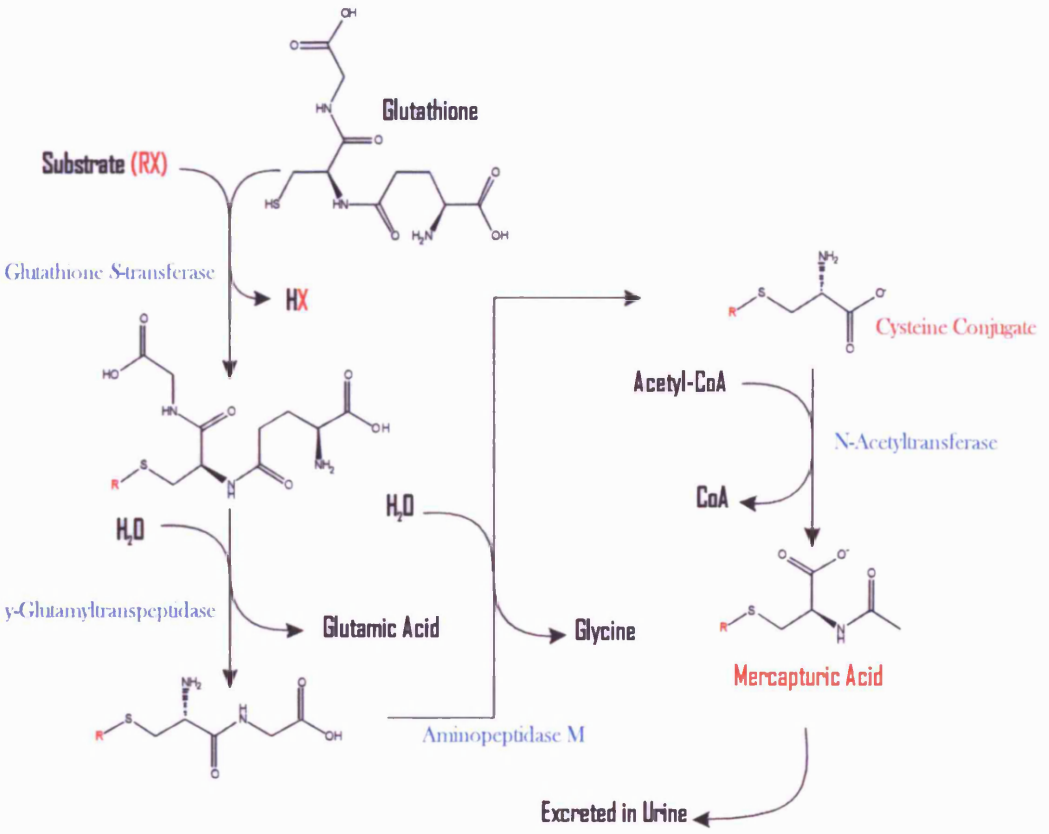


Figure 1.8) **Glutathione conjugation and mercapturic acid biosynthesis.** Adapted from Casarett and Doull (Casarett, Klaassen et al. 2003). The substrate is shown in red and enzymes in blue.

Reactive oxygen species include oxygen ions, free radicals and peroxides. They are highly reactive due to an incomplete electron complement in their outer shells. The high reactivity of ROS poses a threat to the cell as ROS attack on DNA can cause

mutations and genome instability(Casarett, Klaassen et al. 2003). The oxidative damage caused by ROS can then progress to cancer and tumour formation(Pelicano, Carney et al. 2004; Vaquero, Edderkaoui et al. 2004).

ROS form as a natural part of metabolism and are usually subject to rapid detoxification by systems such as superoxide dismutase and cytochrome oxidase. In the $Fech^{m1PAS/m1PAS}$ mouse, the generation of ROS may be from multiple sources (Table 1.3). The accumulation of protoporphyrin can lead to ROS generation owing to the reactive nature of porphyrins and their ability to be activated by light, allowing formation of singlet oxygen free radicals(Milgrom 1997). The hyperlipidemia associated with EPP can also lead to peroxidation of lipids acting as another source of oxidative stress. Peroxyl radicals may then cause damage to further macromolecules .

The results presented in this thesis led to the hypothesis that the mitochondrial respiratory chain (MRC) is disrupted (Section 5.4.4) with this another mechanism of ROS generation occurs. The leakage of cytochrome *c* from the MRC allows electron leakage from the ubiquinone complex III, allowing the generation of free radicals. The free radicals can then either be utilised by cytochrome *c* in the pro apoptotic oxidation of Phosphatidylserine or can oxidise the cytochrome *c* allowing the release haem group to cause further oxidative damage. Chronic inflammation is also observed in the $Fech^{m1PAS/m1PAS}$ mice which is also a source of ROS as phagocytes excrete multiple ROS as a method of destroying foreign bodies and signalling apoptotic pathways.

**Table 1.3**

| Source | Radical Type | Mechanism |
|---|---|---|
| **Protoporphyrin IX Accumulation** | Singlet Oxygen | Activated by visual light, protoporphyrin IX enters an excited state before passing on its excitation energy to oxygen. This generates the raised oxygen states $O_2(a^1\Delta g)$ and $O_2(b^1\Sigma g^+)$. $O_2(a^1\Delta g)$ is quickly quenched leaving the excited $O_2(b^1\Sigma g^+)$ form available to cause oxidative damage. (Cui, Zhou et al. 2003; Molnar, Dedic et al. 2005) |
| **Hyperlipidemia** | Peroxyl Radical | Hyperlipidemia is observed in the $Fech^{m1PAS/m1PAS}$ mice. The presence of hyperlipidemia causes a localised proapoptopic response through the activation of platelets. As part of the platelet response ROS are generated. These lead to peroxidation of the accumulated lipids and further oxidative stress.(Sener, Ozsavci et al. 2005) |
| **Cytochrome *c* leakage** | Hydrogen Peroxide Generation | The effect of cytochrome *c* leakage is two fold. Primarily the leakage of cytochrome *c* decouples the electron transport chain allowing rapid production of ROS. The cytochrome *c* then has two possible consequences. Firstly it can act as a catalyst in the utilisation of the ROS to oxidise phosphatidylserine in the Phosphatidylserine (PS)-dependent pathway for recognition of apoptotic cells (Jiang, Serinkan et al. 2003). Secondly oxidation of cytochrome *c* can lead to the release of its haem group allowing the iron ion to cleave DNA through the Fenton-like generation of ·OH (Kim and Kang 2006). |
| **Inflammation** | Multiple Types | During phagocytic activation molecular oxygen undergoes sequential univalent reduction forming ROS. These ROS and reactive nitrogen species are actively produced and excreted by the activated phagocyte to assist in the breakdown of potential pathogens and the resolution of the inflammation. (Splettstoesser and Schuff-Werner 2002) |

Table 1.3) **Possible Mechanisms of ROS Generation in the $Fech^{m1PAS/m1PAS}$ Mouse.**

The table shows the source of ROS generation, the likely type and the possible mechanism by which generation occurs.

### *1.4.3 Reponse to ROS in the Activation of Multiple Detoxification Pathways by the Transcription Factor Nrf2*

With the dangers posed by ROS, the capability for a rapid response to detoxify them becomes essential. The mechanisms that have evolved for the biotransformation of metabolites and xenobiotics discussed in this section and the catabolism of haem (section 1.1.2) share a common regulatory path for their induction.

This coordinated induction is achieved by transcriptional control from the antioxidant response elements (AREs)(McMahon, Itoh et al. 2001). The ARE is a motif found in the promoter region of the antioxidant response genes with the consensus sequence 5'-RTGANNNGCR-3'. The ARE sequence is bound by the nuclear factor (erythroid-derived 2)-like 2 (Nrf2) transcription factor. Table 1.4 identifies some of the gene modulated by the action of Nrf2 binding.

**Table 1.4**

| Gene | Role |
|---|---|
| **Haem Oxygenase** | **Haem Catabolism** |
| **UGT1A6** | **Glucuronidation** |
| **GSTA1 & 2** | **Glutathione Conjugation** |
| **GSTM1, 2, 3 and 4** | **Glutathione Conjugation** |
| **GSTP1 & 2** | **Glutathione Biosynthesis** |
| **GCLM** | **Glutathione Biosynthesis** |
| **AKR7A2** | **Aldo-ketone Reduction** |

Table 1.4) **Table showing ARE containing genes and their roles**(Itoh, Chiba et al. 1997; McMahon, Itoh et al. 2001; Chanas 2002).

Nrf2 can both induce and repress the transcription of the ARE mediated genes; the choice of co-factor determining its action. When bound to the basic-region leucine-zipper (bZIP) transcription factors, Nrf2 drives expression of the ARE genes, conversely, when bound to small Maf proteins expression is repressed(Chanas 2002). The balance between Nrf2s binding to bZIPs and Mafs that determines the level of expression of the ARE containing genes allowing maintenance of the intracellular environment.

Figure 1.9 summarises the activation of ARE containing genes by Nrf2. Inactive Nrf2 is maintained in the cytosol by association with kelch-like ECH-associated protein 1 (Keap1), a cytoskeletal protein. In the presence of ROS, protein kinase C (PKC)

becomes activated and phosphorylates Nrf2 via the Mitogen-activated protein kinase (MAPK) pathway. Phosphorylation of Nrf2 causes its activation and translocation to the nucleus where it binds either Maf or bZIP transcription factors modulating expression of the ARE containing genes.

**Figure 1.9**

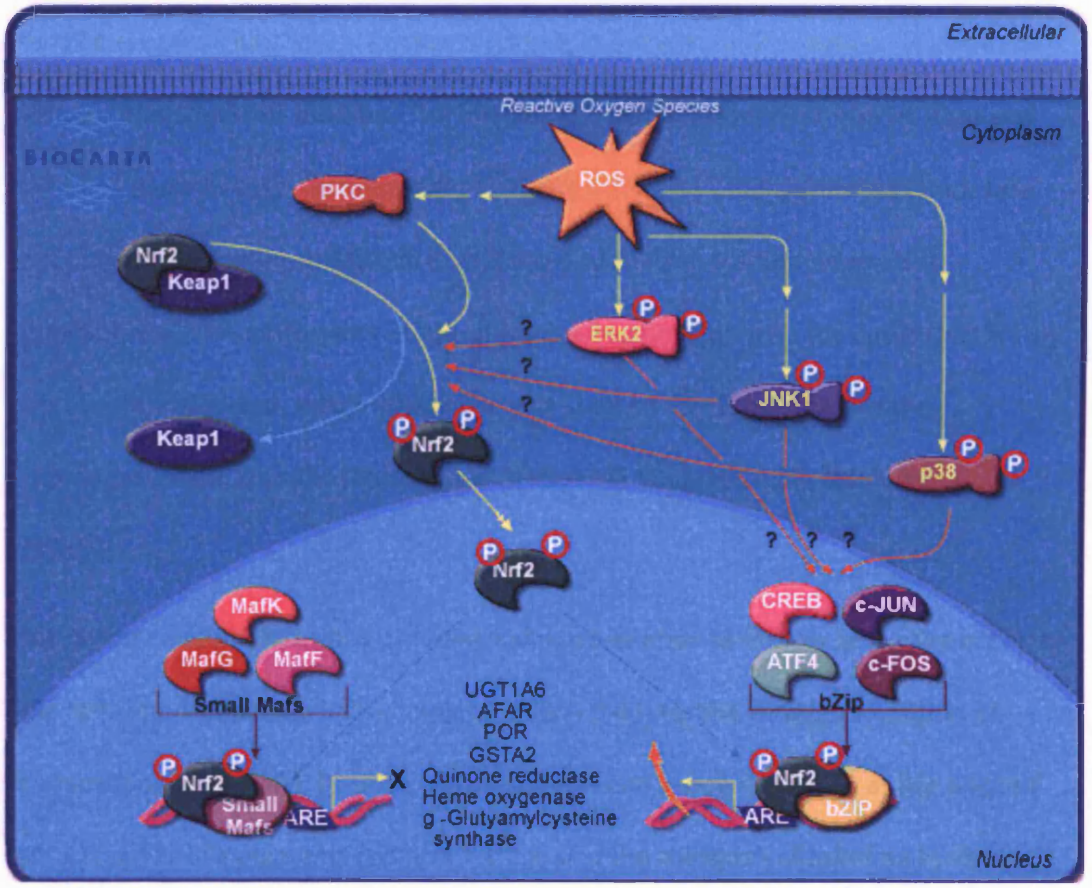


Figure 1.9) **A Graphical representation of the regulatory control of ARE containing genes**. (Obtained from http://www.biocarta.co.uk)

## 1.5 Bile Metabolism and Flow

One of the major functions of the liver is the production and secretion of bile. Bile composition varies from species to species however its key components remain the same, water, the inorganic electrolytes $Na^+$, $Ca^+$, $Mg^{2+}$, $Cl^-$ and $HCO3^-$ and the organic solutes, bile salts, GSH, cholesterol, the phospholipid lecithin and other proteins. Bile is formed through the action of transport processes in the hepatocytes and excreted into the bile canaliculi where it is further modified. Leaving the bile canaliculi, it then empties into small bile ductiles. The bile ductiles join together forming the right and left hepatic ducts which further merge to form the common hepatic duct. Once bile has entered the common hepatic duct it flows to the gall bladder where it is concentrated. The conjunction of the common hepatic duct with the cystic duct forms the common bile duct, which allows bile excretion to the duodenum via the hepatopancreatic ampulla (Tortora and Grabowski 1993; Williams, Bannister et al. 1995).

Bile serves multiple functions including aiding absorption of dietary fat by the action of bile salts and lecithin; an immunological role in the intestine through excretion of immunoglobulin A (IgA); Disposal of metabolites and xenobiotics such as the disposal of bilirubin as bile pigments (section 1.4.2.1) and the transport of substances via a continuing enterohepatic circulation(Tuchweber 1996).

### *1.5.1 Bile Acids and their Synthesis*

Bile acids are the major component of bile. They are polar derivatives of cholesterol with glycine or taurine (glycocholate and taurocholate respectively). Containing both polar and non-polar regions, their role is to emulsify fats, increasing their solubility to facilitate absorption in the digestive tract and to increase their surface areas allowing more efficient action by lipases. This process is enhanced by the phospholipid lectithin which combines with bile salts in the breakdown of fat globules. The lipophillic region binds with lipids whilst the hydrophilic region associates with water allowing emulsification of the fats and the further action of the bile salts in fatty acid metabolism.

Bile acids are synthesised in the liver from cholesterol via a complex pathway containing 17 separate enzyme catalysed reactions in steps localised to the cytosol, endoplasmic reticulum (ER), mitochondria and peroxisome. (Russell 2003) The synthesis can be broken into four main processes, initiation, modification of ring structures, oxidation and shortening of side chains and amino acid conjugation.

Initiation begins with the conversion of cholesterol to hydroxycholesterol by the microsomal P450 hydroxylases by four possible pathways the main being the action of 7α-hydroxylase (CYP7A1). The other pathways catalysed by CYP46A1 and CYP27A1 still require 7α-hydroxylation which is provided an additional hydroxylation step catalysed by CYP39A1 oxysterol 7α-hydroxylase in the CYP46A1 pathway and CYP7B1 oxysterol 7α-hydroxylase in the remaining two.

The 7α-hydroxylated intermediates enter the ring modification stage with an isomerisation from the 5$^{th}$ position to the 4$^{th}$ and oxidation of the 3β-hydroxyl group, catalysed by 3β-hydroxy-$\Delta^5$-$C_{27}$-steroid oxidoreductase ($C_{27}$ 3β-HSD). The products of this step can then take one of two routes dependant on the action of sterol 12α-hydroxylase (CYP8B1); if acted upon by CYP8B1 the resultant bile acid will be a cholic acid, without this action the product will be a chenode-oxycholic acid. It is the abundance of CYP8B1 which determines the balance between the two routes(Li-Hawkins, Gafvels et al. 2002). The intermediates (irrespective of the action of CYP8B1) are then subject to a reduction of the A-ring double bond by $\Delta^4$-3-ketosteroid 5β-reductase (AKR1D1) in the cytosol. The final step of ring modification is the reduction of the 3-oxo group to an α-OH by chlordecone reductase. Prior to conjugation with amino acids, the products of ring modification must undergo a shortening of the sterol side chain by a progressive oxidation. The first reaction is the carboxylation of $C_{27}$ by the action of sterol 27-hydroxylase (CYP27A1) in the mitochondria before the products are transported to the peroxisome where the terminal three carbons are removed by bile acid coenzyme A ligase conjugating CoA to the sterol. The CoA conjugate undergoes an isomerisation from the 25(R) isome to 25(S) by 2-methylacyl-CoA racemase (AMACR) before dehydrogenation by branched chain acyl-coenzyme A oxidase (ACOX2) yielding 24,25-*trans*-unsaturated derivatives(Van Veldhoven, Vanhove et al. 1992). The derivatives then undergo a hydration and oxidation to a $C_{24}$-oxo product by both hydrolysis and oxidation being catalysed by *D*-bifunctional protein. The last oxidation step is the cleavage of the $C_{24}$-$C_{25}$ bond by peroxisomal 3-oxoacyl-

Coenzyme A thiolase (ACAA) resulting in a $C_{24}$-CoA bile acid intermediate and propionyl-CoA. The $C_{24}$-CoA intermediate is then passed on to conjugation with an amino acid; the final step in bile acid synthesis.

Bile acid Coenzyme A: amino acid N-acyltransferase (BAAT)catalyses the amide linkage of either taurine or glycine to $C_{24}$ of the bile acid intermediate; the ratio of taurine versus glycine as a substrate is solely dependent upon their relative abundance in the liver and does not affect function (figure 1.10). The product of this reaction are the final excreted bile salts, glycocholate and taurocholate.

**Figure 1.10**

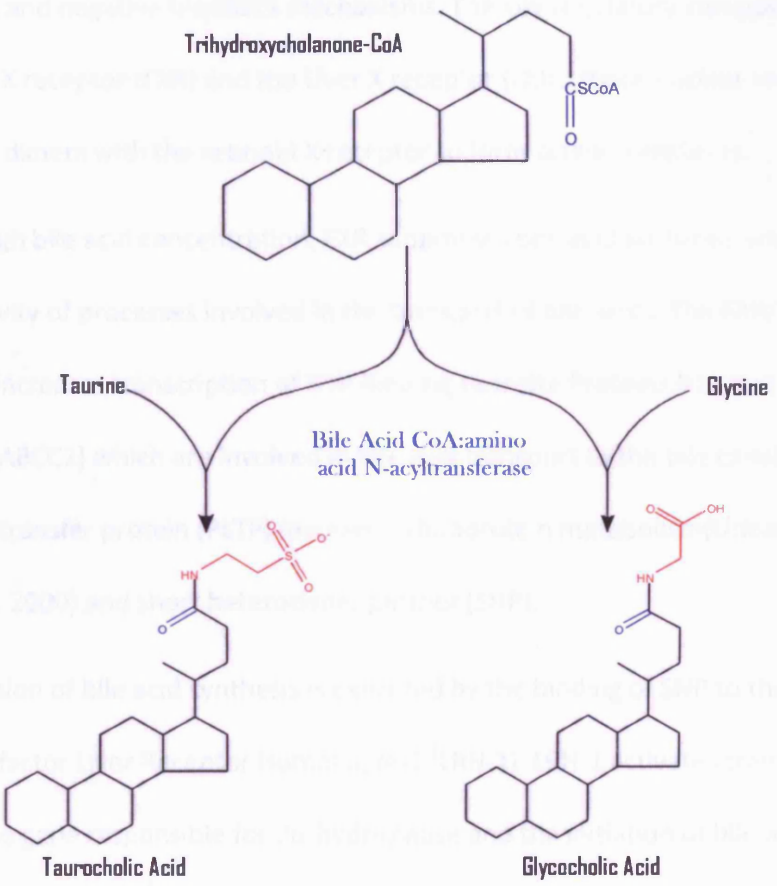


Figure 1.10) **Amino acid conjugation in bile synthesis.** The chemical modifications are shown in red, the enzyme is shown in blue. The conjugation of amino acids increases the solubility of bile acids as the oxygens in the amino acids are ionized at normal physiological pH.

### *1.5.2 Regulation of Bile Acid Synthesis*

The synthesis of bile acids is a tightly regulated process modulated by the availability of cholesterol and negative feedback mechanisms. The key regulatory components are the farnesoid X receptor (FXR) and the Liver X receptor (LXR); these nuclear receptors form obligate dimers with the retinoid X receptor to form active complexes.

In states of high bile acid concentration, FXR suppresses bile acid synthesis and increases activity of processes involved in the transport of bile acids. The FXR/RXR heterodimer increases transcription of ATP Binding Cassette Proteins B11 and C2 (ABCB11 and ABCC2) which are involved in bile acid transport to the bile canaliculi, Phospholipid transfer protein (PLTP) involved in lipoprotein metabolism(Urizar, Dowhan et al. 2000) and short heterodimer partner (SHP).

FXRs suppression of bile acid synthesis is executed by the binding of SHP to the transcription factor Liver Receptor Homologue-1 (LRH-1). LRH-1 activates transcription of CYP7A1, the gene responsible for 7α-hydroxylase and the initiation of bile acid synthesis. When LRH-1 is bound to SHP, CYP7A1 is transcriptionally repressed reducing bile acid synthesis. In addition to SHPs transcriptional control by FXR, the SHPs promoter contains an LRH-1 response element; LRH-1 is titrated by binding to SHP, as the available level of LRH-1 decreases it leaves the response element resulting in attenuation of SHP transcription by an auto regulatory mechanism.

LXR is responsible for the induction of bile acid synthesis by cholesterol. LXR binds oxysterol ligands allowing it to induce transcription of 7α-hydroxylase but not sterol 12α-hydroxylase. In addition to inducing bile synthesis it also changes the bile acid

composition by causing less cholic acid to form in the favour of the other bile acids. The reduction in cholate has the further effect of reducing absorption of dietary cholesterol, due to cholate causing an increase in the solubilisation of cholesterol. Direct attenuation of bile synthesis as cholate is a strong ligand of FXR. In addition to increasing bile acid metabolism, LXR stimulates the direct efflux of cholesterol by induction of ABCA1, ABCG5 and ABCG8(Repa, Turley et al. 2000). The role of these ATP-Binding Cassette transporters is the direct transport of cholesterol and other sterols into the bile.

The result of this myriad of regulation processes with negative feedback loops is that bile synthesis is precisely controlled and can adapt to both assault by excess or starvation through lack of both product or substrate.

### *1.5.3 Bile flow and Toxicity*

Bile flow is a cyclic process; bile acids are excreted in the liver and reabsorbed by enterocytes in the ileum for transport back to the liver reducing the need for *de novo* bile synthesis; This enterohepatic circulation forms the major flow of bile salts (Redinger 2003).

The force behind the flow of bile is generated by the active transport of osmotically active agents into the bile canaliculi resulting in an increase in the osmotic movement of water to rebalance equilibrium. Therefore regulation of osmotically active agents will regulate the rate of bile flow. The active transport of bile salts across the bile

canaliculi membrane correlates directly with an increase in bile flow (Kullak-Ublick, Stieger et al. 2004). However, bile salts exist in a micellar form and therefore have little osmotic activity indicating that it is the accompanying ions that determine flow rate as bile flow will persist in the absence of bile salt secretion. The action of the ions accompanying bile acids on the rate of bile flow forms the basis of bile acid dependant flow (BADF) with the contribution of other osmotic agents being bile acid independent flow (BAIF).

The enterohepatic flow of bile salts relies on the uptake of bile acids across the basolateral membrane and the efflux via the canalicular bile salt export pump (BSEP/ ABCB11). In a normal state these processes are tightly coupled. Bile acids are carried from the blood into the hepatocyte by the $Na^+$-taurocholate transporter (NTCP) and the organic anion-transporting protein (OATP) family as well as other carrier proteins and $Na^+$-independent anion transporters(Kullak-Ublick, Stieger et al. 2004). Once in the cell the bile acids are rapidly diffused to the canalicular membrane by cytosolic bile acid binding proteins before being pumped into the canaliculi by ABCB11(Stanca, Jung et al. 2001).

Impairment and alteration of bile formation and flow may be resultant of metabolic, autoimmune or genetic disease, infection or trauma. The impairment of bile secretion in the $Fech^{m1PAS}$ mouse is unclear and may be a result of intrahepatocytic or extrahepatic changes. These may be related to the accumulation of protoporhyrin in the hepatocytes and canaliculi, or a knock on effect of the changes in cell metabolism. Fibrosis is observed in the bile ducts of the protoporphyric mouse(Tutois, Montagutelli

et al. 1991) but even if the insult is only to the bile ducts hepatocellular injury will occur although the question arises as to whether it is the damage to the bile duct which results in insult to the hepatocytes or the converse.

In the $Fech^{m1PAS}$ mouse bile flow is increased, however the concentration of primary bile acids is also increased to a cytotoxic level(Meerman, Koopen et al. 1999). Although secondary bile acids are more toxic than primary bile acids their concentrations are seen to decrease in cholestatic disease, this is also reflected in the $Fech^{m1PAS}$ mouse suggesting that the cytotoxicity is a result of the increase in primary bile acid concentration. The increase in hydrophobic salts can cause toxicity by several mechanisms.

The most radical is an alteration in cell function; cell death has been shown to be triggered by bile salt accumulation by either necrosis or apoptosis with thresholds of ≥250μM and ≥100μM respectively. Although the bile salt concentration in the $Fech^{m1PAS}$ mouse is not sufficient to cause necrosis it can reach levels that would trigger apoptosis (Meerman, Koopen et al. 1999).

The increase in concentration can cause induction of the mitochondrial permeability transition disrupting electron transfer in the mitochondria and releasing cytochrome *c* which can then lead to ROS generation by electron leakage from the ubiquinone-complex III. This adds to the severity of the liver damage in the porphyric mouse through the cumulative effect of ROS generation through cytochrome *c* release and protoporphyrin accumulation (Palmeira and Rolo 2004) as well as the disruption of electron supply to the detoxification pathways. This may be exacerbated by the

reduced cellular haem levels potentially reducing the capacity of the electron transport chain in the first instance.

## 1.6. Microarrays

### *1.6.1 History of the microarray*

The rapid advances in technology, computing and molecular biology have made available many new opportunities to biologists. In the last couple of decades, computer and nucleic acid sequencing technology has leaped forward leading to dramatic increases in speed, quality and cost; In 2001 the first draft of the human genome was released(Lander, Linton et al. 2001) and in the near future with the advent of pyrosequencing the sequencing of whole genomes will become routine. This increase in sequence availability spear headed a plethora of tools designed to exploit these new data to understand biological systems more fully. Of the many resultant technologies, one of the most powerful to arise was the microarray.

The role of aberrant transcriptional regulation in the manifestation of disease had long been established but techniques such as northern blotting were restrictive due to the small number of genes that could be studied at any one time; DNA arrays on a macroscopic level had been around but were crude. With the advent of microarrays came the ability to analyse many targets at the same time on the same platform.

The expression microarray was first introduced by Patrick Brown and Ronald Davies in 1995, who published a study on changes in gene expression in *Arabidopsis thaliana*

using 45 oligonucleotide probes deposited on a glass slide in a serial manner(Schena, Shalon et al. 1995). Although this was new technology the concept traces back to 1975 and to Ed Southern and the Southern Blot whereby RNA was immobilised on a nylon membrane and a labelled probe hybridised(Southern 1975). Microarray technology took this principle and inverted it; fixing the probe to a coated glass substrate in a series of small features and labelling the biological sample with a fluorophore, the target. Once the samples had been hybridised to the array the results were read by an adapted fluorescence microscope. Now purpose built scanners are used.

### *1.6.2 Production methods of microarrays*

There are two main approaches to the manufacture of nucleic acid micro arrays, synthesis directly on the substrate or printing the probe onto the substrate..

The first method, photolithography is best known from the Affymetrix arrays. Affymetrix microarrays or Affy-chips are produced by synthesising the target oligonucleotide on the substrate, a quartz wafer, using a photolithographic process that was developed in the early 90s by Fodor *et al(Fodor, Read et al. 1991).*; the quartz is washed with a light sensitive protective solution preventing the binding of nucleotides until exposed to light. Each nucleic acid is flooded over the wafer in turn with the features being deprotected by a light mask as required i.e if the next nucleotide is thymine the feature will be exposed to light prior to the thymine wash. The nucleotide added in each step also contains a light sensitive protective group

allowing the next base to be added only after exposure to light. The result is that approximately 25-mer oligonucleotides are built up in discrete features directly on the substrate as defined by the light photo mask. The current Affy-chips routinely have a density of over 1.3 million discrete features per array (http:\\www.affymetrix.com).

The second method of array production is the printing method. Either an oligonucleotide or PCR product is printed onto a glass slide by a print head containing sping loaded pins or by a non-contact method utilising piezo-electric driven print heads (http://www.arrayjet.co.uk/) similar to that used in inkjet desktop printers. Home made versions of the inkjet array printers have recently been successfully employed using print heads from domestic desktop printers (http://bioinformatics.org/pogo/). This approach was mostly pioneered by Joe DeRisi (Stanford) who in 1996 published a paper on the induction and repression of genes in human cancer(DeRisi, Penland et al. 1996) using arrays produced by an in house built micro array printer. Between DeRisi and Patrick Brown, a guide was produced allowing other labs to set up a spotted array facility. This design was used in the production of the facility at the MRC Toxicology Unit and used to manufacture the arrays for this study. With oligonucleotide arrays the sequence arrayed is flexible as the oligo synthesised can be altered by computer, in addition the concentration of the oligos to be printed is easily determined as part of the synthesis process. The drawback of the oligonucleotide spotted array is cost. A cheaper alternative is the cDNA spotted array; the array is printed with PCR products produced from a cDNA expression sequence tag (EST) or genomic library. These libraries are maintained normally in the form of

bacterial artificial chromosomes (BACS) cultured in *E.coli*. This approach has benefits over the other methods; the library is a constant resource, compared with oligo libraries that must be re-synthesised when they are used. For cDNA libraries, when the PCR product runs out it is a simple job to re-PCR them (in our laboratory this is carried out in a semi-automated process). There is also a large cost saving as PCR equipment and reagents are significantly cheaper for a standalone research group than those involving oligonucleotide synthesis. However these benefits must be balanced with the bad points. The PCR even once optimised will tend to have a greater variation in yield leading to variation in the amount of DNA spotted onto the array, this can lead to issues in the downstream analysis as the less probe the less the signal from the array post hybridisation will be. In addition the integrity of the library must be monitored as mismatch errors may be introduced as the library is grown for subsequent generations as well as errors being incorporated into the PCR product as error correcting polymerases are often economically unviable at the level of usage required. However this is not a problem if longer sequences are used. The other major drawback is that there is less flexibility; in order to add to the array the target must be cloned and verified which takes a large quantity of work. However after the initial outlay regeneration of the PCR products for further array printing is relatively inexpensive.

### *1.6.3. Design and applications of Microarrays.*

Irrespective of the fabrication method used in production of the array, the most important design considerations are the choice of probes to be deposited on the array

and the information that one hopes to retrieve from the experiment. The choice of probes defines not only the biological information that can be gained from a microarray experiment but also determines the method used to analyse the results. The main DNA array applications are Sequencing arrays, Expression arrays and Comparative Genome Hybridisation (CGH) arrays.

*Comparative Genome Hybridisation* arrays compare the gene complement between two samples. Variation in gene complement or DNA copy number and gene dosage is common in many genetic based disorders and cancers. CGH arrays were first introduced in 1992 by Kallioniemi *et al.*(Kallioniemi, Kallioniemi et al. 1992) allowing an overview of chromosomal amplifications and deletions across the whole genome in a single hybridisation. This is carried out by the comparison of labelled genomic samples that have been hybridised to an array with the ratio of fluorescence indicating variation in copy number. The array design may be either oligonucleotide or a gene library and can therefore be produced by any of the production methods described above. There are however limitations associated with this technique owing to the nature of genomic DNA. At metaphase regions of the chromosomes are highly condensed preventing a CGH approach at these regions. This has limited detection of amplifications and deletions to those amplifications above 2Mb and deletions of 12Mb and above(Piper, Rutovitz et al. 1995; Bentz, Plesch et al. 1998). These limits have been improved upon with the advent of High Resolution CGH (HR-CGH) and coupled with degenerate oligonucleotide primed PCR have increased deletion resolution between 3-8Mb(Larsen, Ottesen et al. 2001). The subject of amplification resolution

has also been improved upon with Dhami *et al.* producing arrays capable of single exon resolution(Dhami, Coffey et al. 2005) .

*Sequencing arrays* are oligonucleotide arrays containing an array of sequential probes tiled by one nucleotide. Each probe has three companion probes whereby the central nucleotide is changed to the alternate three bases. Thus four probes in total are used for each SNP. This allows rapid screening of sequence and the identification of single nucleotide polymorphisms (SNPs)(Hacia 1999). SNPs are point mutations and are the main form of genetic variation. They are contributory towards human disease and have also been used as biomarkers for disease susceptibility (Chiang, Beck et al. 2006) and to identify unstable regions of the genome (those with high recombination rates) allowing definition of possible breakpoints in the genome associated with disease(Kojima, Mukai et al. 2006). Korsching *et al.* have described the use of SNP arrays as a high resolution alternative to array CGH(Korsching, Agelopolous et al. 2006). The ability to identify a single base change has also led to SNP arrays being employed as a rapid method of genotyping large samples.(Ji, Hou et al. 2004)

*Expression Microarrays* represent the largest area of microarray use. Gene expression is analysed by the comparison of mRNA levels between a test subject and a control as the modulation of mRNA levels changes the abundance of functional proteins through the availability of template for the translations machinery. In general the relationship between mRNA species abundance and the level of the protein product show a linear relationship. (Lockhart and Winzeler 2000) There are many techniques available to measure protein levels directly including western blots, mass spectrometry and

protein arrays which benefit from being able to show regulation at a post transcriptional level. However these approaches are either less sensitive or require a significant amount of extra work or the requirement for more specialised equipment.

The capability of rapidly monitoring gene expression levels of many genes provides us with a powerful tool to further understand the intricacies of the cell and the many processes within it. This information can be applied to several areas, in medicine expression levels can potentially be used for diagnostic purposes through the formation of "biomarkers" associated with disease (Dietel and Sers 2006). From a toxicology and pharmaceutical perspective, expression arrays have had an impact at both ends of the drug discovery and validation process; rapid screening techniques using expression arrays have allowed identification of new drug targets and at the other end of the process allowed investigation of drug candidates mechanisms and interactions allowing determination of compound toxicity including the effect of xenobiotics on the liver (LaFramboise, Bombach et al. 2006).

The ability to study multiple biological pathways simultaneously renders expression arrays an effective tool to study complex metabolic disorders and cancers as approached in this thesis. One of the complicating factors in the study of EPP is it is unclear how the observed phenotypes are linked making it difficult to construct hypotheses as to how the different biological processes interact. Microarrays have successfully been employed to study cholestatic liver disease, inflammation and fibrosis(Gant, Baus et al. 2003) as well as profiling hepatic adenomas and their differentiation from other cancers(Chen, Crone et al. 2005) and may be able to aid in

the elucidation of the progression of the individual phenotypes and also their interactions. This may help to determine which phenotypes are causative in EPP and which of those are resultant from the other phenotypes.

### *1.6.4 Microarray Laboratory at MRC Toxicology Unit, Leicester*

The microarray laboratory at the MRC Toxicology Unit, Leicester is based around a spotted microarray printer built in house to the design from Stanford, USA by Joe DeRisi and Patrick Brown (http://cmgm.stanford.edu/pbrown/mguide/). The printer has a capacity of 137 slides and uses a Majer 32-pin printhead (http://www.majerprecision.com/) to deposit PCR product obtained from both mouse and human EST clone libraries. The Majer printing pins are made from high grade stainless steel and are slotted allowing all 137 slides to be printed from a single loading of printing solution (Figure 1.11).

**Figure 1.11**

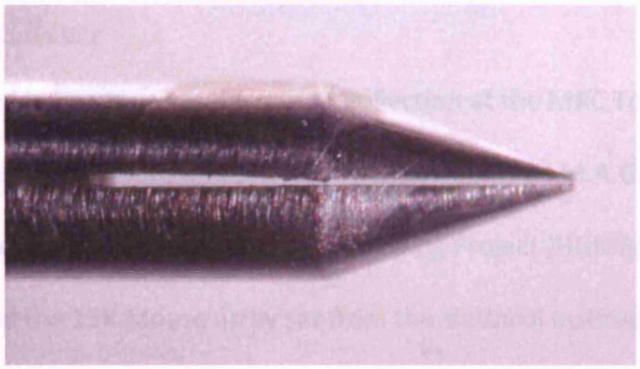

Figure 1.11) **Majer Precision Microquill spotted microarray printing pin**. Pin taken from Majer 32-pin print head at the MRC Toxicology Unit, Leicester.

*1.6.4.1 Array Support*

There are many support materials available for the production of arrays, these include quartz (as in the Affymetrix arrays), nylon membranes and glass. The main materials used in spotted arrays are coated glass microscope slides as the quartz slides are used for photolithographic production methods and nylon filters do not provide as higher sensitivity(Allain, Stratis-Cullum et al. 2004). The glass slides are cleaned prior to use and then coated prior to printing. The purpose of coating the slide is to allow the DNA to be cross-linked to the array. Several different types of coating are available including poly-L-lysine, aldehyde and amine. Although they all allow crosslinkage of

DNA to the slide we have found that poly-L-lysine coating provides the best results using the clones and equipment available at the unit.

*1.6.4.2 The Clone Library*

The clone set used in this thesis is the mouse collection at the MRC Toxicology Unit. It consists of a collection of approximately 6500 genes from the I.M.A.G.E collection formerly available from the Human Genome Mapping Project (HGMP), the Beddington 7.5dpc Library and the 15K Mouse array set from the National Institute on Ageing (NIA), USA. A subset of clones have been verified by sequencing. The clones are stored in glycerol preserved stocks and undergo PCR amplification and suspension in printing solution in a semi-automatic process.

*1.6.4.3 Probe Labelling*

The comparison of RNA levels between two subjects revolves around the competitive hybridisation of the samples, labelled with a fluorophore to the probe printed on the array. There are two main forms of labelling, direct linkage where the dye is directly incorporated into the product of a reverse transcription and indirect labelling where an amino group is introduced during the reverse transcription and the fluorophore conjugated to it in a following step. The latter approach was found to be more sensitive and was introduced to the methods used in this thesis when the process became available.

The direct incorporation method used the cyanine dyes, Cy3 dUTP and Cy5 dUTP and the indirect method uses an amino-allyl dUTP coupled to the Alexa 555 and Alexa 647

dyes (Molecular Probes). Once labelled, a dual hybridisation is carried out on the array with both the test subject and the control on the same slide. The array is then repeated with the labelling reversed to account for any bias in the emission intensities of the dyes.

#### *1.6.4.4 Scanning Microarrays*

Once the hybridisation has been carried out the data is obtained by scanning the microarray. The slides are scanned with lasers to excite the fluorophore at their respective wavelengths. Cy3 and Alexa 555 are scanned at a wavelength of 532nm and Cy5 and Alexa 647 at 635nm. The raw data is then captured in the form of a tagged image file format (TIFF) file using the GenePix Software from Molecular Devices,USA. The scanners used at the MRC Toxicology Unit are an Axon 4000 and an Axon 4200 (Molecular Devices, USA).

### *1.6.5 Analysis of Microarray Data*

After scanning the raw data is in the form of a grey scale image. This image is then mapped to a file containing the locations and masks for each clone on the array. Once the image has been mapped the boundaries for each individual are adjusted to allow the feature intensity to be calculated. The feature intensity is measured as the sum intensity of the pixels within the features mask. Previously, the background intensity of the feature would then be subtracted, however it has been shown that considering the background intensity to be 0 yields better results and also deals with the phenomenon

of "black holes" where the feature intensity is less than the background((Gant and Zhang 2005) and personal communication with Zhang SD, MRC Toxicology Unit, Leicester).

From this point the results are normalised to adjust for systematic differences in the relative intensities of each channel using a global normalisation based on the assumption that the two channels intensities are related by a constant factor for the entire slide. An alternative approach is to consider that the two channels are not constant but vary as a function of signal intensity using locally weighted scatterplot smoothing (LOWESS). As the method used in this thesis addresses the dye bias by reverse labelling the LOWESS style approach is not used.

The data is then presented in the form of the ratio of the median intensity of each channel. This shows whether the gene of interest (GOI) is either upregulated or downregulated relative to the control, to assess this statistically a student type T-test is carried out to give results showing the gene expression change and the statistical probability of a false positive (p-value).

Microarray experiments generate large quantities of data. The key to the application of the data is the interpretation. Once the data has been generated by the process detailed above it is then parsed into a graphical representation, there are many software tools, both commercial and free, designed for the downstream representation and further analysis of expression arrays. The main software used within this thesis is The Institute for Genomic Researchs' Multiple Array Viewer (TIGR MEV, http://www.tigr.org). This allows the representation of the array in a graphical

manner and further analysis to profile the gene expression changes into meaningful results such as cluster analysis.

Cluster analysis organises gene expression data into hierarchical groups that share related gene expression profiles. There are many forms of cluster analysis including hierarchical, *k*-means, self organising maps (SOM) and principal component analysis (PCA). Hierarchical clustering builds relationships between genes based on their gene expression profiles, for example, in the case of the $Fech^{m1PAS}$ timecourse those genes sharing the same gene expression profiles across time. This is a powerful approach as it does not consider the biological relationships between genes and can therefore provide insight as to the interaction between biological pathways that appear unrelated and therefore those observed phenotypes that appear unrelated.

In order to consider the gene expression changes in groups of genes with known biological relationships other methods of handling data have arisen. The Gene Ontology Consortium (http://www.geneontology.org) is a worldwide collaboration of researchers who have attempted to classify all genes based on their function. This has led to genes being assigned Gene Ontology terms (GO terms). Gene expression data can be parsed by GO terms to reduce the data into groups based on known function allowing an in depth study into individual processes. This approach has been applied to great effect in many cancers, including hepatic (Choi, Choi et al. 2004; Patil, Chua et al. 2005; Gamberoni, Storari et al. 2006).

## 1.7 Thesis Aims and Objectives

The objective of this project was to apply microarray technology and bioinformatics to gain genetic information on the progression of disease in the $Fech^{m1PAS}$ mouse model of erythropoeitic protoporphyria. The project consisted of several aspects; production of a robust genotyping method (Chapter 3), the phenotypic progression of the disease (Chapter 4), the changes in gene expression (Chapter 5 & 6) and finally their association with the observed phenotypes.

Data within this thesis extends our knowledge of the progression of complex diseases and the relationships between the multiple phenotypes arising, as well as elucidating some of the possible mechanisms for the presented phenotypes including the development of hepatic adenoma in the $Fech^{m1PAS}$ mouse.

# Chapter 2) Materials and Methods

## 2.1 Buffers and Solutions

### *2.1.1 Nucleic Acid Extraction*

| SNET Buffer |
| --- |
| 20 mM Tris-HCl (pH 8.0) |
| 5mM EDTA (pH 8.0) |
| 400 mM NaCl |
| 1% (w/v) SDS |

| TE |
| --- |
| 10mM Tris-HCl (pH 8.0) |
| 1mM EDTA (pH 8.0) |

| Proteinase K |
| --- |
| 20mg $ml^{-1}$ Proteinase K in SNET buffer |

### *2.1.2 Agarose Gel Electrophoresis*

| 5X TBE | |
|---|---|
| **In 1L of molecular grade water:** | |
| **54g Tris** | Giving a final concentration of 450mM Tris-borate and 10mM EDTA |
| **27.5g Boric Acid** | |
| **20ml 0.5M EDTA (pH8.0)** | |

| Staining Solution |
|---|
| **0.5µg $ml^{-1}$ Ethidium Bromide (Stock 10mg $ml^{-1}$, Sigma) in 1X TBE** |

| 6X Gel Loading Buffer |
|---|
| **50% Glycerol** |
| **0.25% (w/v) Bromophenol blue** |
| **0.25% (w/v) Xylene Cyanol FF** |

| 1kb+ ladder |
| --- |
| Load 10µl per well: |
| 0.05µg µl$^{-1}$ 1kb Plus Ladder (Promega) |
| 1X Gel Loading Buffer |

### *2.1.3 Porphyrin Assays*

| Acid Mix |
| --- |
| 1:1 mix 1M Perchloric Acid:<br>Isopropanol |

| HPLC Solvent A |
| --- |
| 9% acetonitrile in 1M ammonium acetate |
| Adjusted to pH 5.16 with glacial acetic acid |

| HPLC Solvent B |
| --- |
| 10% acetonitrile in methanol |

### *2.1.4 Printing of Microarray Slides*

| Printing Solution |
| --- |
| 1.5M Betaine Monohydrate |
| 3X SSC |
| 0.01% SDS (Optional) |
| 0.005% CHAPS(Optional) |

The composition varies between print runs. On the whole the majority of slides are printed without the SDS or CHAPS.

### *2.1.5 Coating of Microarray Slides*

| Slide Washing Solution |
| --- |
| 2.5N NaOH |
| 60% Ethanol |

| Slide Coating Solution |
| --- |
| 0.01% Poly-L-lysine (From 0.1% Stock obtained from Sigma (Cat: P8920)) |
| 0.1% PBS |

### *2.1.6 Microarray Sample Preparation and Labelling*

| Direct Labelling Mix |
| --- |
| 1X First Strand Buffer (5X stock supplied with the Reverse Transcriptase) |
| 0.01M DTT |
| 0.5mM each of dATP, dGTP, dCTP |
| 0.2mM dTTP |

| Indirect Labelling Mix |
| --- |
| 1X First Strand Buffer (5X stock supplied with the Reverse Transcriptase) |
| 0.01M DTT |
| 0.5mM each of dATP, dGTP, dCTP |
| 0.2mM dTTP |
| 0.3mM Amino-allyl dUTP (Sigma-Aldrich) |

| 50X Denhardts |
| --- |
| 1% (w/v) Ficoll 400 |
| 1% (w/v) polyvinylpyrrolidone |
| 1% (w/v) Bovine Serum Albumin (Sigma Fraction V) |
| Store at -20°C |

| Hybridisation Buffer |
| --- |
| Made as a batch, aliquoted and stored at -20°C |
| 5ml de ionised Formamide |
| 500µl 50X Denhardts |
| 1.0ml distilled Water |
| 500µl 10% SDS |
| The solution was then filtered through a 0.45µ syringe filter. |

| 20X SSPE |
| --- |
| 3M NaCl |
| 10mM $NaH_2PO_4$ |
| 20mM EDTA |
| Adjusted to pH7.4 with NaOH |

### *2.1.7 Pre-hybridisation slide processing*

| Pre-hybridisation Wash Solution |
|---|
| 4X SSC |
| 0.25% SDS |
| Kept at 65°C prior to use. |

| Sodium Borohydride Solution |
|---|
| 65mM $NaBH_4$ |
| 0.25% SDS |
| Kept at 65°C prior to use. |

### *2.1.8 Post-hybridisation Washing*

| Wash Solution 1 |
| --- |
| 1X SSC |
| 0.03% SDS |
| Made from a 20X SSC and 10% SDS stock. Made fresh each use. |

| Wash Solution 2 |
| --- |
| 0.2X SSC |
| Made from a 20X SSC stock. Made fresh each use. |

| Wash Solution 3 |
| --- |
| 0.05X SSC |
| Made from a 20X SSC stock. Made fresh each use. |

### *2.1.9 RT-PCR*

| First Strand Master Mix | |
|---|---|
| **Reagent** | **Volume** |
| **Gibco PCR Buffer (X10)** | **100µl** |
| **$MgCl_2$ (50mM)** | **50µl** |
| **dATP (100mM)** | **10µl** |
| **dTTP (100mM)** | **10µl** |
| **dCTP (100mM)** | **10µl** |
| **dGTP (100mM)** | **10µl** |
| **Random Hexamers 9000 units $ml^{-1}$** | **9.9µl** |
| **DTT (100mM)** | **10µl** |
| **Dd $H_2O$** | **615.1µl** |
| **Made in bulk, split into 50µl aliquots and stored at -20°C** | |

## 2.2 The Fech$^{m1PAS}$ Time Course

All animal work was carried out in accordance with the Animal Scientific Procedures Act (ASPA) 1986 under project licence PPL 80/1690 and personal licence PIL 40/7451

### *2.2.1 Animals*

*ARF20279:* The Fech$^{m1PAS}$ mice were obtained from a colony maintained by the Jackson Laboratory (Strain 002662) donated from the Pasteur Institute (Tutois, Montagutelli et al. 1991) Fech$^{m1PAS}$ Heterozygotes were bred with Balb/C Wild Type mice. The progeny were marked by ear punch and the spare tissue used to identify the genotype by PCR and Digestion with *BspHI* Restriction Endonuclease to identify the restriction length polymorphism (RFLP) arising from the point mutation in the ferrochelatase gene.

Once identified, animals were assigned to time points at 1, 2, 4, 8, 16, 24 and 32 weeks. These animals were then culled at the corresponding age as described in section 2.2.2.

*ARF21556:* A second experiment was carried out breeding Fech$^{m1PAS}$ homozygotes. Progeny were taken at one week of age and also at 18 days gestation.

Pure bred Balb/C mice were also taken at the above time points as controls. The progenies sex was determined post-mortem by PCR of Testis specific protein, Y-linked (Tspy) to confirm maleness.

### *2.2.2. Tissue Removal*

*ARF20279:* Animals were placed under terminal halothane inhalation anaesthesia. Blood was taken by cardiac puncture with or without thorectomy and placed in heparin tubes to prevent clotting. Death was confirmed by cervical dislocation and the liver removed. The liver was sectioned with the majority stored immediately in liquid nitrogen. The rest was fixed in 10% formalin for histopathology. The blood was centrifuged at 13000rpm for 10mins to pellet the blood cells and the blood plasma removed to a new 1.5ml micro-centrifuge tube. Blood plasma was stored at -20°C.

*ARF21556:* Animals were euthanized by cervical dislocation and the livers removed and stored in liquid nitrogen.

## 2.3 Nucleic Acid Extraction

### *2.3.1 RNA Extraction*

RNA was extracted from liver tissue using the Tri Reagent method. All benches were swabbed with 1%SDS/ 70% IMS to reduce the chances of RNase contamination.

100mg of tissue was cut over dry ice to prevent thawing and placed in a Falcon 2052 tube. To each tissue 500µl of Tri Reagent was added and the tissue homogenised by Ultra-Turrax. An additional 500µl of Tri Reagent was added and the lysate mixed. The lysate was incubated for 5 minutes at room temperature before 200µl of chloroform added. The lysate was then incubated for a further 10 minutes at room temperature before being spun for 10 minutes at 13000rpm at 4°C.

After centrifugation, the aqueous phase was transferred to a new 1.5ml micro-centrifuge tube and 1ml of isopropanol added. The sample was mixed by gentle vortexing and then left to incubate for 10 minutes at room temperature. The samples were then spun at 13200 rpm for 20 minutes to pellet the RNA. After centrifugation the supernatant was removed and the pellet washed twice with 70% ethanol (2x 1ml, centrifuged at 13000rpm for 10 minutes). The remaining ethanol was completely removed by air drying the pellet in a laminar flow hood and the pellet resuspended in 40µl of RNase free water. The extracted RNA was then quantitated as described in section 2.3.3.

### *2.3.2 DNA Extraction*

DNA was extracted using the method described in Molecular Cloning section 6.23(Sambrook and Russell 2001)

The lysis buffer was prepared by adding proteinase K to SNET buffer (section 2.1.1) to achieve a working concentration of 400µg $ml^{-1}$.

Ear punch tissue was added to a clean 1.5ml micro-centrifuge tube and 700µl of lysis buffer added. The sample was then incubated horizontally at 55°C overnight in a shaking incubator. 700µl of phenol:chloroform:isoamyl alcohol (Sigma-Aldrich) was added and the sample incubated on a rocking platform (to reduce damage to the DNA in comparison to vortexing) for 40 minutes. Samples were then centrifuged for 5 minutes at 13000rpm to separate the aqueous and organic phase. The aqueous phase

was then transferred to a new 1.5ml micro-centrifuge tube and 700µl of Chloroform added to remove excess phenol. The samples were incubated on a rocking platform for a further 30mins before being centrifuged for 10mins at 13000rpm. The aqueous phase was then transferred to a new 1.5ml micro-centrifuge tube and 1ml isopropanol added. The DNA was then precipitated by centrifugation at 13000rpm for 15mins at 4°C. The pellet was then washed with 70% ethanol and resuspended with TE.

### *2.3.3 Quantitation and Quality Control*

Quantitation was carried out by the $OD_{260}$ absorbance method. 1OD unit was taken as 40µg for RNA and 50µg for DNA. Two different UV-Vis spectrophotometers were used, a BioPhotometer (Eppendorf, Germany) and the NanoDrop ND-1000 (NanoDrop Technologies, USA).

Quality control was carried out by agarose gel electrophoresis and by calculating the $OD_{260/280}$ ratio taking between 1.8 and 2.0 to be good for DNA and over 2.0 for RNA.

200ng of each sample in loading buffer was run on a 1% agarose gel (section 2.1.2) in 1xTBE using 1kB Ladder (Promega, UK) as a size marker. The gel was then post-stained with ethidium bromide staining solution and visualised using a transilluminator. The presence of the ribosomal RNA (rRNA) bands was ascertained as an indication of good quality. If the rRNA bands were not present the sample was discarded and a fresh isolation carried out.

## 2.4 Genotyping the Fech$^{m1PAS}$ Mouse

### *2.4.1 Primer Design*

The Fech$^{m1PAS}$ allele contains a T to A transversion at nucleotide 293. This mutation introduced an RFLP preventing restriction by BspHI restriction endonuclease (Fermentas International Inc. USA). Primers were designed to flank nucleotide 293 producing a 1.4kb amplicon.

**Figure 2.1)**

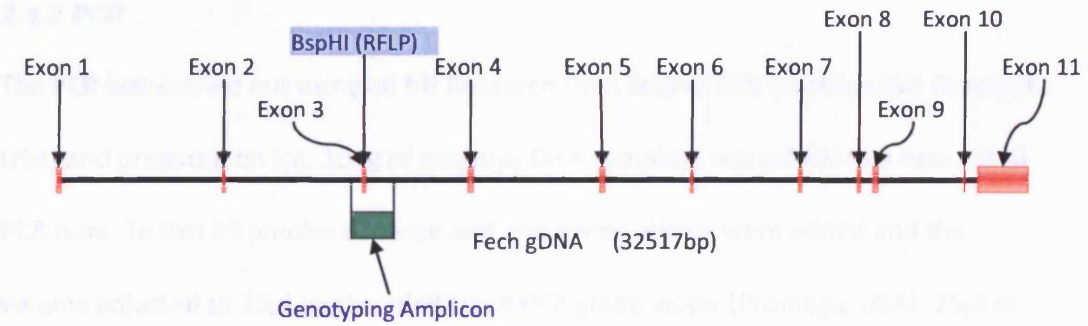


Figure 2.1) **The alignment of the Genotyping Amplicon on Fech Genomic DNA, the *BspHI* RFLP and the intron/exon boundaries.**

**Table 2.1**

| | |
|---|---|
| **Sense** | TAA CCT CTG GAA AGC CAG ACC |
| **Anti-Sense** | GAA CTT ACT GAG CAA GCA AGG C |

Table 2.1) **Primer sequences for genotyping the Fech$^{m1PAS}$ mouse from genomic DNA**

### *2.4.2 PCR*

The PCR was carried out using an MJ Research DNA Engine PCR machine (MJ Research, USA) and prepared on ice. 10ng of genomic DNA template was added to a new 200µl PCR tube. To this 20 pmoles of sense and anti-sense primer were added and the volume adjusted to 25µl by the addition of PCR grade water (Promega, USA). 25µl of Promega 2X PCR master mix was then added, the solution was mixed by vortexing and then spun down in a micro-centrifuge.

The PCR was then run according to the profile in table 2.2.

**Table 2.2**

| Time | **Temperature** | Role |
|---|---|---|
| 5mins | 95 $^{O}$C | Initial Denature |
| 45s | 55 $^{O}$C | Annealing |
| 45s | 72 $^{O}$C | Extending |
| For one cycle | | |
| 30s | 95$^{O}$C | Denature |
| 45s | 55$^{O}$C | Annealing |
| 45s | 72$^{O}$C | Extending |
| For 33 cycles | | |
| 30s | 95$^{O}$C | Denature |
| 45s | 55$^{O}$C | Annealing |
| 5mins | 72$^{O}$C | Final Extension |
| For one cycle followed by soak at 4$^{O}$C | | |

Table 2.2) **DNA Engine thermal profile for amplification of the Fech$^{m1PAS}$ RFLP for genotyping**

### *2.4.3 Restriction Digest with BspHI*

The restriction digest was run as a 10µl reaction.

To a new 1.5ml micro-centrifuge tube, 8µl of the PCR product was added to 1µl of 10X Restriction buffer (supplied with the restriction enzyme) and mixed by vortexing. 1µl of *BspHI* (also known as *PagI*) was added, mixed by vortexing and spun down before being incubated for 3 hours at $37^0$C.

### *2.4.4 Gel Electrophoresis*

A 1% agarose gel was prepared by boiling agarose in 1X TBE (at 10g $l^{-1}$) in sufficient volume to fill the gel tray in use (section 2.1.2).

Samples were prepared by addition of 2µl 6X gel loading buffer to the completed digest.

These samples were then run on the gel at 50V for 1hr to allow good separation of the digest products with 1kb+ ladder (Promega) to act as a sizing marker. After running, gels were post-stained with ethidium bromide to allow visualisation of the nucleic acids. The gels were soaked in staining buffer for 15mins before being carefully removed and photographed using a GelDoc-IT transilluminator (Ultra-Violet Products Inc, USA).

## 2.5 Sex Determination by Testis Specific Protein, Y-linked

### *2.5.1 Primers*

Primers were designed to a region on the Y chromosome with no homology to the other chromosomes to produce a product in male samples only. The region chosen was the testis specific protein-Y pseudogene, TSpy-ps (NG_001475.1)

The following primers produce a 960bp Amplicon in male mice only.

**Table 2.3**

| | |
|---|---|
| **Sense** | ATG GAG AAC TGT GGG GTG G |
| **Anti-Sense** | GGT TGC TGA TGA TGG ACG AC |

Table 2.3) **Primer sequences for sex determination in the mouse by amplification of TSpy-ps.**

### *2.5.2 PCR*

The PCR was carried out as per section 2.4.2 with the presence of a product being checked by gel electrophoresis using a 1% agarose gel as described in section 2.4.4. In addition to the test samples, samples from a known male and known female were also run as positive and negative controls respectively.

## 2.6 Histopathology

Haematoxylin and eosin staining were carried out on liver sections that had been fixed in 10% formalin. A selection of samples was made such that a representation of all genotypes at all time points with n≥3 was achieved. These samples were then analysed on a semi-quantitative basis (scoring as minimal, moderate or marked) by pathologist Dr Peter Greaves (MRC Toxicology Unit, Leicester)

## 2.7 Blood Chemistry

### *2.7.1 Alanine Amino-Transferase analysis of Liver Damage*

Levels of liver damage were assayed from blood plasma by quantitation of alanine amino-transferase activity using a Randox ALT Kit (AL 1205, Randox Laboratories Ltd, UK). The kit comprises of a buffer/substrate solution and vials of enzyme/coenzyme/α-oxoglutarate mix. The assay uses the increase in $NAD^+$ measured by absorbance at 340nm to quantify the level of ALT activity as a result of the reactions summarised in figure 2.2.

**Figure 2.2**

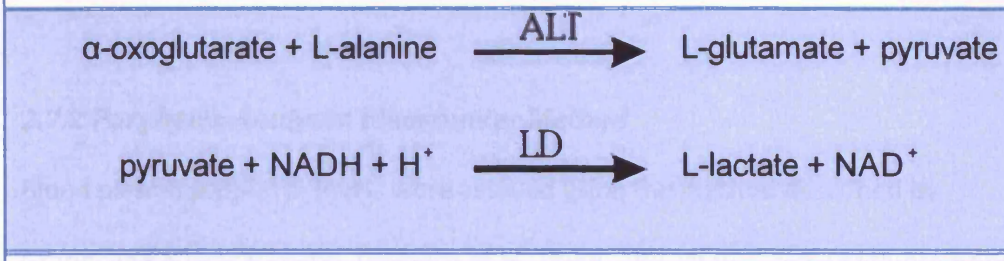


Figure 2.2) **Determination of the levels of alanine amino-transferase (ALT) resultant of liver damage. ALT catalyses the first reaction.** The pyruvate from the first reaction is then used by lactate dehydrogenase (LD) in the oxidation of NADH to $NAD^+$ which absorbs light at 340nm.

A fresh vial of enzyme mix was reconstituted in 10ml of the buffer/substrate solution and mixed thoroughly. The spectrophotometer cuvette holder was warmed to 25°C and blanked against 1ml of the reconstituted enzyme mix. 1ml of the reconstituted solution was added to a new cuvette and 100µl of heparinised blood plasma added and mixed.

The cuvette was then immediately placed in the UV/Vis spectrophotometer and the absorbance at 340nm recorded over 4mins. This produced a curve where the gradient of the curve is in correlation with the ALT activity.

The data were accumulated and the change in absorbance over time

($\Delta A_{340nm}$ $min^{-1}$) calculated for all samples. The ALT activity was then calculated by the equation: Units $l^{-1}$ = 1746 x $\Delta A_{340nm}$ $min^{-1}$

### *2.7.2 Porphyrin Analysis: Fluorimeter Method*

Blood plasma prophyrin levels were assayed using the method described by Grandchamp(Grandchamp, Deybach et al. 1980). The assay compares fluorescence of the biological sample at three wavelengths against a calibrated matrix made using Protoporphyrin, Uroprophyrin and Coproporphyrin standards (Sigma).

Standards were prepared by dissolving 2mg of the standard in 1M ammonia in a new 1.5ml micro-centrifuge tube. Excess ammonia was then vented with nitrogen and 200µl 1N NaOH added. The concentration of the standards was then determined by diluting the standards with hydrocholoric acid to the concentrations detailed in table 2.4 and measuring the fluorescence at the corresponding wavelengths using UV/Vis Spectrophotometry (Perkin Elmer, USA). The standards were then diluted in porphyrin acid mix (section 2.1.3) to 100nM.

**Table 2.4**

| Standard | Hydrochloric Acid Concentration (N) | Wavelength (nm) | Extinction Coefficient |
|---|---|---|---|
| Coproporphyrin | 0.1N | 399.5 | 489000 |
| Uroporphyrin | 0.5N | 405.5 | 541000 |
| Protoporphyrin | 2.7N | 408 | 262000 |

Table 2.4) **Determination of Porphyrin Standard Concentration by UV/Vis Spectrophotometry.**

Liver samples were prepared by producing a 10% homogenate with water. From the 10% homogenate 0.5ml was taken to a clean 15ml falcon tube and mixed with 4.5ml porphyrin acid mix which causes the protein to precipitate. The aqueous phase was then removed to a new tube ready for analysis.

The fluorescence of the three standards and the liver samples was then measured by fluorimeter (Perkin Elmer, USA) using the optimum excitation-emission wavelength pairs shown in table 2.5.

| Table 2.5 | | |
|---|---|---|
| **Standard** | **Excitation Wavelength (nm)** | **Emission Wavelength (nm)** |
| **Coproporphyrin** | 400 | 595 |
| **Uroporphyrin** | 405 | 595 |
| **Protoporphyrin** | 410 | 605 |

Table 2.5) **Porphyrin Assay Optimum Excitation and Emission Wavelengths for Fluorometric Quantitation of Concentration.**

The fluorescence of the standards was then used to create a matrix that allowed determination of the liver samples concentration. The matrix uses the linear relationship between the fluorescence emission mixture of porphyrins and the emission of the individual porphyrins within the mixture such that

$$Fluorescence\ of\ the\ Mixture = \frac{(F_c\, X_c) + (F_u\, X_u) + (F_p\, X_p)}{C}$$

Where $F_c$, $F_u$ and $F_p$ represent the fluorescence of the coproporphyrin, uroporphyrin and protoporphyrin standards respectively; $X_c$, $X_u$ and $X_p$ the unknown concentrations of the samples and $C$ the concentration of the standards.

### *2.7.3 Porphyrin Analysis: HPLC Method*

To confirm the results obtained from the Fluorimeter based porphyrin assay were solely due to the presence of protoporphyrin a separation was performed using High Performance Liquid Chromatography (HPLC). The separation was performed using a 250mm Hypersil BDS C18 Column (Fisher Scientific) across an acetonitrile gradient as described in Luo and Lim.(Luo and Lim 1995). 10% homogenates from section 2.7.2 were taken and mixed 1:1 with DMSO/10% TCA. The mixture was then centrifuged at 13000rpm for 5mins in a benchtop centrifuge to precipitate the protein from the sample. The supernatant was transferred to a clean tube ready for analysis by HPLC.

Solvents were prepared as detailed in 2.1.3

Samples were injected automatically by the HPLC into a 500µl loop and run through the HPLC at a flow rate of 1ml $min^{-1}$ with 10mins at 100% Solvent A, then a linear gradient of 0 to 90% Solvent B over 90mins. The column was then recalibrated with 10mins at 100% Solvent A prior to the next sample being injected. Detection was by a fluorescence detector set at an excitation wavelength of 405nm and an emission wavelength of 618nm.

### *2.7.4 Bilirubin Assay*

Total bilirubin was measured from blood plasma using a commercial diagnostics kit (Randox Laboratories, UK). The method measures the total bilirubin load consisting of both conjugated and non-conjugated bilirubin using a colourmetric method adapted

from Jendrassik and Grof (1938)(Jendrassik and Grof 1938). The method uses the principle that bilirubin forms a blue coloured complex when reacted with diazotised sulphanilic acid in an alkaline medium. This blue complex can be measured by UV/Vis spectrophotometry at a wavelength of 578nm.

Experiments were carried out as directed by the instructions provided with the kit with a 75% reduction of all volumes to allow for the small volumes of plasma available.

## 2.8 The Microarray Process

### *2.8.1 Overview of the Process*

Microarray experiments are complex systems comprised of several key components. These components have been summarised in figure 2.3.

**Figure 2.3**

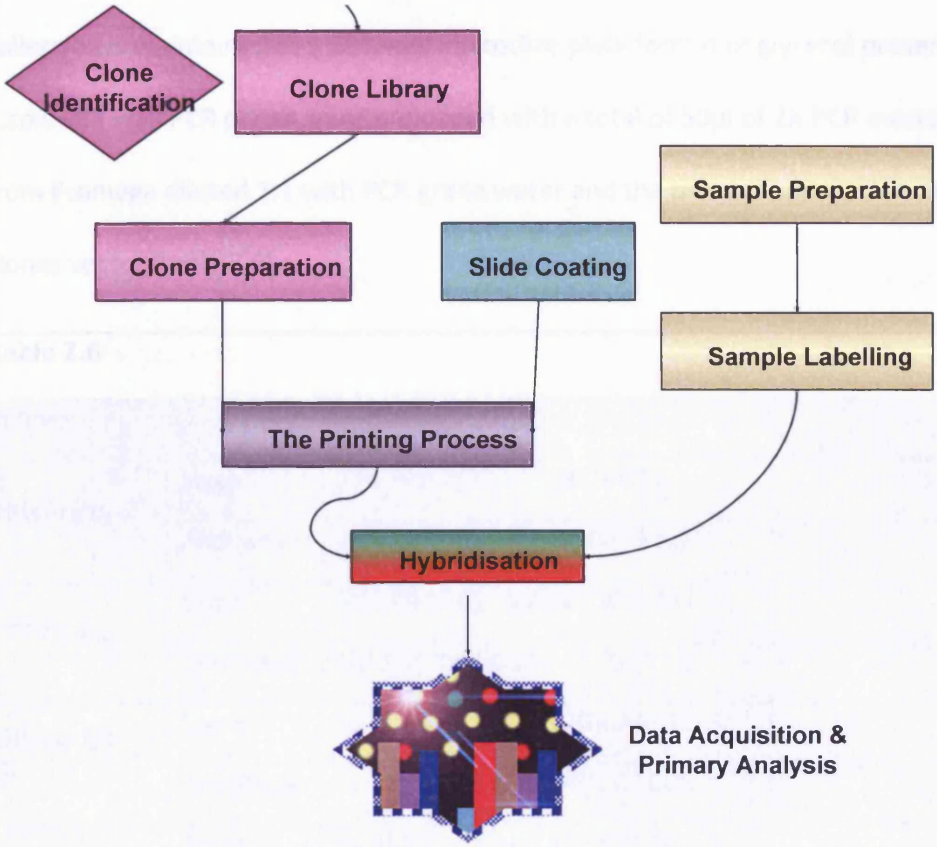


Figure 2.3) **An overview of the array process and its components.** cDNA Clone Libraries are maintained and printed on poly-L-lysine coated slides. Samples are prepared and labelled with fluorophores prior to hybridisation on the printed arrays. Data is acquired by scanning the array and initial data analysis performed.

### *2.8.1 Clone Preparation*

Clones to be printed were amplified by PCR in a semi-automated process. The clone collection is maintained in a 384-well microtitre plate format of glycerol preserved *E.coli*. 384 well PCR plates were preloaded with a total of 50µl of 2X PCR mastermix from Promega diluted 1:1 with PCR grade water and the primers appropriate to the clones vector (table 2.6).

**Table 2.6**

| **Primer** | | **Sequence** |
|---|---|---|
| **Universal** | Sense | GTA AAA ACG ACG GCC AGT G |
| | Anti-Sense | ACA CAG GAA ACA GCT ATG ACC |
| **pT7T3-pac** | Sense | GGC CAG TGC CAA GCT AAA AT |
| | Anti-Sense | TCA CTA TAG GGA ATT TGG CCC |
| **Bluescript-SK** | Sense | GAC TCA CTA TAG GGG AAA TTG G |
| | Anti-Sense | CTA GAA CTA GTG GAT CCC CCG |
| **PcmvSPORT** | Sense | AGA GCT ATG ACG TCG CAT GC |
| | Anti-Sense | AGG TAC CGG TCC GGA ATT C |
| **PcmvSPORT6** | Sense | AGA AAG CTG GGT ACG CGT AA |
| | Anti-Sense | AAA AAG CAG GCT GGT ACC G |

Table 2.6) **Primer Sequence for PCR Amplification of Clone Library Prior to Printing.** Clone well locations are held in a database with their respective plasmid allowing identification of which primers should be loaded into which wells on the PCR plate.

PCR mix was made in bulk and loaded into the wells using a Hydra-96 pipetting station (Robbins Scientific, now Matrix Technologies, USA). Each clone was then picked into the preloaded 384 well PCR plate using a QPix 2 colony picking robot (Genetix, UK) equipped with a honeypicker style 96 pin head.

The PCR reaction was carried out in a MJ Research DNA Engine Tetrad using the thermal profile in table 2.7. The primer annealing temperature was varied dependent on the primers used; the universal primers required an annealing temperature of 52°C whereas the others anneal at 56°C.

The PCR products were then aliquoted into 384 well printing source plates (Costar) using the Hydra 96 pipetting station and dried in a vacuum centrifuge (SpeedVac). The dried down product was then resuspended in printing solution (section 2.1.4) overnight on a shaking platform.

**Table 2.7**

| Time | Temperature | Role |
|---|---|---|
| **5mins** | 95 $^{o}$C | **Initial Denature** |
| **3mins 30s** | 72 $^{o}$C | |
| For one cycle | | |
| **30s** | 95$^{o}$C | **Denature** |
| **45s** | 52/56$^{o}$C | **Annealing** |
| **3mins 30s** | 72$^{o}$C | **Extending** |
| For 28 cycles | | |
| **5mins** | 72$^{o}$C | **Final Extension** |
| For one cycle followed by soak at 4$^{o}$C | | |

Table 2.7) **DNA Engine thermal profile for amplification of the Clone Library for Printing.**

### *2.8.2 Slide Preparation*

Glass slides (Erie Scientific, USA) were coated with poly-L-lysine to allow the printed cDNA clones to be covalently bonded to the array platform.

The slides were arranged in slide racks (produced in house, see appendix I.i) and washed in Slide Washing Solution (see 2.1.5) for two hours with rocking in a parallel plane to the slides.

The slides were then washed in distilled purified water four times to remove all traces of the washing solution. After rinsing the slides were dried in a bench top centrifuge (Eppendorf 5804), using a microtitre plate rotor, at 1500rpm for 5mins. Once dry the slides were protected from dust by being kept in sealed plastic boxes at all times prior to the next step.

The slides were then coated with poly-L-lysine by immersing the slides in the Slide Coating Solution (see 2.1.5) in polypropylene boxes with slow rocking in a parallel plane to the slides for one hour. After this the slides were then washed with five changes of distilled purified water before drying in the bench top centrifuge for 5mins at 1500rpm, removing all traces of the Slide Coating Solution.

The slides were then placed in a dry heat oven at 45°C for 15mins to complete the drying process without water spots forming on the slides.

The completed slides were then transferred to slide boxes containing silica gel packets and allowed to cure for two weeks prior to printing.

### *2.8.3 Coverslip Preparation*

The coverslips used in the hybridisation must be clean and free from dust to assure that nothing will interfere with the hybridisation process. Coverslips were loaded into coverslip racks and immersed in 1% SDS for 30mins with rocking in a parallel plane to the coverslips and then rinsed in a continuous flow of ultra-purified water (18mΩ resistance, ELGA Lab Water, UK) for 20mins. After rinsing, the coverslips were dried by incubation in a dry heat oven at 55°C and then transferred to sealed polypropylene boxes for storage.

### *2.8.4 The Printing Process*

#### *2.8.4.1 The Printer*

The array printer was built in house to the plans made available by Joe DeRisi and Patrick Brown at Stanford (figure 2.4a). It is a sprung pin based spotted microarray print run by a standard windows PC using Arraymaker software also obtained from Joe DeRisi.

The 32pin print head used was manufactured by Majer Precision Engineering in conjunction with Stanford University (figure 2.4b). The pins used were Majer MicroQuill 3001 DNA array pins.

**Figure 2.4**

a)

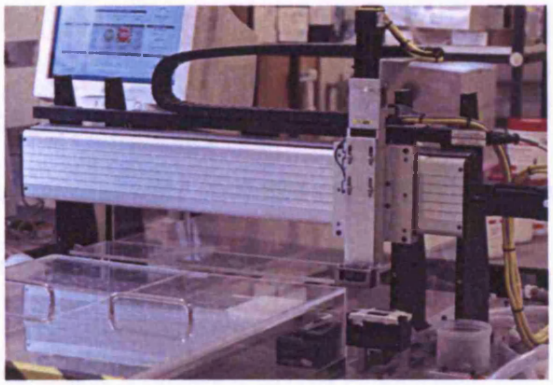

b)

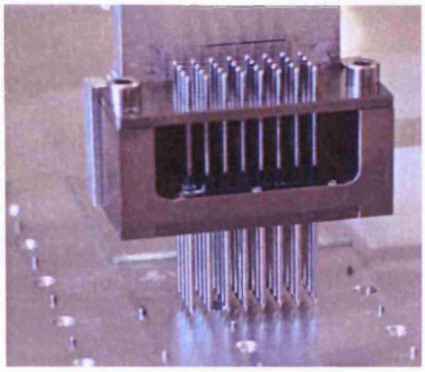

Figure 2.4) a) **The array printer built in house from Joe DeRisi's plans** (UCSF). b) **The Majer 32pin print head fitted with MicroQuill DNA array pins.**

*2.8.4.2 The Printing Method*

The printing method used is as described Schena *et al.*(Schena, Shalon et al. 1995); The printing head is introduced into the printing solution of the printing source plate where capillary action draws printing solution into the split at the end of the pin. The pin is then blotted on an empty slide to remove excess solution before it is deposited on the poly-L-lysine coated slides by a gentle tap of the print head against the slide. Once all 137 slides have been tapped with the current clone the print head is washed in purified water and blown dry, the next clones are drawn up and the position of the print head indexed to give ≈150µm spacing from the centre of one feature to the next allow the printing of discreet features. Once printing is complete the arrays are labelled and stored in a cool, dry and dark place. A file containing the identity of each

feature on the array is also generated (the .GAL file) to allow analysis post-hybridisation.

### *2.8.5 Sample Preparation and Labelling*

All benches were swabbed with 1%SDS/ 70% IMS to reduce the chances of RNase contamination. RNA was extracted from tissue as described in section 2.3.1.

#### *2.8.5.1 Direct Labelling*

Direct labelling using Cy-dyes was used for some of the initial arrays and was then superseded by the indirect method (section 2.8.5.2). Two cy-dyes were used; Cy3 dUTP with an wavelength of 532nm on the green channel and Cy5 dUTP with a wavelength of 647nm on the red channel.

50µg of total RNA was added to a new RNase free 0.5ml micro-centrifuge tube in 10µl DEPC treated water. The sample was then denatured by heating to 95$^{O}$C for 3mins and then snap-cooled on ice. Oligonucleotide $dT_{25}$ primers were then annealed for first strand synthesis by adding 0.5µl oligo $dT_{25}$ (8µg $\mu l^{-1}$). The samples were then incubated at 70$^{O}$C for 8mins and then the temperature reduced slowly to 50$^{O}$C over 30mins. The temperatures were achieved by the incubation being carried out in an MJ Research DNA Engine.

Whilst maintaining the sample at 50$^{O}$C, 6.5µl of Direct Labelling Mix (section 2.1.6) was added with 2.0µl of the appropriate Cy dye , 0.5µl RNAsin (Promega) and 0.5µl Superscript III Reverse Transcriptase (Invitrogen). The sample was then incubated for 2

hours at 50$^{O}$C to allow first strand synthesis and incorporation of the cyanine dye. After incubation 20.5µl molecular grade water was added.

The residual RNA was hydrolysed by the sequential addition of 1µl EDTA (0.5M), 1µl SDS (10% w/v) and 3µl NaOH (3M) followed by an incubation at 70$^{O}$C for 15mins with the resultant cDNA being neutralised with the addition of 3µl 2M HCl and 10µl 1M Tris/HCl (pH7.5).

The next step in the labelling protocol was to purify the labelled sample and prevent it from binding non-specific sequences. To purify the labelled probes, 1µl of tRNA (4µg $\mu l^{-1}$) was added to the probe to act as a carrier and then purified using Centri-sep columns (Princeton Seperations, USA) according to the manufacturer's instructions. The presence of the tRNA at this point help ensure that all of the labelled probe is carried through the column and retrieves. At this point the two samples to be hybridised together were combined in one tube and to prevent the sample from binding non-specific fragments, 1µl Cot1 DNA (10mg $ml^{-1}$) and 1µl poly A (1µg $\mu l^{-1}$) was added. Alu fragments are repetitive elements found in most genomes and the addition of excess Cot1 DNA prevents binding by competitive binding to any Alu fragments present on the array.

Samples were then dried down using a DNA speedvac (Savant).

Before hybridisation the samples were resuspended in 24.5µl Hybridisation Buffer (section 2.1.6) and 10.5µl of 20X SSPE and the hybridisation carried out as in section 2.8.7.

*2.8.5.2 Indirect Labelling*

Indirect labelling was introduced due to the increased emission levels generated by the utilisation of the Alexa dyes (Molecular Probes) in comparison to the Cyanine dyes and to stream line the protocol to make it less prone to user error.

20µg of total RNA was added to a new RNase free 1.5ml micro-centrifuge tube with 1.0µl of oligonucleotide $dT_{25}$ (8µg $\mu l^{-1}$) and 1.0µl of random hexamers (3µg $\mu l^{-1}$) (Amersham Biosciences). The volume was then adjusted to 13µl using DEPC treated water.

The samples were then heated to 95°C for 5mins to denature then RNA and then taken to 70°C for 10mins to allow annealing of the $dT_{25}$ and the hexamers before being snap cooled on ice. To each sample 14µl of Indirect Labelling Mix (section 2.1.6) and 1µl of Superscript III RNA Polymerase (Invitrogen, USA) was added and the sample mixed by vortexing. Samples were then incubated at 50°C for 3 hours to produce cDNA with incorporated amino-allyl dUTP. After 3 hours 10µl of 0.5M EDTA was added to stop enzymatic reactions and the RNA hydrolysed by addition of 10µl of 1N NaOH and incubation at 65°C for 15mins. After the hydrolysis reaction the samples were neutralised by the addition of 25µl 1M HEPES (pH7.0)

The first strand synthesis was then cleaned using Microcon YM-30 filters (Millipore) as follows. For each sample a new column was labelled and 400µl of water paced on the filter. The sample was then added to the water on the filter and the column assembly spun in a micro-centrifuge for 7mins at 12000rpm. The flow through was discarded

and a further 450µl of water added to the top of the column. The samples were then spun for 13mins at 12000rpm or until the filter membrane was dry.

To recover the sample, 7µl molecular grade water and 1µl 1M sodium carbonate buffer were added to the filter and left to stand for 5mins. The columns were then inverted and placed into new 1.5ml micro-centrifuge tubes before being pulse spun in a micro-centrifuge to recover the sample.

The next series of steps attach the Alexa fluorophore (Molecular Probes, Invitrogen) to the aa-dUTP by means of a covalent condensation reaction between the carboxylic acid group on the dye and the amine group in the aa-dUTP. Different Alexa dUTPs were used dependent on the intended fluorescence channel of the sample (table 2.8).

**Table 2.8**

| Alexa Dye | Microarray Channel |
|---|---|
| Alexa Fluor 647 | Red |
| Alexa Fluor 555 | Green |
| Alexa Fluor 594 | Yellow |
| Alexa Fluor 488 | Blue |

Table 2.8) **A table showing the Alexa dyes used in the microarray experiments and their corresponding colour.**

The dyes were prepared by addition of 8µl of DMSO to a new vial of Alexa dye. To each sample in carbonate buffer, 2µl of the appropriate dye was added and the reaction mixed by stirring without centrifugation. The carbonate buffer maintains pH8.5 to pH9, the required pH for the amine linkage. The reaction was then incubated in the dark for one hour at room temperature. After incubation, 4.5µl of 4M hydroxylamine was added to quench the reaction, and the reaction incubated for a further 15mins to prevent linkage of excess dye to the other channel once the reactions are combined. The reactions for each array were then combined and 35µl of 0.1M NaOAc (pH5.2) added to buffer the reactions ready for the following clean up.

**Table 2.8**

| Alexa Dye | Microarray Channel |
|---|---|
| Alexa Fluor 647 | Red |
| Alexa Fluor 555 | Green |
| Alexa Fluor 594 | Yellow |
| Alexa Fluor 488 | Blue |

Table 2.8) **A table showing the Alexa dyes used in the microarray experiments and their corresponding colour.**

The dyes were prepared by addition of 8µl of DMSO to a new vial of Alexa dye. To each sample in carbonate buffer, 2µl of the appropriate dye was added and the reaction mixed by stirring without centrifugation. The carbonate buffer maintains pH8.5 to pH9, the required pH for the amine linkage. The reaction was then incubated in the dark for one hour at room temperature. After incubation, 4.5µl of 4M hydroxylamine was added to quench the reaction, and the reaction incubated for a further 15mins to prevent linkage of excess dye to the other channel once the reactions are combined.

The reactions for each array were then combined and 35µl of 0.1M NaOAc (pH5.2) added to buffer the reactions ready for the following clean up.

Using a QiaQuick PCR cleanup kit (Qiagen, USA) 250µl of buffer PB was added to each combined reaction and then the whole sample was loaded onto a new qiaquick column. The column was spun in a micro-centrifuge for 1min at 13000rpm and the flow through discarded. 750µl of wash buffer PE was then added to each column before centrifugation for 1min at 13000rpm. The flow through was discarded and the sample dried by a further centrifugation for 1min at 13000rpm.

The columns were then placed into new 1.5ml micro-centrifuge tubes and 30µl of elution buffer EB added to the centre of the filter. The tubes were then incubated for 1min at room temperature to allow the elution buffer to permeate the filter before being spun for 1min at 13000rpm to retrieve the purified sample. A further 30µl of EB was then placed on the filter, incubated for a minute and spun as previously to ensure that all sample had been retrieved from the column.

The recovered sample was then checked for fluorophore incorporation using a NanoDrop spectrophotometer and the microarray application within the NanoDrop software.

Each sample was then added to a new Microcon 30 column (Millipore) with 400µl of molecular grade water, 1.0µl Poly Adenosine Oligonucleotide (1µg $\mu l^{-1}$), 1.0µl Yeast tRNA (4µg $\mu l^{-1}$, Invitrogen) and 10µl species specific Cot1 DNA (1µg $\mu l^{-1}$, Invitrogen). The samples were then spun in a micro-centrifuge for 12mins at 12000rpm until the volume of sample retained on the filter decreased to 10µl and then recovered to a new 1.5ml micro-centrifuge tube. The concentrated samples were then dried using a

DNA SpeedVac (Savant) before being resuspended in 24.5µl Hybridisation Buffer and 10.5µl of 20X SSPE.

Samples were denatured at 100$^{O}$C for 2mins then incubated at 50$^{O}$C for 1 hour prior to hybridisation allowing the samples to reach equilibrium.

### *2.8.6 Pre-Hybridisation Slide Processing*

Printed microarray slides were selected and the printed DNA denatured by heating the slides to 100OC for 2mins using an MJ Research DNA Engine with a slide holding block. The printed DNA was then cross-linked to the slide surface by a further incubation at 80OC for 2 hours.

The slides were then loaded into racks and washed in pre-hybridisation wash solution (section 2.1.7) for 5mins with periodic agitation. The excess solution was washed off by immersing the slides in ultra-pure water for 2mins before being washed in Sodium Borohydride Solution (section 2.1.7) for 20mins with periodic agitation to reduce intrinsic background. After 20mins the slides were washed in 0.2% SDS for 2mins and then twice with ultra-pure water for 2mins each before being dried in a bench top centrifuge (Eppendorf 5804), using a microtitre plate rotor, at 1500rpm for 5mins. Once dry the slides were protected from dust by being kept in sealed plastic boxes at all times prior to hybridisation.

### *2.8.7 Hybridisation and Post-Hybridisation Processing*

A template slide was prepared using an unwashed printed slide from the same batch as the hybridisation to indicate the position of the features on the slide.

The array to be hybridised was then placed over the template slide and the sample loaded onto the edge of the array boundary. Using forceps, a clean coverslip was then gently lowered onto the array as shown in figure 2.5. The array was then placed in a hybridisation chamber (produced in house to the specifications of Dr. M Marvin, Department of Genetics, University of Leicester) with 25µl 3X SSC at the end of the chamber to maintain the humidity. The chamber was then sealed and placed in a 50OC water bath for 24hrs.

After hybridisation the slides were removed from the hybridisation chambers and racked. Wash solutions were made as detailed in section 2.1.8. The slides were then washed in Array Wash Solution 1 for 10mins, Array Wash Solution 2 for 5mins and then Array Wash Solution 3 for 5mins. The arrays were then dried in a bench top centrifuge (Eppendorf 5804), using a microtitre plate rotor, at 1500rpm for 5mins. After drying the slides were kept in an opaque slide box to protect them from light prior to scanning.

**Figure 2.5**

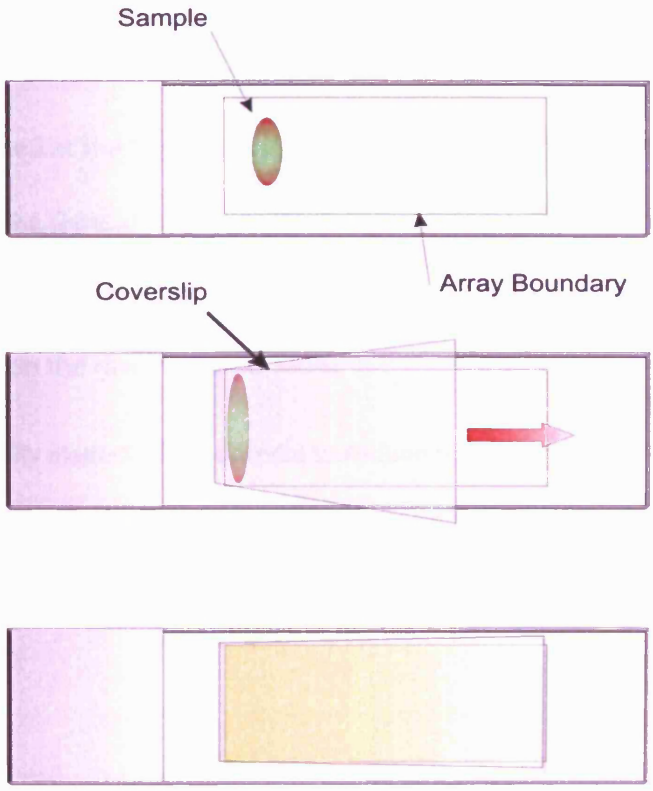


Figure 2.5) **Diagram demonstrating the proper placement of the coverslip when setting up a hybridisation.**

### *2.8.8 Data Acquisition and Primary Analysis*

Hybridised microarrays were scanned using an Axon 4000 and later an Axon 4200A Microarray scanner (Molecular Devices (formerly Axon Instruments), USA)

The slides were scanned at the highest possible resolution (10µm for the 4000, 5µm for the 4200A) using the Genepix software (Molecular Devices). The raw images were converted to pixel intensities by overlaying a GAL file (See 2.8.4.2 ) and fitting the GAL file features to those on the raw image.

Features were manually inspected for defects to reduce incident of false readings and the array analysed in the manner discussed in section 1.6.5.

## 2.9 Real-Time PCR

### *2.9.1 Overview of the Process*

Real time PCR is an accurate method for the quantification of rates of gene expression. Although Microarray technology provides insight into the intricacies of gene expression changes it cannot provide the sensitivity that real time PCR can.

Real time PCR monitors the progress of a PCR reaction as it occurs using the detection of a fluorescent dye which increases in emission the more PCR product is present. This allows characterization of samples by the point of time at which the reaction can be detected (the cycle threshold, $C_t$) as opposed to the amount of target accumulated after a fixed number of cycles as in a northern blot. The higher the copy number of a

species of RNA the sooner an increase in fluorescence emission will be detected. Real time PCR was carried out using the ABI 7000 Sequence Detector and SYBR Green Dye (Applied Biosystems Inc.) which fluoresces when bound to double stranded DNA.

### *2.9.2 Primer Design.*

Primers were designed using Primer Express 2.0 Software (Applied Biosystems Inc.) so that they span an exon/exon boundary to prevent DNA contamination and a melting temperature just below 60°C.

### *2.9.3 cDNA First Strand Synthesis*

Prior to real time PCR is the whole RNA sample is reverse transcribed to a cDNA. It is the cDNA that is used as the template in the real time detector.

To reverse transcribe the sample, 1µl whole RNA (100ng $\mu l^{-1}$) was added to 8.25µl First Strand Master Mix (section 2.1.9). The samples were denatured at 95°C for 5mins and then cooled on ice to allow annealing of the random hexamer primers in the master mix.

After the sample had cooled, 0.25µl RNasin (Promega 1unit $\mu l^{-1}$) and 0.5µl Superscript III Reverse Transcriptase (Invitrogen) were added. The samples were then placed in an MJ Research DNA engine to be incubated at 23°C for 10mins, 50°C for 45mins, 99°C for 10mins and then held at 4°C.

### *2.9.4 SYBR Green Real Time PCR Reaction and Analysis*

SYBR Green Real Time PCR reactions were carried out in triplicate for each sample and a non-template control to check for contamination. Reactions were set up either by hand or using a 6-Station liquid handling robot (Corbett Robotics, Australia) in 96-well optically clear microtitre plates (Applied Biosystems Inc.) as per table 2.9 to a final volume of 25µl.

**Table 2.9**

| **Reagent** | **Volume (µl)** |
|---|---|
| SYBR Green PCR Master Mix (2X) (ABI) | 12.5 |
| Sense Primer (50µM) | 0.15 |
| Anti-Sense Primer (50µM) | 0.15 |
| cDNA Template from 2.9.3 | 1.00 |
| PCR Grade Water | 11.20 |

Table 2.9) **Components of the SYBR Green Real Time PCR Reaction.**

The plates were then mixed by vortexing and spun down in a centrifuge before being loaded into the real time PCR machine. The real time PCR was run on the default

thermal program for the detector (table 2.10) with a dissociation protocol at 60°C to check for the presence of non-specific amplification.

Analysis of the results was carried out using the $\Delta\Delta C_t$ relative quantitation method. The mean $C_t$ was calculated for each gene and normalised against the endogenous control gene β-actin. β-actin was chosen due to its unchanging, ubiquitous expression. Each gene in the $Fech^{m1PAS/m1PAS}$ mouse was then calibrated against the data from Balb/C controls.

**Table 2.10**

| Time | Temperature | Role |
|---|---|---|
| **2mins** | 50 $^{O}$C | Initial Denature |
| **10mins** | 95 $^{O}$C | Annealing |
| For one cycle | | |
| **15s** | 95$^{O}$C | Denature |
| **1min** | 60$^{O}$C | Anneal, Extend and Read |
| For 40 cycles | | |
| **15s** | 95$^{O}$C | Denature |
| **20s** | 60$^{O}$C | Dissociation Protocol Read |
| **15s** | 95$^{O}$C | |
| For one cycle | | |

Table 2.10) **ABI 7000 Sequence Detector thermal profile for SYBR Green Real Time PCR.**

# Chapter 3) Genotyping and Experimental Design

## 3.1 Introduction

The generation of the Fech$^{m1PAS}$ time course required that a sufficient number of animals of each genotype be assigned to each time point to attain statistical power. The known variability of gene expression and the technical limitations have an adverse effect on statistical power which has been articulated in the paper of Zhang and Gant (Zhang and Gant 2004). This method has been used to statistically model the power of the experimental design or rate of successful differential gene expression (DGE) detection for a given set of parameters; $n_f$ being the number of forward labelled arrays for a given experiment, $n_r$ being the number of reverse labelled arrays for the same experiment, $P_{th}$ the P-value at which a DGE will be declared significant and $|\mu|/\sigma_T$ is the mean to standard deviation ratio for the magnitude of differential expression. The S value depicts the percentage of DGE's that will be successfully identified.

The model used in the S calculation summarises the log-intensity fluorescence of each feature as

$$G_{v,i,s,c} = I_{v,i} + A_s + D_c + \in_{v,i,s,c} \qquad \text{(eq.1)}$$

Where $G_{v,i,s,c}$ is the $\log_2$ fluorescence of the feature, $I_{v,i}$ is the expression level of the *i*-$^{th}$ member of group *v* (in this experiment v = t for the Fech$^{m1PAS}$ mouse, v = c for the wild type mouse and $i = 1, \ldots, n$ where *n* is the number of individuals in group *v*) based on the assumption that $I_{v,i}$ is independent of other factors and is normally distributed with a mean $E_v$.

$A_s$ is the effect of spot quality on array *s* and is independent of the dye used but assumed to be constant across any given slide *s*. $D_c$ is the effect of the fluorophore used in the labelling (*c*) and is assumed to be independent of the slide used, where *c* = *g* when the green dye is used or *c* = *r* when the red dye is used.

$\in_{v,i,s,c}$ denotes the random error which cannot be predicted but is assumed to have a normal distribution about a mean of 0.

$E_v$ is the mean expression level of the gene in sample group *v* showing that the comparision of gene expression levels between the Fech$^{m1PAS}$ mice and the Balb/C controls would be summarised as $E_t - E_c$. Using the model in eq.1 we can derive a summary of the simultaneous hybridisation of both the test and control to a single array

$$G_{c,j,a,g} = I_{c,j} + A_a + D_g + \in_{c,j,a,g}$$

$$G_{t,i,a,r} = I_{t,i} + A_a + D_r + \in_{t,i,a,r} \qquad \text{(eq.2)}$$

Where *j* is an individual from the Balb/C control group *c* and *i* is an individual from the Fech$^{m1PAS}$ group *t*. This shows us that the difference ($F_a$) between the two fluorescence $\log_2$ intensities for slide *a* is

$$F_a = G_{t,i,a,r} - G_{c,j,a,g} = (I_{t,i} - I_{c,j}) + (D_r - D_g) + (\in_{t,i,a,r} - \in_{c,j,a,g}) \qquad \text{(eq.3)}$$

This shows that the quality of the individual spot does not matter as $A_a$ becomes cancelled out as the two equations are combined but it does show that the effect of dye bias remains ($D_r - D_g$) and demonstrates the requirement for reverse labelling.

Using this model Zhang and Gant have derived the *S* calculation to provide an assessment of the successful detection of DGE to assist in experimental design. Table 3.1 shows the application of this model to the experimental design of the Fech$^{m1PAS}$ time course.

**Table 3.1**

| Number of Individuals per Group | $n_f$ | $n_r$ | $P_{th}$ | $\|\mu\|/\sigma_T$ | S-Value |
|---|---|---|---|---|---|
| **2** | 2 | 2 | 0.05 | 2 | **0.564515** |
| **3** | 3 | 3 | 0.05 | 2 | **0.947938** |
| **4** | 4 | 4 | 0.05 | 2 | **0.996157** |
| **5** | 5 | 5 | 0.05 | 2 | **0.999766** |
| **6** | 6 | 6 | 0.05 | 2 | **0.999987** |

Table 3.1) **S-Value Results for Experimental Design**. The table shows the S-value depicting the percentage of DGE's that will be successfully identified for a different number of individuals (column 1) per genotype per timepoint in the Fech$^{m1PAS}$ time course. $|\mu|/\sigma_T$ was set to 2 as expected differential DGE changes were in the region of 4-fold.

The calculation shows that if 3 individuals are chosen for the control and Fech$^{m1PAS}$ groups at each time point 95% of all DGE will be identified with a certainty of p=0.05. The S value for 4 individuals shows a higher success rate and appears preferable, however the model used for the S calculation assumes that each gene is only

represented once on the array; this is not the case as the majority of genes are duplicated on the array indicating that value of S value should be considered slightly higher.

Using the results in table 3.1 the number of subjects per genotype at each time point was set to 3 as this provided a suitable success rate with S≈94% as the gain of using 4 subjects did not sufficiently justify the extra animals required.

The application of microarrays deviates from a classical experiment whereby a single hypothesis is tested against a single statistic. In a single hypothesis style experiment, the formation of false positives and negatives must be controlled. One of the key benefits of microarray technology is that multiple hypotheses may be tested simultaneously. In this multiple hypothesis environment, the false positives and negatives must be controlled for each individual hypothesis, in this case for each gene represented on the array. Benjamini and Hochberg(Benjamini and Hochberg 1995) introduced a measure for testing the error in multiple hypothesis experiments which they called the False Discovery Rate (FDR)63. Although the statistical power calculation above predicts a successful detection rate of ≈94%, the actual value will be less owing to the FDR. However, after consideration of the FDR the difference successful detection rates between n=3 and n=4 was not sufficient to justify the extra animals required for n=4 in the $Fech^{m1PAS}$ time course.

As ferrochelatase inhibition in EPP is an autosomally recessive inherited trait a medelian ratio was expected in the litters. However, any *in utero* mortality would cause the mendelian ratio to deviate from the theoretical. To ascertain whether this was happening, the breeding data was analysed for deviation from the mendelian ratio as an addition to the overall experimental strategy. In a standard, autosomal single allele 2$^{nd}$ generation back cross the progeny are expected to show a 1:2:1 ratio of wild type to heterozygote to homozygote.

However, there was no efficient method to assess the genotype of the litters. Previous papers had used hybridisation of oligonucleotides to PCR generated products over the SNP mutation (Boulechfar, Lamoril et al. 1993; Abitbol, Bernex et al. 2005). This though is a cumbersome method and so the generation of a restriction fragment length polymorphism (RFLP) at the site of the T/A transversion was used on PCR products to determine the genotypes. This method was essentially similar to that previously used in the laboratory (personal communication with T.W Gant, Leicester) but did not rely on the amplification of cDNA as had been utilised previously. The generation of cDNA had been used by Gant because the genomic sequence at that time was not available and as tissues were being genotyped at post-mortem and there was no restriction on the amount of RNA, PCR from the cDNA was appropriate. Here though the genotyping method had to retrieve the biological sample in the least invasive manner such that animals could be assigned to groups that were then allowed to live for up to a further 8 months. Two routes for obtaining tissue were used; stools and ear punch tissue removed for animal identification. The use of stool samples for

genotyping has been shown effective by Broome *et al.*(Broome, Feng et al. 1999) and many others in both the laboratory and field settings; the DNA obtained from the stool is due to the sloughing of intestinal epithelial cells however there are concerns about contamination of the PCR template resulting from nucleic acids in the food source.

Due to a lack of ferrochelatase transcription in the ear, use of mRNA as a PCR template was not applicable and therefore genomic DNA had to be used. The completion of the mouse genome sequencing project (Waterston, Lindblad-Toh et al. 2002) allowed the discernment of the intron/exon structure of the ferrochelatase gene. Examination of this revealed that the original primers designed for genotyping the $Fech^{m1PAS}$ mouse spanned a large intron and could not be used with a gDNA template as the product size was beyond the limits of standard PCR. Therefore new primers were designed. The RFLP as previously described was then used on this genomic DNA fragment obtained to determine the genotype of the mice.

In order to accurately sex the mice primers against the Testis Specific Y Pseudogene on the Y chromosome were designed which then specifically amplified from the male but not female mice.

The aim of this chapter is to show the results of the new genotyping method, to show that non-invasive routes of obtaining samples for genotyping is a viable approach and to analyse the distribution of genotypes in the Fech time course to identify any deviation from patterns of Mendelian inheritance.

## 3.2 Results

### *3.2.1 Comparison of PCR product from Ear Punch Tissue and Stools*

Genomic DNA was extracted from ear punch tissue and freshly obtained stools. The cleaned DNA was used as a template for PCR of the ferrochelatase gene including the RFLP and for TSpy another gene chosen as a control. Figure 3.1 shows 10µl of each 50µl PCR reaction run out on a 1% agarose gel; Although TSpy amplified consistently between the Ear punch and Stool based templates the Fech PCR was more efficient using the ear punch based gDNA.

**Figure 3.1**

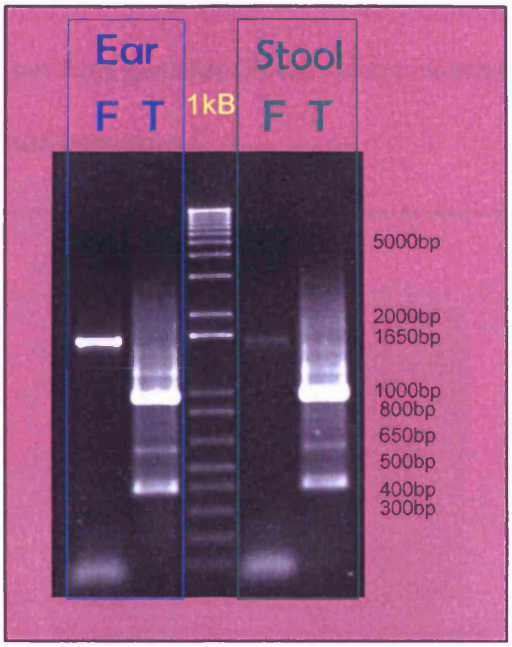


Figure 3.1 **Figure showing the Fech PCR and a Control PCR using a Genomic DNA obtained from Ear Tissue and Stools.** A 1% agarose gel with each lane containing 10µl of a 50µl PCR reaction. From the left, lane 1 is the Fech PCR (F) and lane 2 the TSpy (T) PCR using a gDNA template obtained from ear tissue, lane 3 contains 1kB DNA marker (Invitrogen), lanes 4 and 5 contain the Fech (F) PCR and the TSpy (T) PCR respectively using a template obtained from stools.

### *3.2.2 Genotyping the Fech$^{m1PAS}$ mouse using the BspH1 RFLP*

PCR primers were designed and optimised such that the genotype of a F2 Fech mouse could be determined from 10ng genomic DNA obtained from either ear punch tissue or genomic DNA extracted from stools.

**Figure 3.2**


Figure 3.2 **Figure showing the genotyping of the Fech mouse m1PAS allele.** A section of a 1% agarose gel showing the product of the restriction digest with BspH1 to identify the RFLP associated with the Fech$^{m1PAS}$ allele. Lane identification for the 3 genotypes are shown in blue. The genotypes shown in lanes 1,2 &3 are wild type, heterozygote and homozygous m1PAS respectively. The 1kB DNA marker has been superimposed onto the image from another part of the gel maintaining its scale.

Figure 3.2 gives an example of the restriction digest of the PCR product demonstrating all three genotypes in the three marked lanes. Lane 1 shows the wild type restriction

digest with *BspH1* which gave rise to two fragments of ≈900bp and ≈500bp of which the sum of their sizes is consistent with the Fech PCR product. Lane 2 shows the heterozygote digest; the two fragments seen in the wild type are present but to a lesser extent and a third larger band shows the undigested PCR product corresponding to the $Fech^{m1PAS}$ allele. Lane 3 is from a mouse homozygous for the $Fech^{m1PAS}$ allele, as such it does not contain a restriction site for *BspH1* resulting in no cleavage and a single 1.4kb band.

One of the issues often seen in the RNA based genotyping was incomplete cleavage by the restriction enzyme leading to false calling of the genotype due to the similar appearance of the wild type and heterozygotes. This situation also arose in the genomic DNA based genotyping. To combat this, the pixel intensity of the gel photograph was plotted against the migration distance (in arbitrary units) of each band as in figure 3.3 allowing differentiation between the heterozygote and wildtype. This was carried out using TotalLab 1D gel software from Nonlinear Dynamics UK.

The homozygous $Fech^{m1PAS/m1PAS}$ mice produce a profile such as that shown in blue with a single peak as position 100. The heterozygote and wildtype show three peaks at 100, 120 and 150. The heterozygote is distinguished from the wild type by a greater peak at position 100 and lesser peaks at 120 and 150.

**Figure 3.3**

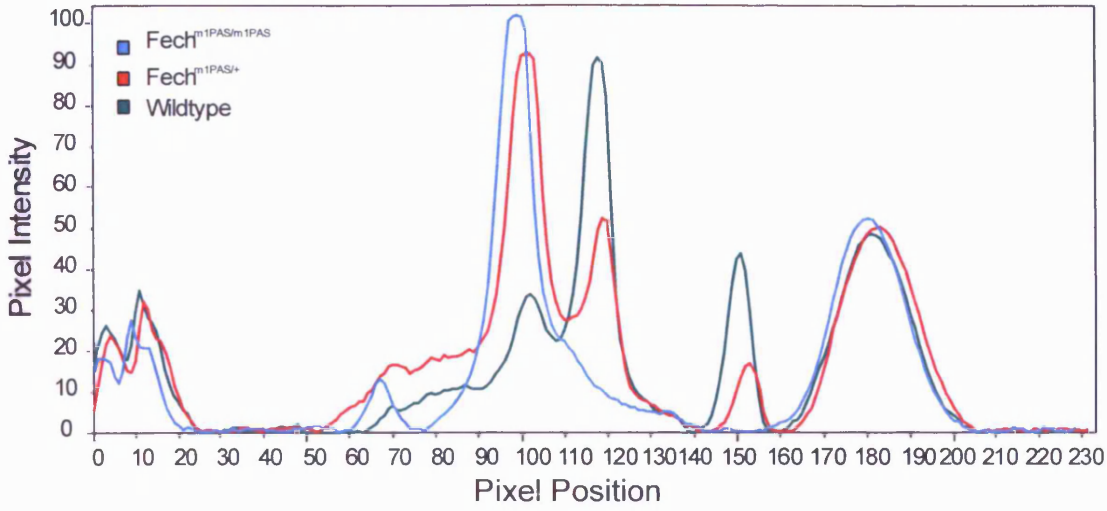


Figure 3.3) **Differentiation between Wild Type and Heterozygous Fech$^{m1PAS}$ by Pixel Density Plot.** The peak at 10 corresponds to the well of the gel The peak at 100 shows the complete PCR product as a result of either incomplete digestion by *BspH1* or in the case of the homozygote a lack of digestion owing to the presence of the RFLP. The peaks at 120 and 150 represent the product of the digest and the peaks at 180 are the primers from the PCR.

### *3.2.3 Analysis of the Distribution of Genotypes in the Fech$^{m1PAS}$ F2 Backcross*

In order to assess the conformation of the breeding of the Fech$^{m1PAS}$ F2 backcross to the expected 1:2:1 ratio Chi squared test was carried out on the raw genotyping data.

The result of this analysis (table 3.1) showed that the distribution of genotypes in the Fech$^{m1PAS}$ F2 backcross matched the mendelian 1:2:1 ratio expected for a backcross between two heterozygotes with $p<0.05$ where p is the probability of a false positive.

**Table 3.1**

$$\text{Using } X^2 = \sum \frac{(observed - expected)^2}{(expected)}$$

| | +/+ | +/- | -/- | Total |
|---|---|---|---|---|
| Observed | 98 | 144 | 89 | 331 |
| Expected | 82.75 | 165.5 | 82.75 | 331 |

| | |
|---|---|
| Degrees of Freedom=2 | |
| | $X^2$= 6.075528701 |
| | p= 0.047942 |

| | |
|---|---|
| **Null Hypothesis:** | **The progeny of the F2 Cross does not meet the mendelian ratio of 1:2:1** |
| **Result:** | **The null hypothesis is disproven, showing that breeding is statistically similar to the mendelian ratio.** |

Table 3.1 **Table showing the Chi Squared analysis of the Fech$^{m1PAS}$ F2 Back cross Genotyping.** All genotyping data was pooled from the genotyping gels taking care to avoid duplications. This produced the observed results shown in the blue table with +/+, +/- and -/- denoting wild type, heterozygote and Fech$^{m1PAS/m1PAS}$ respectively. From the total the expected values were calculated. The red box shows the $\chi^2$ result and its associated p-value using 2 degrees of freedom. A low value of $\chi^2$ is an indicator of independence; the value of 6.08 is high denoting close dependence towards the expected results and as $p<0.05$ we can disprove the null hypothesis.

## 3.3 Discussion

The requirement of a robust method to genotype the Fech mouse was paramount to the successful outcome of the genomic assessment. The previous method which relied on the amplification of cDNA was inapplicable because the Fech gene is not expressed in the tissue available for the genotyping, and ear punch biopsy. Therefore another approach was required. The approach used was to utilise the same RLFP previously described but on a piece of genomic DNA. This is a simpler approach that had previously not been possible because the genomic sequence of the Fech gene was not known. However the completion of the mouse genome sequencing project derived this information and allowed the approach to be used on this occasion.

The use of the RLFP approach has advantages over the hybridisation approach of wild type and mutant oligos previously utilised by Boulchefar *et al. (Boulechfar, Lamoril et al. 1993)*in terms of being both simpler and more quantitative.

The new method once optimised allowed rapid genotyping of the progeny in a non invasive manner and the PCR was successful in 98% of all reactions. With the 2% that failed, a combination of repeating the PCR from the original template or reproducing the template from freshly collected stools allowed gaps in the genotyping to be filled.

Concerns that the use of stools as a template for genotyping may contain contamination from food sources proved unfounded as the specificity of the genotyping primers was sufficient to produce a clearly defined PCR product of the correct 1.4kb size.

The problem of incomplete cleavage by *BspH1* was solved through the graphical representation of the gel bands. This method allowed a rapid calling of the digest products that were unclear to visual inspection of the gel as well as a useful tool to validate those genotypes that were called directly from the gel. With the combination of visual inspection of the genotyping gels and computer based image analysis mice were assigned to genotype groups for each time point in the time course.

One of the key areas of interest forming this thesis was the progression of the disease state, in particular, the question of how the mutation affects younger animals is unanswered; chapter 6 will show the gene expression changes observed *in utero* in the $Fech^{m1PAS/m1PAS}$ mouse. To show whether the m1PAS allele has an effect on the viability of the progeny, the genotyping data was subjected to analysis by the Chi Squared test. This considers the Mendelian principles of inheritance and compares the observed genotype ratios against those expected.

Figure 3.4 shows the cross between two $Fech^{m1PAS}$ heterozygotes and demonstrates the 1:2:1 ratio expected. The main reason for deviations from this ratio are the presence of *in utero* lethalities caused by the presence of the $Fech^{m1PAS}$ allele. Section 3.2.3 demonstrated that there was no statistically relevant deviation from the expected ratio; this shows that the influence of the $Fech^{m1PAS}$ allele is not detrimental *in utero* and that the negative effects propagate after birth at later time points.

**Figure 3.4**

Let $F^{+}$ equal the Fech wild type allele
$F^{m1PAS}$ equal the $Fech^{m1PAS}$ allele

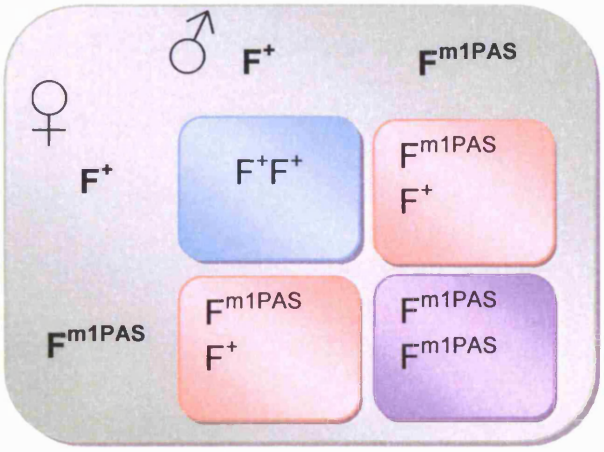


Figure 3.4) **Figure Demonstrating the Expected 1:2:1 Ratio of Genotypes in Animals Bred in the $Fech^{m1PAS}$ Time Course.** The diagram shows a cross between two mice heterozygous for the $Fech^{m1PAS}$ allele; the female gametes are shown on the left with the male gametes across the top. The progeny genotype are shown in the centre in the form of a Punett Square, clearly showing a 1:2:1 ratio of genotypes.

# Chapter 4) Blood Chemistry and Histopathology- Establishing the Phenotype.

## 4.1 Introduction

The reduced ferrochelatase activity of the $Fech^{m1PAS}$ mutant decreases the incorporation of reduced iron into the protoporphyrin IX ring as described in section 1.2.1. The hydrophobic protoporphyrin that remains accumulates within the hepatocytes and bile canaliculi occluding the bile duct at later time points and unbalancing the normal function of the liver(Meerman, Koopen et al. 1999). Accumulated bile is toxic and damages the liver. In addition, bilirubin levels in the blood increase leading to jaundice.

The main objective of this chapter was to establish the phenotype of the $Fech^{m1PAS}$ mice throughout the time course and their progression towards the disease state. In order to achieve the objective several analytical approaches were used. First accumulation of the protoporphyrin was measured; second, the biochemical changes indicative of the integrity of the liver and third, the histopathological changes.

The protoporphyrin was assayed by two methods. First, a modified version of the method described by Grandchamp(Grandchamp, Deybach et al. 1980) was used and second HPLC separation using a methanol gradient. The HPLC method allowed a resolution as to the relative concentrations of the three porphyrin types. The HPLC method allowed a secondary objective of this chapter to be addressed; to determine that the porphyrin accumulation observed in the liver is solely due to protoporphyrin IX.

Alanine aminotransferase (ALT) assays were used to quantify the level of damage to the liver. Alanine aminotransferase is a cytosolic enzyme found in high concentrations in the liver where it catalyses the transfer of α-amino groups from alanine to α-ketoglutaric acid(Kaplan 2002). On liver injury, the ALT is released into the blood where it can be detected in the plasma.

Bilirubin is a metabolite of haem. Haem is degraded by haem oxygenase to produce reduced iron, carbon monoxide and bilirubin (via a biliverdin intermediate)(Section 1.3.2). The cyclic tetrapyrrole haem is oxidised by haem oxygenase using the iron in the haem as its cofactor resulting in an open chain of the four pyrroles. Due to the haem oxygenase requirement for the iron cofactor, bilirubin cannot be formed from the accumulated protoporphyrin. Bilirubin is conjugated with glucuronic acid before removal to the bile canaliculi. In the $Fech^{m1PAS}$ mouse, disruption of normal bile duct function prevents removal of Bilirubin leading to its accumulation in the blood plasma and jaundice. Therefore by assaying the time point at which bilirubin levels increase we can obtain an indication of when liver function becomes impaired.

The pathological changes in the $Fech^{m1PAS}$ mouse have been characterised at the later stages of the associated EPP(Libbrecht, Meerman et al. 2003) but not in the earlier stages of the disease where the animals are asymptomatic. At post-mortem, sections were taken from the livers of all animals in the time course. The haemotoxylin and eosin stained slides were assessed for pathological changes with the aid of Dr Peter Greaves (University of Leicester).

The analysis of pathological and biochemical changes presented in this chapter aimed to establish the phenotypic progression of EPP.

## 4.2 ALT Results

Alanine aminotransferase assays were carried out on blood plasma obtained from mice varying in age from 2 to 32 weeks with a sample size where n≥3 for each genotype at each time point.

Figure 4.1 shows a graphical representation of the increased ALT levels over the time course for wild type mice and mice heterozygous and homozygous for the $Fech^{m1PAS}$ allele. To determine whether a result may be called elevated a normal range was established. The threshold value is defined as the mean activity observed in healthy animals ±2SD. This value was calculated using the pooled results for all wild type animals and defined the maximum healthy activity as 26units $L^{-1}$ ±61.

ALT activity was observed in the wild type mice and those heterozygous for the $Fech^{m1PAS}$ allele. In the heterozygous mouse ALT levels were below the threshold value and therefore not significantly different from the wild type. All mice homozygous for the $Fech^{m1PAS}$ alleles showed an increase in ALT activity beyond the threshold value indicating that liver damage was present. Liver damage was observed from 2 weeks with ALT activity 13 times greater than the normal level. The ALT activity decreased slightly from 2 weeks through the time course until 6 months when the ALT activity had dropped to approximately 7 times above normal. After this point liver damage

increased to 12 times the normal level at the 32 week point coinciding with the presentation of the more acute symptoms associated with protoporphyria (Figure 4.1).

**Figure 4.1**

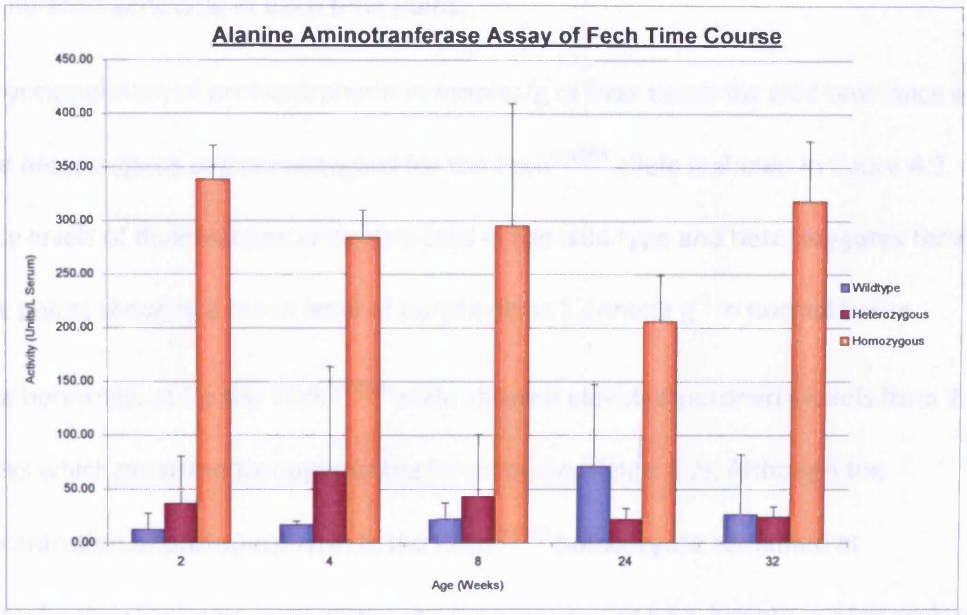


Figure 4.1) **Figure showing the level of alanine aminotransferase activity of the Fech$^{m1PAS}$ time mice over a 32 week time course.** The graph shows ALT activity levels for wild type male mice and mice heterozygous and homozygous for the Fech$^{m1PAS}$ allele. n≥3

## 4.3 Porphyrin Assay Results: Fluorimeter Method

Porphyrin assays were carried out on a selection of livers from the $Fech^{m1PAS}$ time course. Tissue was taken from mice ranging from 2 weeks to 32 weeks in age where $n \geq 3$ for each genotype at each time point.

The accumulation of protoporphyrin in nmoles/g of liver tissue for wild type mice and mice heterozygous and homozygous for the $Fech^{m1PAS}$ allele is shown in figure 4.2. Trace levels of fluorescence were detected in the wild type and heterozygotes for all time points showing a mean level of porphyrin at 1.4nmole $g^{-1}$ in normal tissue.

Mice homozygous for the $Fech^{m1PAS}$ allele showed elevated porphyrin levels from 2 weeks which persisted throughout the time course (figure 4.2). Although the concentration of protoporphyrin in the $Fech^{m1PAS}$ homozygote remained at approximately the same level across the time course the total hepatic protoporphyrin load increased over time to a peak at 24 weeks of age. This was shown using the data shown in figure 4.2 and the mean liver weight for mice of each genotype at each time point (figure 4.3).

**Figure 4.2**

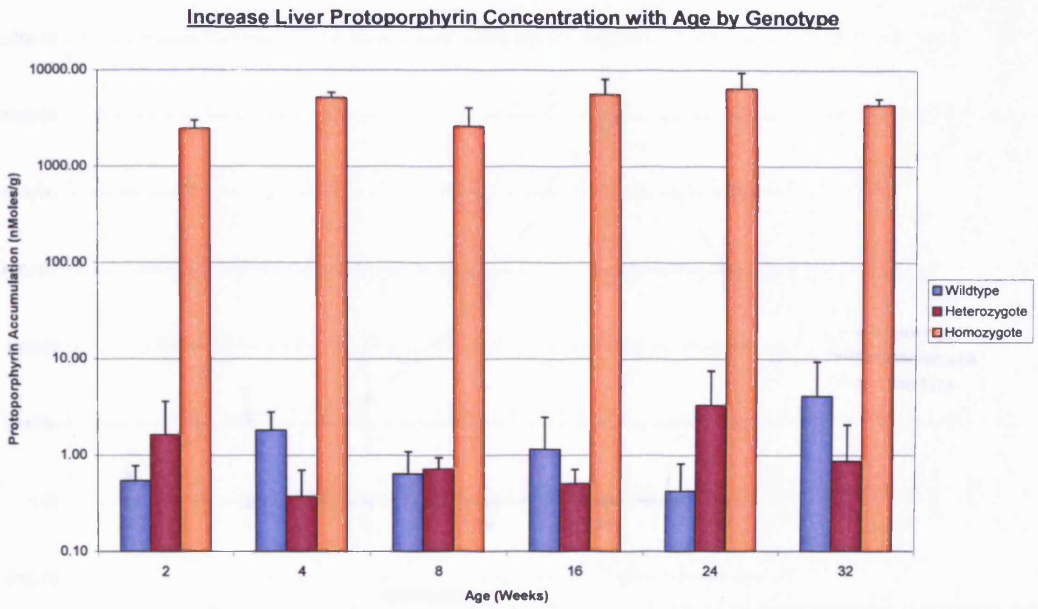


Figure 4.2) **Protoporphyrin levels in liver tissue from the Fech mouse time course as determined by the fluorescence.** The graph shows protoporphyrin levels for wild type mice and mice heterozygous and homozygous for the Fech$^{m1PAS}$ Allele. n ≥3

**Figure 4.3**

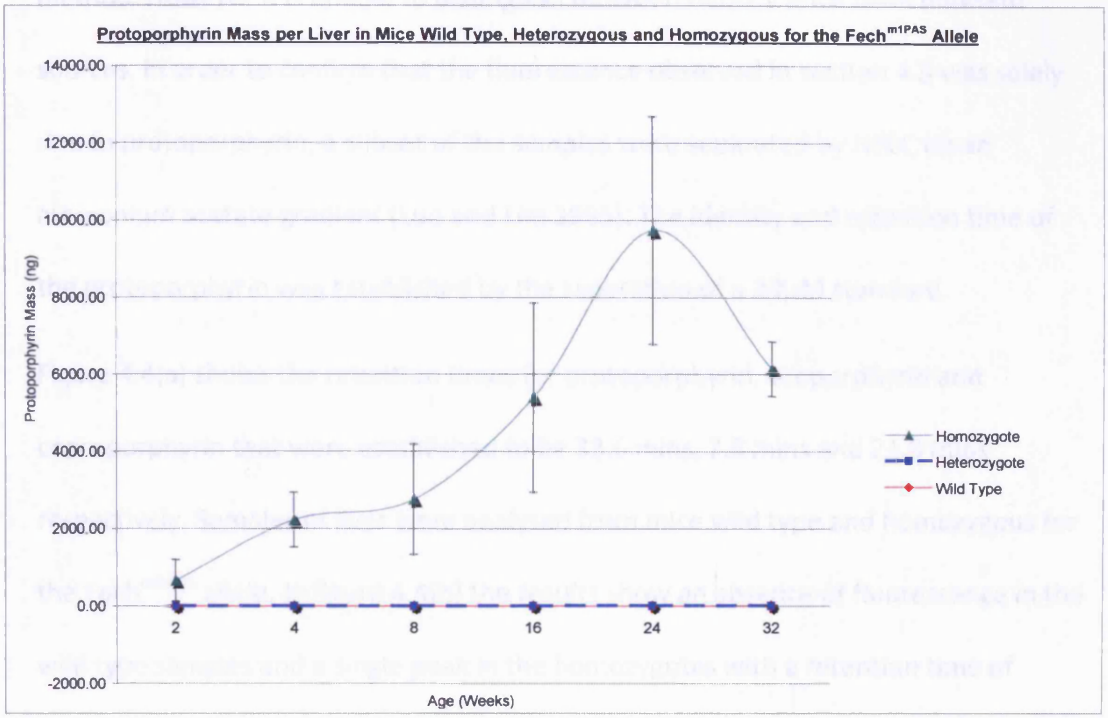


Figure 4.3) **Mass of Protoporphyrin per Liver .** This graph shows the total protoporphyrin load in the liver of wildtype mice and mice heterozygous and homozygous for the Fech$^{m1PAS}$ allele. n≥3.

Levels of uroporphyrin and coproporphyrin were also established. The results showed an absence of uroporphyrin and coproporphyrin in all genotypes at all time points.

## 4.4 Porphyrin Assay Results: HPLC Method

The Grandchamp method for quantitation of protoporphyrin is a quick and efficient method. However it is unable to distinguish between fluorescence from different sources. In order to confirm that the fluorescence observed in section 4.3 was solely due to protoporphyrin, a subset of the samples were separated by HPLC on an ammonium acetate gradient (Luo and Lim 1995). The identity and retention time of the protoporphyrin was established by the separation of a 20μM standard.

Figure 4.4(a) shows the retention times for protoporphyrin, uroporphyrin and coproporphyrin that were established to be 33.6 mins, 7.8 mins and 21.9 mins respectively. Samples of liver were analysed from mice wild type and homozygous for the $Fech^{m1PAS}$ allele. In figure 4.4(b) the results show an absence of fluorescence in the wild type samples and a single peak in the homozygotes with a retention time of ≈33.6mins identifying the fluorescent source as protoporphyrin.

**Figure 4.4**

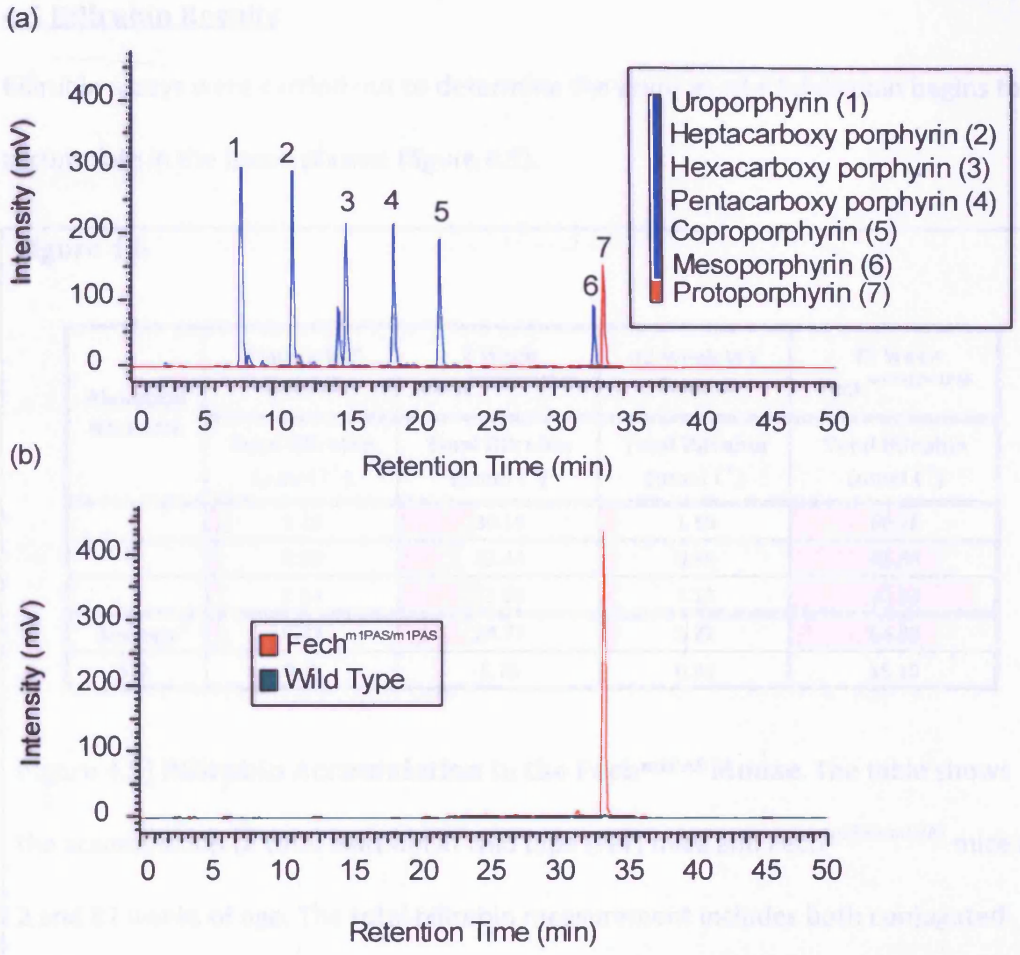


Figure 4.4) **Figure showing HPLC traces of liver homogenate identifying protoporphyrin as the source of fluorescence and its accumulation.**

Protoporphyrin is shown in orange. Figure 4.4a shows the separation of the porphyrin standards as defined in the legend on the right. Figure 4.4b shows the separation of the Fech$^{m1PAS/m1PAS}$ porphyrin sample vs. the wild type. Increases in detector voltage (y-axis) indicate increases in fluorescent intensity.

## 4.5 Bilirubin Results

Bilirubin assays were carried out to determine the point at which bilirubin begins to accumulate in the blood plasma (figure 4.5).

**Figure 4.5**

| Biological Replicate | 2 Week WT Control | 2 Week $Fech^{m1PAS/m1PAS}$ | 32 Week WT Control | 32 Week $Fech^{m1PAS/m1PAS}$ |
|---|---|---|---|---|
| | Total Bilrubin ($\mu mol\ l^{-1}$) | Total Bilrubin ($\mu mol\ l^{-1}$) | Total Bilrubin ($\mu mol\ l^{-1}$) | Total Bilrubin ($\mu mol\ l^{-1}$) |
| 1 | 1.20 | 30.19 | 1.55 | 50.75 |
| 2 | 0.93 | 22.44 | 0.98 | 63.38 |
| 3 | 0.54 | 33.69 | 1.13 | 80.83 |
| **Average** | **0.89** | **28.77** | **1.22** | **64.98** |
| **S.D.** | 0.33 | 5.76 | 0.30 | 15.10 |

Figure 4.5) **Bilirubin Accumulation in the $Fech^{m1PAS}$ Mouse.** The table shows the accumulation of total bilirubin in wild type (WT) mice and $Fech^{m1PAS/m1PAS}$ mice at 2 and 32 weeks of age. The total bilirubin measurement includes both conjugated and non-conjugated bilirubin.

Blood plasma total bilirubin levels were elevated in mice homozygous for the $Fech^{m1PAS}$ allele. Defining normal total bilirubin levels as the mean concentration in the wild type ±2S.D. would set the normal total bilirubin concentration at 1.54µmole $l^{-1}$ bilirubin was found to have accumulated in the $Fech^{m1PAS/m1PAS}$ mouse to a level of ≈30µmole $l^{-1}$ at just 2 weeks, a ≈65 fold increase over normal. Measurements at 1 week were not

possible due to a lack of blood plasma and attempts made to scale down the assay showed a large deviation between results implying that the data was not trustworthy.

## 4.6 Histopathology

Samples were taken from all genotypes across the whole timecourse.

Table 4.1 shows a summary of the observed pathology. From 1 to 4 weeks there were no histopathological changes obvious hepatic pathology exists showing the importance of an accurate genotyping method (chapter 3). The observed round cell aggregates are representative of extra-medullary haematopoiesis; this process is normal in young mice (personal communication from P. Greaves, University of Leicester). At 4 weeks pathology begins to form with visible accumulation of protoporphyrin, bile duct hyperplasia and inflammation of the portal tract. The inflammation continues to advance to a more severe chronic inflammation and fibrosis by 8 weeks of age.

At 16 weeks foci begin to form leading to adenoma by 24 weeks of age.

This data is supported by histology plates 1 to 3 (located at the end of this chapter) which show photomicrographs of the liver sections obtained in this experiment. The plates show the progression of the disease from inflammation through to adenoma. Plate 1A shows a section of normal wild type liver as a reference. Plate 1B shows white cell infiltration indicating inflammation in a 24 week $Fech^{m1PAS/m1PAS}$ liver, this inflammation starts at one week and persists throughout the timecourse. The initial

stage of inflammation is shown in plate 1C, showing a one week old homozygote with neutrophil and eosinophil inflammation around a portal vein with bile canaliculi to the top left of the vein. Although pigment is not evident at this point by 8 and 16 weeks of age protoporphyrin can be clearly seen in tissues and occluding the bile canaliculi (plate 2A and 2B). The bile canaliculi occluded by protoporphyrin also shows hyperplasia in the surrounding tissues as shown in plate 2B by the irregular shape of the bile canaliculi. Inflammation can also be seen with white cell infiltration in the surrounding tissue. By 24 weeks foci of cellular alteration can be seen as well as large fatty deposits indicating the hyperlipidaemia associated with EPP (plate 3A). By 32 weeks the foci of cellular alteration have developed into suspected adenoma (shown in plate 3B as a darkly stained cellular mass).

On a macroscopic level the Fech homozygotes livers were visibly increased in size. Figure 4.6 shows how the enlargement in liver mass of the $Fech^{m1PAS/m1PAS}$ mice increased relative to body mass. The data shows a steady increase in relative liver mass to a critical point at 24 weeks after which a decrease in relative liver mass was observed.

**Figure 4.6**

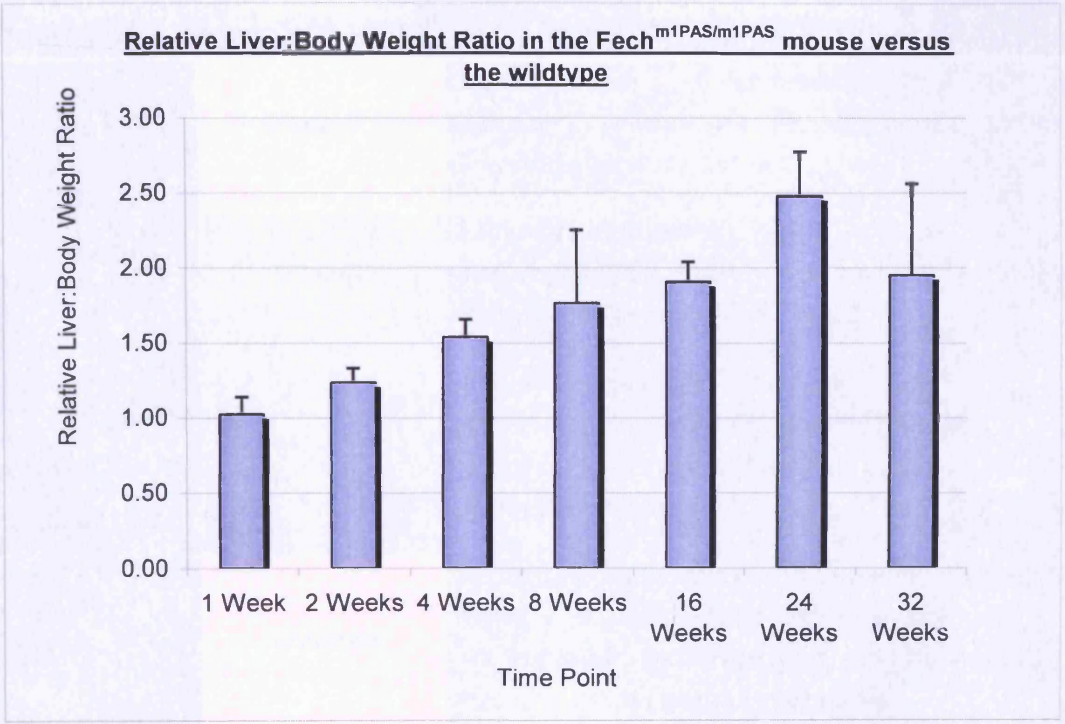


Figure 4.6) **Liver:Body Mass Ratio in Fech$^{m1PAS/m1PAS}$ mice Relative to Wild Type.** The graph shows the increase in Liver:Body mass ratio in the Fech$^{m1PAS/m1PAS}$ mice relative to the wild type over the time course. The mean liver:body weight ratio of controls was 0.2±0.15. n≥3.

**Table 4.1**

| Age (Weeks) | Severity Rating | Observed Pathology |
|---|---|---|
| 1 | Moderate | Moderate round cell aggregate, minimal neutrophil infiltrate in the hepatic portal tract. A few odd megakaryocytes. |
| 2 | Minimal | Minimal round cell aggregates, minimal neutrophil infiltration and minimal pigment in the hepatic portal tract. |
| 4 | Minimal | Minimal parenchymal and portal tract inflammation, moderate accumulation of pigment in the hepatic portal tract. Bile duct hyperplasia. |
| 8 | Moderate | Moderate portal tract chronic inflammation and fibrosis. Moderate chronic parenchymal inflammation. Moderate pigment in the hepatic portal tract and bile duct hyperplasia. |
| 16 | Moderate | Moderate pigment in hepatic portal ducts and hepatocytes, moderate periportal fibrosis and chronic inflammation. Bile duct epithelial hyperplasia. Minimal hepatocellular degeneration and anisocytosis. |
| 24 | Marked | Marked anisocytosis, minimal chronic portal tract inflammation. Foci of cellular alteration (eosinophillic), Mallory hyaline and adenoma |
| 32 | Marked | Hepatic anisocytosis, minimal chronic portal tract inflammation. Foci of cellular alteration, Mallory hyaline and adenoma |

Table 4.1) **Table showing the observed pathology in mice homozygous for the Fech$^{m1PAS}$ allele from 1 to 32 weeks of age.**

## 4.7 Discussion

The experiments within this chapter were designed to allow the phenotypic progression of EPP to be characterised. In addition to this the results above also give us insight into the underlying mechanisms of toxicity and tumour formation.

### *4.7.1 Liver damage is apparent from 2 weeks of age without the formation of pathological change.*

One of the aims of this chapter was to analyse the progression of the EPP in the $Fech^{m1PAS}$ mouse from birth. The results showed an increase in ALT activity from 2 weeks of age (figure 4.1), this is supportive of liver damage associated with the increased porphyrin levels (figure 4.2). This evidence shows that even from the earliest time point the $Fech^{m1PAS}$ homozygote liver is undergoing toxic insult from the protoporphyrin despite there being no overt pathological change. These data alignswith observations made by Gant *et al. (Gant, Baus et al. 2003)* of increased ALT and porphyrin levels in a chemically induced model of EPP. Gant *et al.* chronically exposed mice to the anti-fungal agent griseofulvin (a strong inhibitor of fech activity (Knasmuller 1997)) over a period of 22 days to produce a hepatic porphyria characterised by accumulation of protoporphyrin IX and the pathological changes found in human EPP. In line with the results shown in section 4.2 and 4.3 they observed increased ALT levels in the liver which coincided with the accumulation of protoporphyrin and of histopathological damage including adenoma.

### *4.7.2 Porphyrin accumulation in EPP is solely protoporphyrin.*

One important aspect of the biochemistry in establishing the phenotypic progression of the $Fech^{m1PAS}$ mouse was to assay the accumulation of protoporphyrin over time. The fluorimeter method employed in this study allowed quantitation of porphyrin levels but not necessarily of the different porphyrins that arise in haem biosynthesis. By using a HPLC separation (section 4.4), it was possible to show that the porphyrin measured in the Grandchamp method was solely protoporphyrin.

The lack of uroporphyrin and coproporphyrin showed that there was no decoupling of haem biosynthesis prior to the terminal step of haem synthesis catalysed by ferrochelatase. If uroporphyrin were present it would suggest a loss of uroporphyrinogen III cosynthase activity resulting in an increase of anaemia and hemolysis through photooxidation as observed in congenital erythropoietic porphyria (Gunthers Disease)(Dsnick and Astrin 2002; Kauppinen 2004). Similarly, an accumulation of coproporphyrin would be associated with neurological dysfunction but more apparent, strong photo-cutaneous legions as seen in hereditary coproporphyria(Milgrom 1997). Although dual porphyrias are possible and have been documented(Poblete-Gutierrez, Badeloe et al. 2006), the porphyrin results in section 4.3 and 4.4 are supported by the lack of these extra phenotypes and by the pure bred background of the mice used in the time course. This has an important bearing on the site of early toxicity as protoporphyrin is produced in the mitochondria (section 1.3.1) it follows that the early stages of disease may be linked to a disruption in mitochondrial function due to the reactive nature of the porphyrins (section 4.7.6).

### *4.7.3 Liver damage and the corresponding porphyrin accumulation supports a critical value of ferrochelatase activity.*

Neither liver damage or significant porphyrin accumulation was detected in mice heterozygous for the $Fech^{m1PAS}$ allele. The trace levels of protoporphyrin detected (figure 4.2) can be accounted for due to the fact that the livers were not perfused at the time of dissection, allowing some iron leakage causing a low, but detectable, basal fluorescence in both the heterozygote and wild type. The porphyrin levels and other phenotypes observed in the $Fech^{m1PAS}$ homozygote and heterozygote were significantly different. The heterozygote remained totally asymptomatic despite a reduced ferrochelatase activity of 45-65%(Tutois, Montagutelli et al. 1991). Whilst the $Fech^{m1PAS}$ homozygote's level of Fech activity is <7% of normal (section 1.2.1) which corresponds to the activity levels that are observed in patients with advanced EPP. This data reinforces the use of the $Fech^{m1PAS}$ mouse as a model of severe human EPP as well as giving insight into the mechanism of penetrance.

The porphyrin accumulation and Fech activity levels seen in the $Fech^{m1PAS}$ heterozygous and homozygous mice mirror those observed in human patients with variable penetrance(Bloomer, Wang et al. 2006). In most symptomatic cases of human EPP the residual level of Fech activity is ≤30% relative to normal. Another mouse model of EPP has been reported which demonstrates phenotypes at two other points of the fech activity spectrum. A Fech ($Fech^{\Delta 10}$) deletion was generated using a gene targeting approach(Magness and Brenner 1999). This deletion resulted in formation of

a null mutant as shown *in vitro* by Fech activity of 50% relative to wildtype. *In vivo* the exon 10 deletion was shown to be homozygous embryonic lethal demonstrating the absolute requirement for basal Fech activity; the heterozygote did not remain at 50% activity but decreased to 37% of normal activity(Magness, Maeda et al. 2002). This was consistent with the mutant allele having a dominant-negative effect on the wild type allele as observed in human EPP with the *IVS3-48C* allele(Gouya, Puy et al. 2004) leading to a reduction in Fech activity to 34% and presenting with mild porphyria. At 37% of normal Fech activity, the $Fech^{\Delta 10}$ heterozygote displayed symptoms of mild EPP; they exhibited mild protoporphyrin accumulation to a 9 fold higher level than normal and necrotic photosensitivity. The photosensitivity could not be established in the $Fech^{m1PAS}$ mice owing to Home Office regulations however the protoporphyrin levels of the $Fech^{\Delta 10}$ mice although elevated are a lot lower than in the case of the $Fech^{m1PAS/m1PAS}$ mouse thus fitting the $Fech^{\Delta 10}$ mouse as a model of low penetrance mild EPP and the $Fech^{m1PAS/m1PAS}$ mouse as a model of high penetrance severe EPP.

### *4.7.4 Cholestatic liver disease in EPP is primarily intrahepatic progressing to extrahepatic at later stages.*

One of the key aims of this thesis was to elucidate the order in which liver disease propagates as a result of a reduction in ferrochelatase activity. The principle phenotype associated with the disease is that of cholestatic injury but the mechanism by which it arises is normally attributed to the accumulation of protoporphyrin(Meerman, Koopen et al. 1999; Libbrecht, Meerman et al. 2003;

Bloomer, Wang et al. 2006). There are two possible forms of cholestatic liver disease associated with EPP; extrahepatic cholestasis arises when accumulation of the highly hydrophobic protoporphyrin occludes the bile duct, preventing normal flow of bile, leading to a cytotoxic build up of bile such as in the griseofulvin model. Intrahepatic cholestasis results in the same cytotoxicity but is the result of aberrations in the cellular mechanisms of bile transport within the hepatocyte.

The data shown in this chapter provides evidence that the cholestatic liver disease in the early stages of EPP is attributable to intrahepatic cholestasis not extrahepatic. As discussed above there are biochemical indications of liver damage of liver damage prior to protoporphyrin occlusion of the bile ducts. The results showed blood plasma bilirubin levels to be elevated to 65 fold that of normal from 2 weeks of age (section 4.5) despite there being no visible occlusion of bile canaliculi at this point (section 4.6). This data in union with the elevated ALT and cellular protoporphyrin concentration support the hypothesis that in the early stages of EPP the cholestatic liver disease is intrahepatic as a result of aberrations in the regulation and activity of bile acid and ABC gene transporters within the hepatocytes and also the effect of cellular protoporphyrin on the osmotic balance of the cell. Progressive familial intrahepatic cholestasis (PFIC) demonstrates the transporters that may be affected; There are three types of PFIC, each associated with a different transporter. PFIC type 1 arises from defective activity of ATP8B1, PFIC type 2 from ABCB11 inhibition and PFIC type 3 from ABCB4(Jansen and Sturm 2003).

This data compliments the findings of Meerman *et al.* who reported a 2 fold increase in bile salt concentration and the findings in this thesis showing an upregulation of ABCB11 transcription (discussed further in chapter 5).

### *4.7.5 Pathological Symptoms in the Fech$^{m1PAS}$ homozygotes are a function of total porphyrin load.*

Protoporphyrin accumulation is the major visible phenotype associated with EPP and was detectable in the Fech$^{m1PAS/m1PAS}$ mouse from 2 weeks of age and clearly visible in liver sections from 4 weeks. However, the pathological changes are gradual over a period of 24 weeks until adenoma is seen, despite ALT increases depicting liver damage and the porphyrin assays showing a variable but consistently high concentration of protoporphyrin. The total load of protoporphyrin within the liver increases (section 4.3) as a function of the size of the liver but the concentration does not vary dramatically over the time course. This suggests that the porphyrin level has a cumulative effect on the pathological changes rather than one directly linked to concentration of protoporphyrin. At 24 weeks the total liver protoporphyrin load is 10 times higher than at 2 weeks and it is at this threshold that we see the presentation of the severe liver disease.

### *4.7.6 Modified bile flow may lead to mitochondrial-mediated toxicity at 32 weeks.*

Section 4.7.5 suggested a critical exposure limit to protoporphyrin mediated toxicity in the liver. The maintenance of protoporphyrin concentration across the time course shows that there is a maximum load of protoporphyrin per mass of liver. Protoporphyrin is excreted in faeces, however the rate of porphyrin excretion is only sufficient to maintain the concentration but not clear the accumulation(Meerman, Koopen et al. 1999). At 32 weeks the hepatic load of protoporphyrin decreases (section 4.3), the ALT level increases (section 4.2) coupled with the presentation of the severe pathological changes (section 4.6), high plasma bilirubin levels (section 4.5) and high bile salt concentrations previously observed. This sudden shift in the phenotypes shows a critical point in the cytotoxicity in EPP progression and suggests a breakdown in mitochondrial function within the hepatocytes.

Mitochondrial-mediated cytotoxicity is likely for several reasons. Firstly, the toxic protoporphyrin is synthesized within the mitochondria and is not being cleared sufficiently as shown by the high porphyrin levels within the liver. Secondly, high bile acid concentrations have been shown to mediate mitochondrial toxicity in cholestatic liver disease(Palmeira and Rolo 2004) by the uncoupling of the mitochondrial respiratory chain (MRC). Increased bile acid concentrations have been shown to initiate mitochondrial permeability transition (MPT)(Rolo, Oliveira et al. 2000) and cause efflux of cytochrome *c*. This could be exacerbated by the elevated concentration

of the hydrophobic protoporphyrin. This indicates that the cytotoxicity is due to a series of defined events rather than just an osmotic imbalance.

The cytochrome *c* release then has a further effect of causing ROS generation through electron leakage from the ubiquinone-complex III. This could cause a multi-faceted attack on the liver inducing the most severe phenotypes as ROS generation may be from the protoporphyrin accumulated and the electron leakage of ubiquinone-complex III. The sustained generation of ROS would then deplete GSH levels which cannot be replenished due to the breakdown of cellular respiration.

## Plate 1) Fech Timecourse Pathology

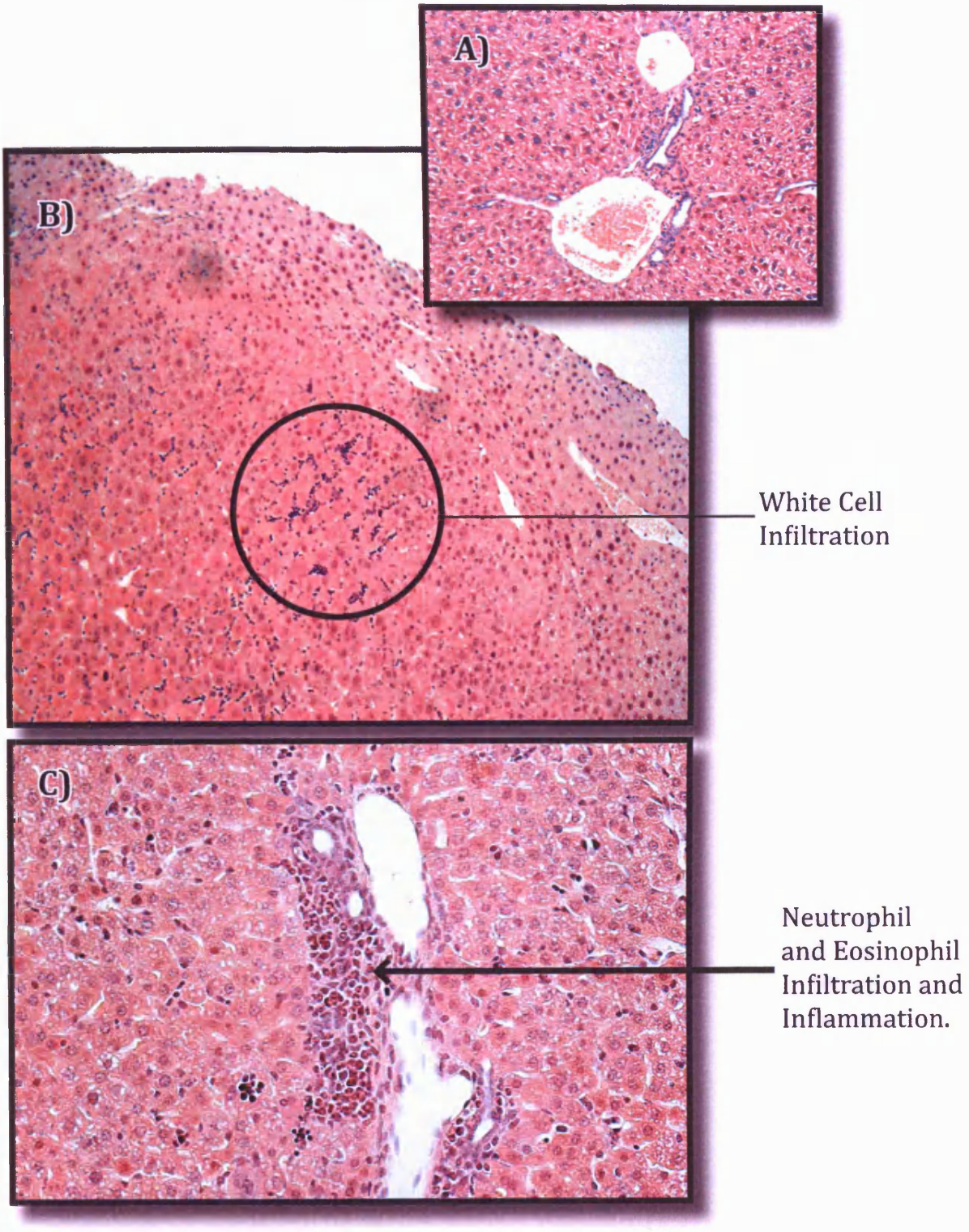


Plate 1. A) Normal Wild Type Liver

B) $Fech^{m1PAS/m1PAS}$ Liver showing White Cell Infiltration.

C) $Fech^{m1PAS/m1PAS}$ Liver showing neutrophil and eosinophil infiltration and inflammation.

## Plate 2) Fech Timecourse Pathology Part 2

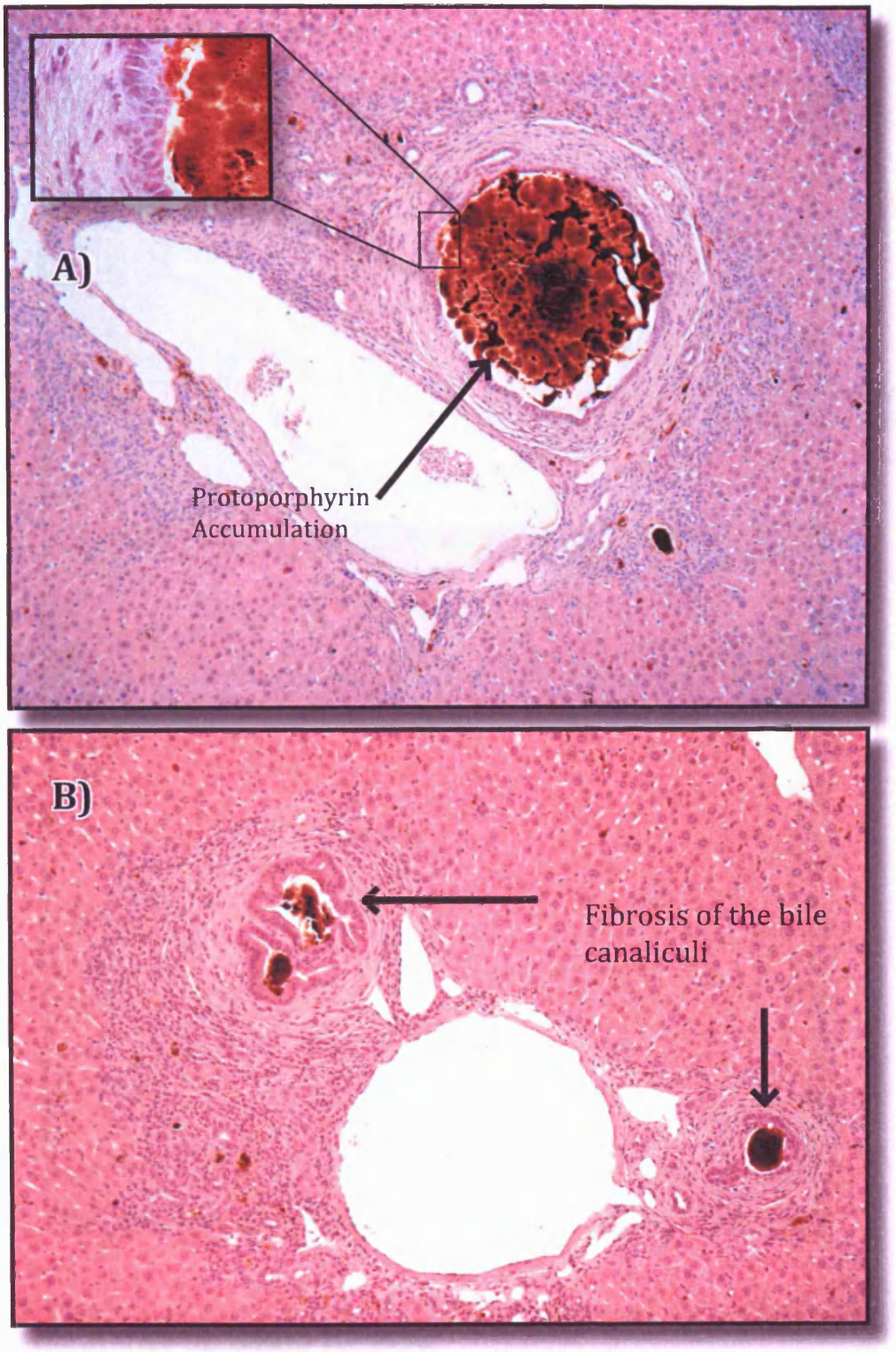


Plate 2. A) Protoporphyrin accumulation in the bile canaliculi of a $Fech^{m1PAS/m1PAS}$ mouse liver.

B) Fibrosis of the bile canaliculi in a $Fech^{m1PAS/m1PAS}$ mouse liver.

## Plate 3) Fech Timecourse Pathology Part 3

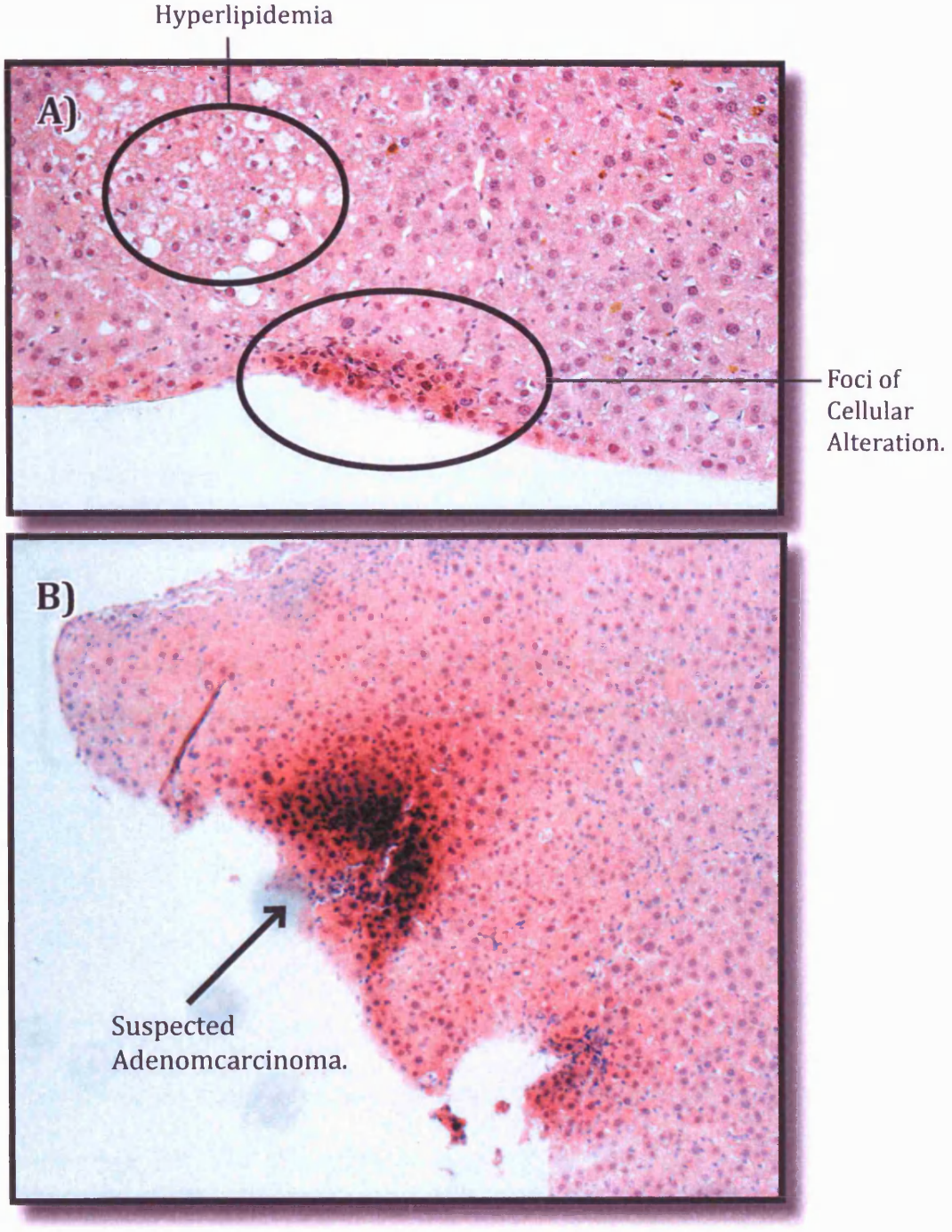


Plate 3. A) Liver from a $Fech^{m1PAS/m1PAS}$ mouse showing hyperlipidemia and a foci of cellular alteration.

B) Liver from a $Fech^{m1PAS/m1PAS}$ mouse with suspected adenomcarcinoma.

# Chapter 5) Differential Gene Expression in the Fech$^{m1PAS/m1PAS}$ Mouse

## 5.1 Introduction

In the previous chapter the phenotypic progression of disease in the $Fech^{m1PAS}$ mouse was established. In humans genetic disease phenotypes are complex and subject to environmental influences in addition to genetic. The advantage of using a model such as the $Fech^{m1PAS}$ mouse is that the environmental component which may influence the disease outcome can be controlled. When the environmental factors are controlled then markers of the disease can be better correlated and with less variability. In this chapter the genomic response to loss of ferrochelatase activity was assessed in a carefully selected set of approximately 15,000 genes that were selected for their relevance to biochemistry and toxicology. The environmental factors were controlled and the mice were inbred with the gene combinations being derived from a mating of the heterozygotes to control for variation in the genetic background.

In the context of the $Fech^{m1PAS}$ mouse the accumulation of protoporphyrin IX contributes the major pathological change. However the effects of the protoporphyrin accumulation are multi-faceted (section 4.7).

Using microarray technology this chapter aims to associate those phenotypic changes observed in the progression of the disease state with gene expression changes. The intention behind this is to gain an insight into the different mechanisms and communication networks affected by the inhibition of ferrochelatase activity.

The quantity of data generated in genomic experiments presents challenges in the interpretation of results which becomes an exercise in the meaningful filtering to extract data to reflect the phenotypic changes observed. Here the application of known gene function and relationships derived from GO terms (section 1.6.5) with the phenotypic results presented in chapter 4 , has allowed gene expression data to be presented in the form of functional groups. The application of cluster analysis to the gene expression data also identifies genes with shared expression profiles over the time course. These data can be insightful in the linking of the differential gene expression within the functional groups to common regulatory mechanisms.

Additional value is gained from experiments such as this by profile mapping across different disease models where patterns of gene expression can dissociate differences and similarities in the disease processes. Such data is now becoming much more readily available through the auspices of databases such as ArrayExpress and GEO. Though not always in a format which makes it easy to analyse, the availability of such data provides a resource for cross comparing of data with the aim of deriving substantial added values from ones own datasets. In this chapter and chapter 6 the gene expression data from the $Fech^{m1PAS}$ time course will be presented and then compared to differential gene expression in the griseofulvin model of EPP (discussed in chapter 4).

## 5.2 Results

The genomic evaluation of the $Fech^{m1PAS/m1PAS}$ timecourse against the wildtype from 4 to 32 weeks of age showed that of the approximately 10500 genes detected on the microarrays, an average of 1670 genes showed differential gene expression to a significant level ($p \leq 0.05$) per time point. Of the detected DGE an average of 980 were upregulations and 690 were downregulated.

### *5.2.1 Haem Biosynthesis & Real-Time PCR*

The $Fech^{m1PAS}$ allele decreases the formation of haem at the last stage of haem synthesis. The reduction in ferrochelatase activity arises not as a result of altered transcription but through a loss of function mutation. Although ferrochelatase does not interact directly with the genes involved in the earlier steps of haem synthesis it was hypothesised that alteration in the expression of these genes may occur as a response to the demand for haem. These genes were therefore extracted from the dataset and their differential expression is shown in figure 5.1. The array data did not show a smooth transition in gene expression across the time course. In this and other gene sets from these data the 4 and 32 week data sets appeared to have greater changes in gene expression than the other time points of the series. The reason for this is not known though it is possible that technical factors were involved here. To control for this a careful protocol of forward and reverse labelling and hybridisation was carried out for each time point. In addition to verify the gene changes QPCR was

**Figure 5.1**

**A)**

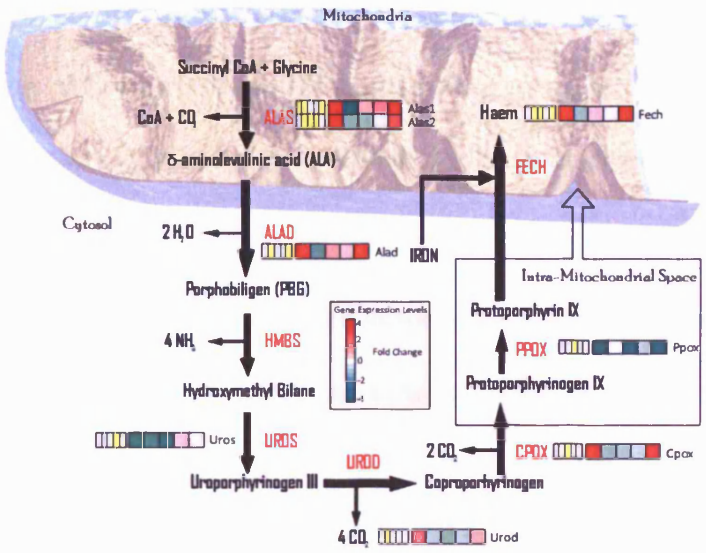


**B)**

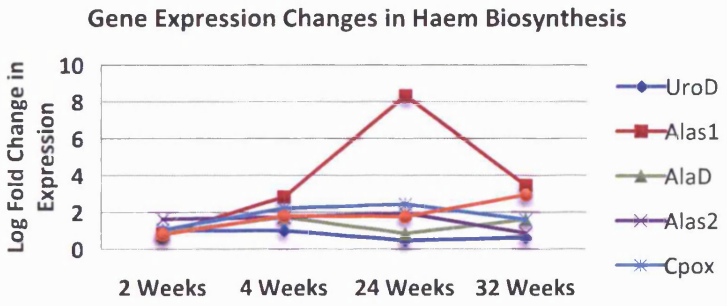


Figure 5.1) **Gene Expression Changes in Haem Biosynthesis.** A) The gene expression changes in Haem Biosynthesis genes determined by microarray for the Fech$^{m1PAS/m1PAS}$ mice compared to the wild type from 4 weeks to 32 weeks of age. The tables to the left of the expression data indicate statistical significance with yellow identifying changes significant to $p<0.05$. Each square represents a time point from left to right of 4, 8, 16, 24 and 32 weeks respectively B) Validation of microarray gene expression changes by real time PCR; The figure shows a subset of genes involved in haem biosynthesis and their expression profile from 2 weeks to 32 weeks.

carried out. Figure 5.1 A shows the gene expression changes from the microarray for those genes which had a significant change in gene expression and are part of the biochemical pathway of haem synthesis. Most genes were upregulated at the first time point of four weeks with the exception of PPox and Uros which are downregulated.

These changes were not absolutely confirmed by the RT-PCR though in general the trend of the altered gene expression across the time course was similar. A possible explanation for the discrepancies in between the methods is the low level of expression of these genes which makes them hard to measure and subject to technical variation.

The results show a modulation of haem synthesis across the time course with *Alas1, Fech, CPox and AlaD* sharing a similar expression profile of up regulation at 4 weeks before an oscillation until 32 weeks where up regulation is also observed. This oscillation is reflected in the RT-PCR results with the greatest changes being observed in *Alas1* the rate limiting enzyme in haem biosynthesis.

The RT-PCR results show a significant increase in haem synthesis activity across the time course; the microarray data indicates the same profile however, the extra resolution of RT-PCR gives a more precise quantitation.

Down regulation is observed in *PPox*, the gene responsible for the synthesis of protoporphyrin IX suggesting a negative feedback regulation by the elevated protoporphyrin levels shown in section 4.3.

### *5.2.2 Cytochrome P450 Genes*

One of the usages in the liver for newly synthesised haem is the cytochrome P450 family of proteins. This large family of genes use haem as an oxygen source in detoxification processes such as phase I biotransformation (See section 1.4.1) and as an electron acceptor in electron transport chains.

Drug metabolism involves several families of Cyp genes with each subfamily catalysing the breakdown of different substrates. The Cyp1 family contains several genes of which two were altered in expression during the course of this study (figure 5.2); the results showed a down regulation of *Cyp1b1* in the earlier time points before expression is raised just above the basal level. Cyp1b1 is thought to eliminate a steroid signalling molecule involved in the repression of tumourgenesis and this link has been shown in congenital glaucoma(Plasilova, Stoilov et al. 1999); although the eye is not linked in function to the liver it is likely that mechanisms of tumour formation remain closely related and this result can be considered in that respect .

Cyp1a2 plays a role in the oxidation of uroporphyrinogen and is implicated in uroporphyria and carcinogenesis(Gant, Baus et al. 2003). The results showed a down regulation of *Cyp1a2* across the time course with a large increase in expression at 16 and 24 weeks, however the increase was not found to be statistically relevant. The DGE relating to haem biosynthesis was shown in section 5.2.1.

**Figure 5.2**

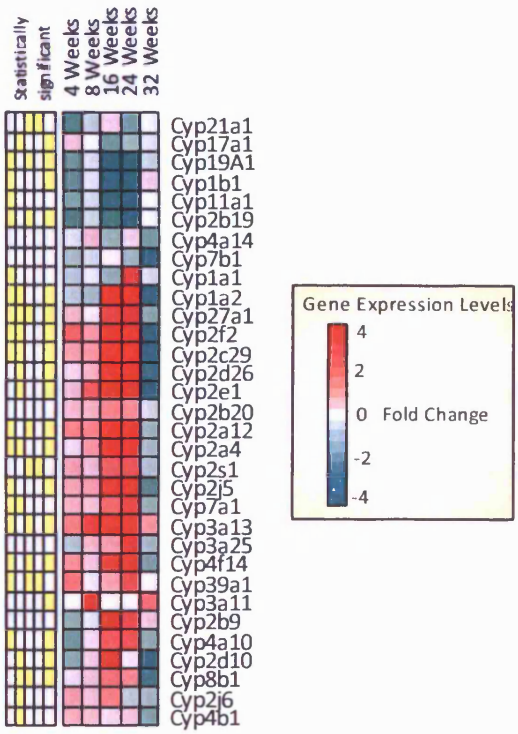


Figure 5.2) **Gene Expression Changes in the Cytochrome P450 Family**

The figure shows the gene expression changes in the cytochrome P450 family observed in the Fech$^{m1PAS}$ homozygote compared with the wild type, from 4 weeks to 32 weeks of age. The table on the left indicates statistical significance with yellow identifying changes significant to $p<0.05$.

The Cyp2 family is the largest of the P450 families in both mice and humans; the Cyp2 genes provide a protective role through the breakdown of steroidal xenobiotics arising

in the form of drugs and directly from diet i.e. toxins produced defensively by plants. With the exception of Cyp2b19 the Cyp2 family show progressive hyper-transcription in the Fech$^{m1PAS}$ until the 32 week time point where transcription is shown to decrease below basal levels; this change in transcription coincides with the presentation of the severe phenotype shown in chapter 4.

This expression profile is shared by Cyp27a1 and mirrored in Cyp11a1. Cyp27a1 is a mitochondrial sterol 27-hydroxylase responsible for the first step in one of the bile acid synthesis pathways (see section 1.5.1) as well as catalysing part of the side chain oxidation pathway in later bile formation(Russell 2003) similarly, acting in the later stages of the same process is Cyp3a11 which also sees an upregulation in gene expression. Cyp11a1 is responsible for the side chain cleavage of cholesterol in steroidogenic tissues(Pikuleva 2006).

### *5.2.3. Genes Relating to Glutathione*

Glutathione conjugation forms the main pathway of phase II biotransformation. The gene expression changes shown in figure 5.3 are genes with either the direct glutathione transferase function or the genes associated with the maintenance of the glutathione pool. As described in section 1.4.2.2, the glutathione pathway is a low capacity pathway and is tightly regulated to prevent glutathione depletion.

Glutamate-cysteine ligase, modifier subunit (Gclm) and Glutamate-cysteine ligase catalytic subunit (Gclc) act together as a dimer in the rate limiting step of glutathione synthesis; both genes share similar expression profiles with up regulation at all time points and peaks at 4 and 32 weeks. This expression profile is shared with all downstream genes involved in GSH synthesis and the GSH transferases indicating increased activity in the glutathione conjugation activity.

**Figure 5.3**

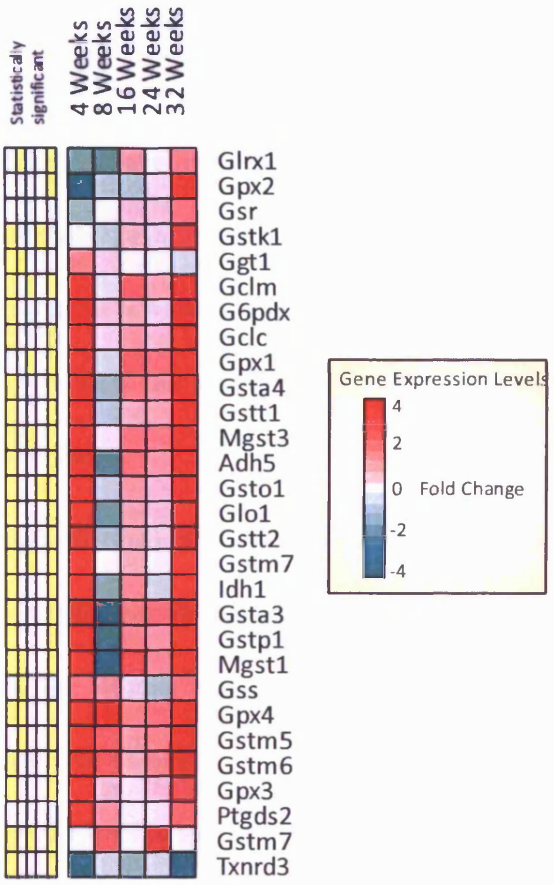


Figure 5.3) **Gene Expression changes in Glutathione Related Genes.**

The figure shows the differential gene expression for genes related to glutathione metabolism observed in the Fech$^{m1PAS}$ homozygote compared with the wild type, from 4 weeks to 32 weeks of age. The table on the left indicates statistical significance with yellow identifying changes significant to $p<0.05$

### *5.2.4 Bile Synthesis and Flow*

One of the major phenotypic changes observed in the Fech$^{m1PAS}$ mouse is an alteration in the composition of bile. Bile composition and flow is regulated tightly at a genetic level and expression changes have implications in the excretion of metabolites and xenobiotics and the normal digestion and absorption of lipids part of the intrahepatic circulation of bile salts. Figure 5.4 shows the gene expression changes in genes associated with the synthesis of bile components and their transport from hepatocytes to the bile canaliculi and ducts.

The main regulatory system in bile biosynthesis and cholesterol metabolism relies on the varied interactions of RXR and FXR dimers. Figure 5.4 shows an upregulation in gene expression of the regulators of bile acid synthesis, *Rxra, Rxrg and Nr1h4* with down regulation of *Rxrb*. The nuclear receptor *Nr1h4* encodes the FXR protein of the FXR/RXR dimer responsible for the transcriptional regulation of bile synthesis (section 1.4.2). The differential expression of the regulatory mechanisms surrounding bile synthesis were then further complimented by DGE in genes responsible for the downstream synthesis of bile acids.

The precursor to all bile acids is cholesterol; *Cyp39a1* and *Cyp7a1* are genes responsible for the rate limiting steps of cholesterol synthesis. These genes were up regulated in the Fech$^{m1PAS/m1PAS}$ mouse compared with the wild type, suggesting increased cholesterol and bile synthesis. This was supported by the increase in expression of *Baat*; a gene involved in the conjugation of glycine in the last stages of bile acid synthesis.

**Figure 5.4**

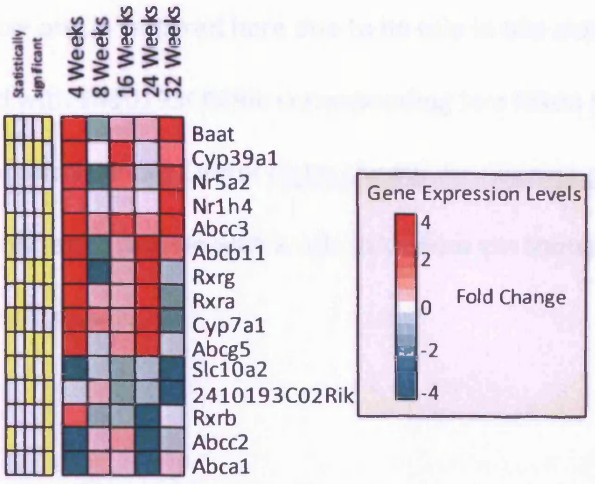


Figure 5.4) **Gene Expression Changes in Bile Biosynthesis and Flow.**

The figure shows the gene expression changes in genes related to bile formation and flow observed in the Fech$^{m1PAS}$ homozygote compared with the wild type, from 4 weeks to 32 weeks of age. The table on the left indicates statistical significance with yellow identifying changes significant to $p<0.05$

Genes responsible for bile salt transport across the canalicular membrane include members of the ATP-binding cassette superfamily, the results show that *Abcc3* and *Abcg5* are upregulated in the Fech$^{m1PAS}$ homozygote and *Abcc2 and Abca1* are down regulated. These changes could lead to a direct change in bile composition and bile dependant flow. *Abcb11* and *Abcc3* upregulation are of particular note as the genes are responsible for the primary transport of bile acids across the hepatocyte/canalicula membrane.

*Slc10a2* an anion transporter which shows significant down regulation in the Fech$^{m1PAS/m1PAS}$ mouse and is featured here due to its role in bile acid independent flow; this profile is shared with 2410193C02Rik corresponding to a Riken Clone obtained from the Riken Genomic Sciences Center (http://www.gsc.riken.co.jp). 2410193C02Rik is a putative protein with a role in sodium ion transport, produced from sequence homology analysis.

### *5.2.5 Cellular Respiration and Electron Transport*

In chapter 4, the hypothesis was advanced that the severe phenotypes seen in the Fech$^{m1PAS/m1PAS}$ mouse could be attributed to a deregulation of the mitochondrial electron transport chain and cellular respiration. In support of this hypothesis the differential gene expression pertaining to mechanisms of ATP synthesis and electron transport within the mitochondria was parsed from the time course and is presented in figure 5.5.

The results showed elevated expression of genes involved in cellular respiration and the synthesis of ATP. The mitochondrial ATP synthase genes (*Atp5*) are split into the production of two units; the proton-conducting $F_0$ unit (*Atp5j2, k, j, g3 & f1*) and the ATP synthesising unit, $F_1$ (*Atp5o, b, c1, a1 & e*). The genes for each subunit formed individual clusters under complete hierarchical clustering with the $F_0$ subunit genes at the top of the diagram and the $F_1$ subunit genes further down implying that the genes for each sub unit share the same DGE profile.

The energy required for ATP synthesis is provided by the electron transport chain; complex I, III and IV are represented in the data in figure 5.5. Complex I contains the NADH (ubiquione) dehydrogenase made up of several protein subunits (the *Ndufl* genes), Complex III is responsible for the reduction of cytochrome *c* and contains the mutli-subunit ubiquinol cytochrome-c reductase (the *Uqcr* genes) and the haem containing cytochrome P450 reductase (*Por*). Complex IV catalyses the final steps of the electron transport chain through the oxidation of cytochrome c by cytochrome oxidase (the *Cox* genes). All three stages of the electron transport chain see hypertranscription over the time course in the $Fech^{m1PAS/m1PAS}$ mouse implying that the respiration mechanism is impaired and that there is a need for increased respiration.

One of the major outcomes of aberration in the electron transport chain is the generation of ROS and oxidative stress. Figure 5.6 shows DGE present in oxidative damage response genes. The data shows an increase in the transcription of mitochondrial heatshock chaperones (*Hspd1 and Hspe1*), superoxide dismutase genes (*Sod1* and *Sod2*) and catalase (*Cat*). The increased transcription of these genes in the $Fech^{m1PAS/m1PAS}$ mouse relative to the wild type suggests an increase in ROS generation and oxidative stress.

**Figure 5.5**

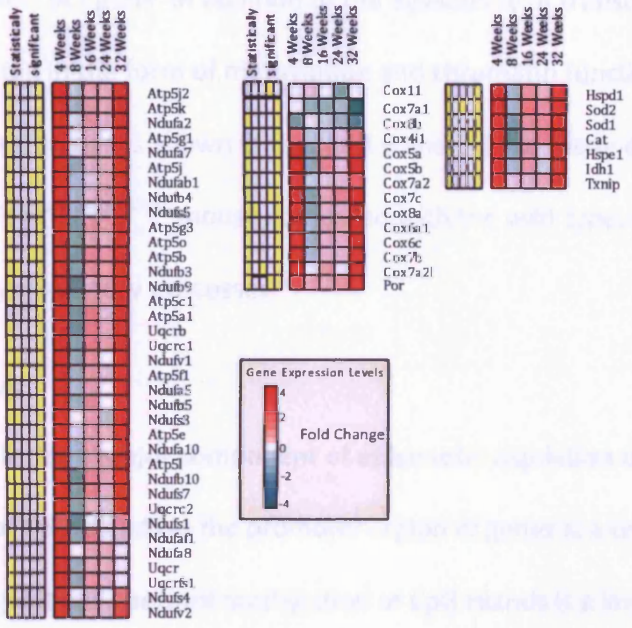


Figure 5.5) **Differential Gene Expression in Genes Associated with ATP Synthesis, Mitochondrial Respiratory Chain and Oxidative Stress.** The column of the left shows genes responsible of complexes I and III of the mitochondrial electron transfer chain and genes responsible for the mitochondrial ATP synthase. The central column shows genes responsible for complex IV; the cytochrome oxidase genes and the haem containing *Por*. The right hand column shows the response to oxidative stress. Mitochondrial heat shock proteins (Hspd1 & Hspe1), superoxide dismutase (SOD) and catalase (Cat) genes are all increased in their expression in the $Fech^{m1PAS/m1PAS}$ mouse relative to the wildtype. The table on the left indicates statistical significance with yellow identifying changes significant to $p<0.05$

### *5.2.6 Regulatory Systems- Methylation, Circadian Rhythm*

The regulation of gene transcription expression is a complex process employing multiple mechanisms per gene. In addition to the availability of transcription factors , epigenetic regulation in the form of methylation and chromatin function can control gene transcription. The genes shown in figures 5.6 and 5.7 are those differentially expressed in the $Fech^{m1PAS/m1PAS}$ mouse compared with the wild type, with roles and associations in key regulatory processes.

#### *5.2.5.1 Methylation*

DNA methylation forms a major component of epigenetic regulation of transcription. The methylation of CpG islands in the promoter region of genes is a critical process in transcriptional regulation. Aberrant methylation of CpG islands is a known mechanism in disease and links have been shown between methylation states and regulation of glutathione metabolism(Lertratanangkoon, Wu et al. 1997; Wang, Qin et al. 2006), response to cytotoxicity(Pogribny, Ross et al. 2006) and hetpatocarcinogenesis(Nagai, Nakamura et al. 2003; Chen, Choo et al. 2005; Wang, Qin et al. 2006).

Methylation of CpG islands is catalysed by the action of the DNA methyltransferases (DNMT). In the $Fech^{m1PAS/m1PAS}$ mouse *Dnmt1, Dnmt3a* and *Dnmt3b* show a down regulation relative to the wild type suggesting a state of hypomethylation (figure 5.5). Dnmt1 catalyses the hemi-methylation in DNA replication with Dnmt3a and Dnmt3b being involved in *de novo* methylation of cytosine residues(Nagai, Nakamura et al. 2003).

**Figure 5.6**

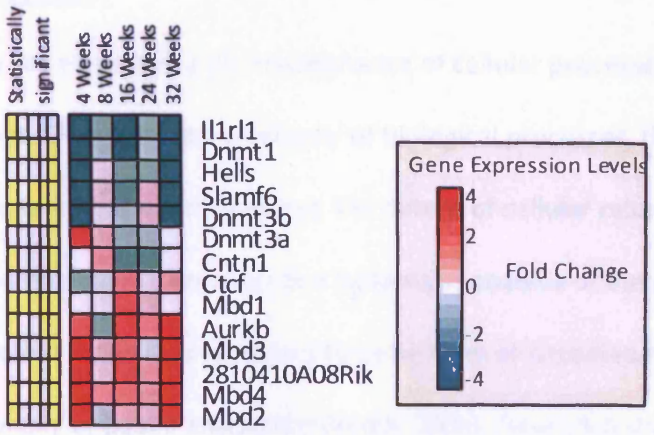


Figure 5.6) **Differential Gene Expression in Genes Associated with Transcriptional Regulation by Differential Methylation.** The table shows genes differentially expressed pertaining to methylation, in the Fech$^{m1PAS/m1PAS}$ mouse compared with the wild type, over 32 weeks. The table on the left indicates statistical significance with yellow identifying changes significant to $p<0.05$.

The methyl-CpG binding proteins (MBD) are responsible for methylation dependent transcriptional regulation and also demethylation. MBDs bind hypermethylated promoters repressing gene transcription(Bakker, Lin et al. 2002). In the Fech$^{m1PAS/m1PAS}$ time course, members of the MBD family, *Mbd1, Mbd2, Mbd3* and *Mbd4* are overexpressed. The genes *Hells* and *Aurkb* are not directly involved in DNA methylation but have an associated role through the remodelling of DNA structure.

*5.2.5.2 Circadian Rhythm*

Circadian rhythms are essential to the maintenance of cellular processes including metabolic pathways. Owing to the complexity of biological processes, the cell must have a way of maintaining temporal control. The extent of cellular reliance on circadian rhythm is not known, however in a systematic analysis of the proteome up to 20% of soluble protein in the liver is subject to some form of circadian regulation either transcriptionally or post transcription(Reddy 2006). Figure 5.6 shows genes differentially expressed in the $Fech^{m1PAS/m1PAS}$ mouse that defined using gene ontology terms, are associated with the maintenance and effect of temporal coordination by the circadian rhythm.

The period genes (*Per*), *Clock* and the Cryptochrome (*Cry*) genes are the most important genes in maintenance of the circadian rhythm. In the $Fech^{m1PAS/m1PAS}$ mouse, *Per1*, *Per2* and *Per3* showed downregulation over the 32 week period. The transcription factors *Clock* and *Npas2* also showed a continued down regulation in line with the expression profile shown by the period genes. *Clock and Npas2* are activated in their role of transcription factors by the gene *Cry1* (Kondratov, Kondratova et al. 2006) which shares the same expression profile.

**Figure 5.7**

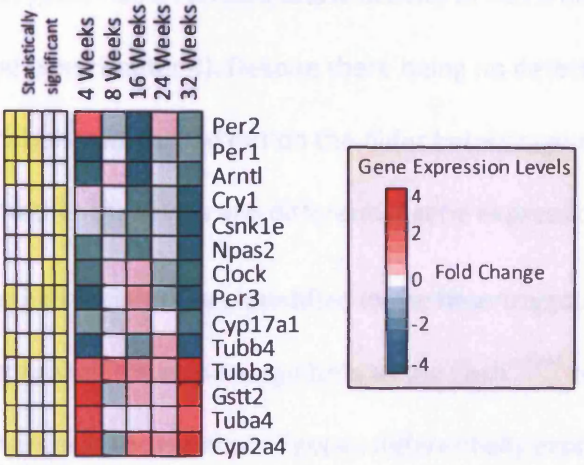


Figure 5.7) **Differential Gene Expression in Genes Associated with Circadian Rhythm Based Regulation.** The table shows genes differentially expressed pertaining to the temporal organisation of the cell, in the Fech$^{m1PAS/m1PAS}$ mouse compared with the wild type, over 32 weeks. The table on the left indicates statistical significance with yellow identifying changes significant to $p<0.05$.

Differential expression was also found in genes known to be affected by circadian regulation, these genes included the cytoskeletal genes *Tubb4*, *Tubb3* and *Tuba4*; the glutathione S-transferase, *Gstt2* and the steroid 15 alpha-hydroxylase *Cyp2a4*.

## 5.3 Differential Gene Expression in Mice Heterozygous for the Fech$^{m1PAS}$ Allele

The Fech$^{m1PAS}$ heterozygote has a Ferrochelatase activity of ≈65% and displays no significant phenotype (see chapter 4). Despite there being no detectable phenotype, microarray based analysis was carried out on the older heterozygous mice in the time course to identify whether there was any differential gene expression.

Some differential gene expression was identified in the heterozygous Fech$^{m1PAS}$ mouse however it did not approach the same magnitude as the Fech$^{m1PAS}$ homozygote in either the level of change or the number of genes differentially expressed (326 genes in the Fech$^{m1PAS/wt}$ vs. 1517 genes in the Fech$^{m1PAS/m1PAS}$ predicted changed at 24 weeks to $p<0.05$).

Genes that did show differential expression in the Fech$^{m1PAS}$ heterozygote are shown in figure 5.8. The *Cyp* genes involved in Stage 1 biotransformation (chapter 1) and the genes involved in glutathione mediated stage II biotransformation showed a slight upregulation in the 32 week mice (figure 5.8 A and B respectively). Figure 5.8C demonstrates slight upregulation in three other processes that are affected in the Fech$^{m1PAS}$ homozygote; the methyl binding domain proteins (*Mbd1, 2 and 4*) responsible for the methyl dependant regulation of gene expression showed a slight increase in expression as observed in the homozygote (section 5.2.5.1) however in contrast there was no downregulation of the period genes (*Per*). A similar upregulation at 32 weeks was observed in genes responsible for complex IV in the mitochondrial electron transport chain (*Cox* genes) and in the ATP synthase subunits *Atp5b* and *Atp5j*.

Genes involved in the earlier stages of the electron transport chain remained at normal levels of gene expression.

**Figure 5.8**

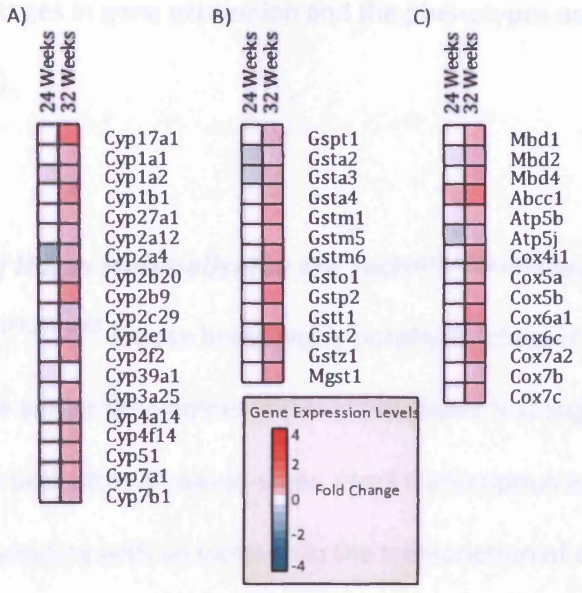


Figure 5.8) **Low Levels of Differential Gene Expression in the Fech$^{m1PAS}$ Heterozygote.** The table shows genes differentially expressed in the Fech$^{m1PAS}$ heterozygote at timepoint where the homozygous mouse presents severe phenotypes. Although expression of biomarkers of oxidative attack are increased they are not to the same extent as the homozygous mouse. All data shown are significant to $p<0.05$.

## 5.4 Discussion

The Fech$^{m1PAS/m1PAS}$ mouse showed differential gene expression throughout the 32 weeks of the time course. Analysis of the gene expression data has allowed correlation between these changes in gene expression and the phenotypes associated with the disease (chapter 4).

### *5.4.1 Response of Haem Metabolism in the Fech$^{m1PAS/m1PAS}$ mouse*

Despite the Fech$^{m1PAS/m1PAS}$ mouse being highly porphyric (chapter 4), the modest upregulation in the earlier time points of this study (figure 5.1) suggests that haem supply is sufficient until after 24 weeks when *Alas1* transcription is seen to peak in its expression corresponding with an increase in the transcription of cytochrome P450 genes (figure 5.2). *Alas1* is the rate limiting component of haem biosynthesis and responds to cellular haem increasing haem biosynthesis (Weiss and Orkin 1995).This suggests that haem synthesis was increased to meet the demand of haem for the cytochrome P450s (section 5.4.3). The increased haem requirement may have been exacerbated further by the increased expression of complex IV in the mitochondrial electron transport chain as cytochrome *c* reductase (*POR*) requires a haem cofactor to function correctly.

The variation in differential gene expression observed in the microarray timecourse (figure 5.1A) may be attributable to a loss of *NPas2* (figure 5.7), the transcriptional regulator of *Alas1(Kaasik 2004)*. *NPas2* is a transcription factor forming part of the circadian clock; *NPas2* has been shown to regulate haem biosynthesis through a

feedback loop mediated by haem binding. The results showed a loss in circadian control across the time course which could cause deregulation of haem biosynthesis (discussed in section 5.4.5.).

### *5.4.2 Response to Oxidative Stress in the Fech$^{m1PAS/m1PAS}$ mouse.*

With ferrochelatase activity reduced in the Fech$^{m1PAS/m1PAS}$ mouse, the mitochondria forms the focus of the protoporphyrin accumulation. It is therefore possible that the primary site of DNA damage mediated by protoporphyrin and ROS arising as a result of its accumulation, would be the mitochondrial genome. Genes in the mitochondrial genome showed differential gene expression compared with the wild type, over the time course; Down regulation was observed in *Cyp27a1*, required for degradation of the $C_{27}$-sterol side chain in bile acid biosynthesis(Norlin, von Bahr et al. 2003); *Cyp11a1* was found upregulated until 24 weeks. Like *Cyp27a1*, Cyp11a1 is also involved in side-chain cleavage of cholesterol.

With the accumulation of protoporphyrin and the altered bile in the Fech$^{m1PAS}$ mouse liver, reactive oxygen species may arise. The gene expression changes shown in figure 5.2 and 5.3 show an activation of the cytochrome P450 detoxification pathway (section 1.4.1) and both the glutathione transferase genes, responsible for the glutathione conjugation in phase II biotransformation (section 1.4.2) and genes involved in GSH biosynthesis to replenish the GSH pool. The mechanism of activation is not clear, however it may be through activation of *Nrf2* (section 1.4.3) and its

subsequent binding to the ARE found in the promoter of the biotransformation gene.(McMahon, Itoh et al. 2001)

The increased activity of the Phase I and II detoxification pathways coupled with activation of the cytochrome oxidase genes (*Cox*) and cytochrome *c* reductase (*Por*) is supportive of the theory of increased ROS; the same genes showed differential gene expression in rat hepatocytes that were exposed to cadmium to illicit a cytotoxic response, to the extent that Tan *et al.* (Tan, Shi et al. 2006) suggested that some of these genes may be used as biomarkers of cytotoxicity. The implication of the above gene inductions as cytotoxic response genes have also been observed in other systems(Goldstein and Faletto 1993; Li and Chan 2004).

Differential gene expression in the $Fech^{m1PAS}$ heterozygous mice showed partial activation of the oxidative response genes (section 5.3) but without pathological change consistant with the theory that although Fech activity is reduced the level at which protoporphyrin is synthesised higher than the rate at which ferrochelatase can process it but not to the extent where severe protoporphyrin accumulation will occur (section 4.3).

### *5.4.3 Differential Gene Expression of RXR in the $Fech^{m1PAS/m1PAS}$ Mouse leads to Aberrant Bile Composition and Flow*

Mice with griseofulvin induced EPP have an altered bile flow with increased levels of β-muricholate(Meerman, Koopen et al. 1999). Although in physiological concentrations

β-muricholate provides a protective role in the form of its tauro- conjugate, the levels seen in the griseofulvin mouse lead to a cytotoxic bile composition. The formation of bile and regulation of its composition is tightly regulated at the level of gene transcription as discussed in section 1.5.2.

In the $Fech^{m1PAS/m1PAS}$ mouse differential gene expression was observed in genes responsible for both the regulation of bile acid independent flow, and regulation of bile composition.

As described in section 1.5.2 the FXR/RXR dimer regulates bile composition through the transcriptional regulation of *Abcb11* and *Cyp7a1(Tuchweber 1996)*. In the $Fech^{m1PAS/m1PAS}$ mouse the RXR homologues alpha and gamma (*Rxra* and *Rxrg*) showed an increase in transcription from 4 to 24 weeks with a drop in expression below the wild type level at 32 week (figure 5.4). This gene expression profile was shared by their regulatory targets *Cyp7a1* and *Abcb11*. The increased expression of *Cyp7a1* elicited an increase in bile salt synthesis which correlated with the increase seen in the expression of other components of bile acid synthesis; the rate limiting oxysterol 7α-hydroxylase *Cyp39a1* and *Baat* which catalyses the final stage of bile synthesis. The increased bile acid metabolism led to an increased concentration of bile acid constituents caused by increased of the genes *Abcb11* and *Abcc3* which encode the bile acid transporter proteins. The increased concentration of bile acid constituents led to an increased efflux of electrolytes across the bile canaliculi membrane.

In addition to the increased bile acid concentrations, the bile composition of the griseofulvin mouse also showed increased protoporphyrin levels (discussed in chapter

4), increased cholesterol levels and increased bile flow. These findings are further supported through gene expression changes detected in the Fech$^{m1PAS/m1PAS}$ mice.

The cholesterol efflux transporter *Abcg5* is transcriptionally regulated by the FXR/RXR dimer(Kullak-Ublick, Stieger et al. 2004); in line with this, *Abcg5* showed a similar expression profile to the RXR transcription factors over the Fech$^{m1PAS/m1PAS}$ time course. The increased levels of Abcg5 led to an increased cholesterol efflux from the hepatocytes into the bile canaliculi causing the elevated levels observed in the griseofulvin model of EPP.

Meerman *et al.*(Meerman, Koopen et al. 1999) predicted that the increase bile flow may be as a result of aberrant bile salt-independent bile flow. The data from this study supports this theory through the down regulation of the anion transporter *Slc10a2* which may result from an imbalance in the osmotic balance across the bile canaliculi/ hepatocyte membrane.

The combination of gene expression changes in bile acid synthesis, flow and regulation were consistent with the biochemical analysis of bile in the griseofulvin mouse, and support the hypothesis that altered bile composition is attributable in part to differential gene expression of the retinoic X receptor.

### *5.4.4 Toxicity in the Fech$^{m1PAS/m1PAS}$ Mouse Leads to Disruption of Mitochondrial Processes.*

The integrity of the mitochondria is essential to the normal function of the cell. In a previous study, Navarro et al.(Navarro, del Hoyo et al. 2005) showed increases in the mitochondrial respiratory chain enzymes in the Fech$^{m1PAS/m1PAS}$ mouse that correlated with observed liver damage. Navarro et al. suggested that the increased activity in the mitochondrial respiratory chain enzymes were due to a modification of intracellular ATP requirements. The data presented in section 5.2.5 showed that in the Fech$^{m1PAS/m1PAS}$ mouse genes responsible for the mitochondrial electron transfer chain were upregulated. Although ATP requirements are most likely to be increased due to the upregulation of protective mechanisms such as phase I and II biotransformation (section 5.4.2) which use the energy supplied by ATP, the increased ATP production led to an accumulation rather than utilisation(Navarro, del Hoyo et al. 2005). This leads to an alternative hypothesis that in addition to elevated ATP requirements, increased bile salt concentration (section 5.4.3) may have lead to decoupling of the mitochondrial respiratory chain, leading to cytochrome c leakage and ROS attack. The observed increase in complex IV transcription may then form a protective response against the released cytochrome c.

It is known that levels of hydrophobic substances have a linear relationship with cell damage(Hansch and Dunn 1972). In murine EPP, the accumulation of hydrophobic protoporphyrin (chapter 4) and bile salts(Meerman, Koopen et al. 1999) reached levels that can cause damage to the cell by altering the mitochondrial membrane

potential(Rolo, Oliveira et al. 2000) and generating ROS. This form of disruption has already been implicated in cholestatic liver disease by Palmeira and Rolo(Palmeira and Rolo 2004).

Although the levels of bile salts do not reach a point where solubilisation and destruction of the mitochondrial membrane may occur, the aggregate effect of the elevated bile salt concentration with the accumulated protoporphyrin levels may induce mitochondrial permeability transition (MPT), which has a known role in cell death(Palmeira and Rolo 2004), allowing leakage of cytochrome c out of the electron transfer chain.

The $Fech^{m1PAS/m1PAS}$ mouse also showed activation of cytochrome oxidase (Por) which is known to provide a protective role against ROS attack and hepatic tumourgenesis(Schulz, Thierbach et al. 2006). The induction of protective mechanisms supports the presence of ROS attack, and combined with the known effects of high bile salt concentrations on the MPT, the disruption of mitochondrial processes appears a valid hypothesis. The increased ATP levels suggest that the electron transport chain is not entirely decoupled however, as Hansch demonstrated that hydrophobicity had a linear relationship to activation of biological processes, the leakage of cytochrome c may be titrated by the level of protoporphyrin and bile salts but sufficient to allow generation of ROS. The generation of ROS by cytochrome c would then excacerbate the effect of the protoporphyrin in the induction of cholestasis. This could also give rise to DNA damage allowing tumourgenesis as observed in the $Fech^{m1PAS/m1PAS}$ mouse after 32 weeks (section 4.6) and the griseofulvin model of EPP(Knasmuller 1997; Gant,

Baus et al. 2003). The combination of DNA damage in the mitochondria and the alteration of other mitochondrial processes including the disruption of the haem biosynthesis pathway has previously been linked to tumour growth in the frataxin deficient mouse(Schoenfeld, Napoli et al. 2005; Thierbach, Schulz et al. 2005) adding further support to this hypothesis.

### *5.4.5 Loss of temporal regulation is associated with altered Haem metabolism and Glutathione Biotransformation Activation*

The temporal organisation of the cell by maintenance of the circadian clock is essential to normal health. The circadian rhythm is primarily maintained in the suprachiasmatic nucleus (SCN) of the brain with peripheral tissues having their own circadian rhythm which is calibrated by the SCN in a hierarchical manner with the SCN as the "master" and the peripheral tissue, in this case the liver, as the "slave"(Reppert and Weaver 2002).

In the liver, 20% of all soluble protein(Reddy 2006) and a large proportion of the hepatic transcriptome (Akhtar, Reddy et al. 2002) have been shown to be under circadian regulation. The disruption of circadian rhythm has a known association with metabolic disease(Turek, Joshu et al. 2005) but has also been identified as a risk factor in cancer(Chen, Choo et al. 2005).

Differential gene expression in the $Fech^{m1PAS/m1PAS}$ showed down regulation of the genes responsible for mediating output of the circadian rhythm, and expression

changes in those genes responsible for the imparting of the circadian rhythm on cellular processes (section 5.2.5.2).

The genes responsible for maintenance of circadian rhythm in the Fech$^{m1PAS/m1PAS}$ mouse were down regulated. The *period* genes, *Per 1, Per2* and *Per3* have been shown to be deregulated in breast carcinoma and were observed to have a decreased transcription in the Fech$^{m1PAS}$ homozygote (figure 5.7). In breast cancers, the loss of regulation of the *Per* genes has been shown to be through aberrant methylation(Chen, Choo et al. 2005) rather than mutation which has an important bearing on this study as the expression data also showed evidence for global hypomethylation (section 5.4.6). The deregulation of *Per1, Per2* and *Per3* is perpetuated further as the transcriptional activator of the period genes, *Clock* was also found to be inhibited preventing recovery of *Period* transcription and synchronisation of the hepatic circadian rhythm with the master clock in the SCN(Reppert and Weaver 2002).

The clinical relevance of the breakdown in hepatic circadian rhythm in the Fech$^{m1PAS/m1PAS}$ mouse is multi-faceted. The reduction of *Clock* expression in the Fech$^{m1PAS/m1PAS}$ mouse has been reported to impair the detoxification of xenobiotics through modulation of several members of the glutathione S-transferases (*Gsta2, Gsta3*), haem oxygenase (*Por*) and *AbcG2(Gachon 2006)*. The results from this study do not support the effect of *Per* on the detoxification pathways as induction of *Gsta2, Gsta3* and *Por* were seen suggesting that *Period*'s regulatory effect may be upstream from the activators of these processes in the Fech$^{m1PAS/m1PAS}$ mice. However, although

not detected in the array analysis, the potential link to *AbcG2* is of interest as AbcG2 activity has been linked to the clearance of protoporphyrin(Zhou, Zong et al. 2005).

The *NPas2* gene is one of the output modulators of the circadian rhythm; Npas2 is a transcription factor and forms a dimer with *Bmal1* to rhythmically activate transcription of downstream effectors. One of the targets of NPas2 mediated activation is *Alas1*. It is feasible that the downregulation of *NPas2* and the rest of the circadian machinery in the $Fech^{m1PAS/m1PAS}$ mouse led to a deregulation of haem synthesis (as shown in section 5.2.1) allowing aberrant modulation of synthesis by other factors that would otherwise have a lesser effect.

The major role of temporal organisation by the circadian clock is the regulation of cell division. Matsuo *et al.* (Matsuo, Yamaguchi et al. 2003) have shown that cell division in mammalian tissues is directly regulated by components of the circadian clock. He showed that mice lacking the circadian regulator cryptochome (*Cry1*) had a complete lack of free-running rhythmicity. In conjunction with a loss of Per1, Per2 and Per3 it was shown that this led to a loss of cell cycle control through Wee1 (down regulated in the $Fech^{m1PAS/m1PAS}$ but not with enough statistical power to confirm the finding). The loss of the *Period* genes and *Cry1* in the $Fech^{m1PAS/m1PAS}$ mouse over the time course (figure 5.7) showed that the mechanisms observed by Matsuo *et al.(Matsuo, Yamaguchi et al. 2003)* and Chen *et al.(Chen, Choo et al. 2005)* may benefit survival of cancer cells in EPP leading to a further promotion of carcinogenesis.

### *5.4.6 Global Hypomethylation as a model for carcinogenesis in the Fech$^{m1pas}$ homozygote.*

Methylation of DNA at CpG dinucleotides forms a major component of the epigenetic regulation; approximately 3-5% of somatic cell cytosines are subject to methylation(Xiong, Dowdy et al. 2005). The degeneration of methylation patterns in the genome has a known association with cancer with both hypermethylation and hypomethylation leading to differential gene expression and tumour formation(Bakker, Lin et al. 2002; Badminton and Elder 2005; Xiong, Dowdy et al. 2005; Yamada, Jackson-Grusby et al. 2005; Bachman, Curtin et al. 2006; Bachman, Kamendulis et al. 2006; Bachman, Phillips et al. 2006).

DNA methylation is catalysed by the DNA methyltransferases (section 5.2.5.1). In the Fech$^{m1PAS/m1PAS}$ time course evidence of global hypomethylation was observed. The DNA methyltransferases *Dnmt1, Dnmt3a* and *Dnmt3b* were transcriptionally down regulated whilst demethylases, *Mbd2, Mbd3* and *Mbd4* were upregulated. The downregulation of the DNMTs prevents methylation of new DNA (*Dnmt1*) and *de novo* methylation (*Dnmt3a* and *Dnmt3b*), combined with the demethylation by the MBD family may have led to a state of hypomethylation. The hypomethylation may have then led to the adenomas observed at 32 weeks in the Fech$^{m1PAS/m1PAS}$ mouse. This is supported by the data of Xiong *et al.* who showed that lower levels of *Dnmt1* and *Dnmt3b* were strongly associated with a severe adenocarcinoma phenotype(Xiong, Dowdy et al. 2005). This is also supported by the similar de-methylation observed in mice with a drug induced choline deficiency. Bachman *et al.* showed that introduction

of phenobarbital (PB) or diethanolamine (DEA) modelled choline deficiency and caused hypomethylation through the deregulation of genes involved in the regulation of methylation(Bachman, Kamendulis et al. 2006).

The altered bile acid synthesis observed in the $Fech^{m1PAS/m1PAS}$ mouse (Section 5.4.3) may have led to the loss of methylation as reported in choline deficiency(Bachman, Kamendulis et al. 2006; Bachman, Phillips et al. 2006). This would have led to a progression towards complete hypomethylation(Bachman, Curtin et al. 2006) in the $Fech^{m1PAS/m1PAS}$ mouse and then loss of heterozygosity and increased DNA mutation rates as previously reported in cases of global hypomethylation(Chen, Pettersson et al. 1998).

# Chapter 6) Early Stage Differential Gene Expression and the Griseofulvin Mouse.

## 6.1) Introduction

The establishment of phenotypic change from birth to 32 weeks of age in the $Fech^{m1PAS/m1PAS}$ mouse (chapter 4) and microarray gene expression analysis allowed correlation between DGE and the observed phenotypes in chapter 5. This has helped to elucidate the mechanisms by which the $Fech^{m1PAS/m1PAS}$ mouse develops a severe form of EPP. From the data generated it became clear that the phenotypic changes were progressive and that the stimuli causing them to arise was acting early in life. To study this further, $Fech^{m1PAS/m1PAS}$ mice were taken at 18 days gestation and 1 week of age and subjected to microarray based gene expression analysis; Balb/c mice were also taken and used as controls as the $Fech^{m1PAS}$ allele was generated in a Blab/c genetic background(Tutois, Montagutelli et al. 1991).

In addition to the study of the $Fech^{m1PAS/m1PAS}$ model of EPP, expression data from mice fed griseofulvin were obtained(Gant, Baus et al. 2003). Griseofulvin is a potent inhibitor of ferrochelatase activity and when fed to mice induces accumulation of protoporphyrin (Knasmuller 1997; Meerman, Koopen et al. 1999). This occurs via a suicide inhibition of ferrochelatase(Knasmuller 1997) and in contrast to the $Fech^{m1PAS/m1PAS}$ mouse, the ferrochelatase inhibition occurs only in the liver and therefore anaemia does not result.

The aim of this chapter is to use the *in utero* and 1 week gene expression data to further understanding of the early stages of disease in the $Fech^{m1PAS/m1PAS}$ mice and to compare and contrast the differential gene expression in the griseofulvin fed mouse with the $Fech^{m1PAS/m1PAS}$ mouse.

## 6.2) Results

### *6.2.1) Overview of Pre-Natal Differential Gene Expression in the Fech$^{m1PAS/m1PAS}$ mouse.*

The gene expression levels of Fech$^{m1PAS/m1PAS}$ mice at 18 day gestation and 1 week of age was established as described in chapter 2.

**Figure 6.1**

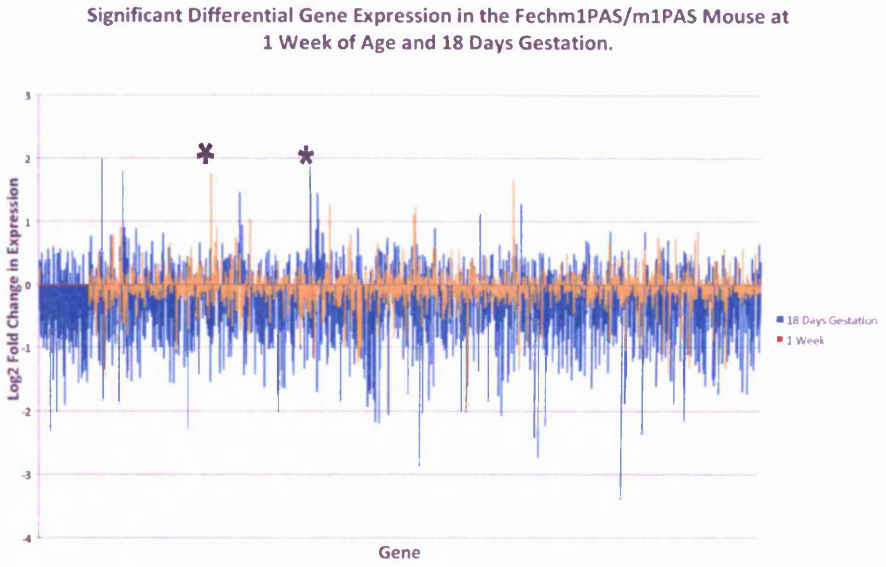


Figure 6.1) **Gross DGE in the Fech$^{m1PAS}$ homozygote at 18 Days Gestation and 1 Week Post-Natal relative to Balb/c Controls.** All significant differential gene expression (DGE) is shown with each gene displayed on the horizontal axis and $\log_2$ fold change in gene expression on the vertical axis. The data show that the majority of DGE in the 18 days gestation mouse are down-regulations as opposed to the more normal distribution observed in the 1 week old mice.

The results showed there was a marked change in gene expression levels in the $Fech^{m1pas/m1pas}$ mouse at 18 days gestation relative to the Balb/C control. Figure 6.1 shows that the gene expression changes observed at 18 days gestation were predominantly downregulation relative to the Balb/C control. This contrasts with the other time points analysed in this thesis which showed normal distributions of upregulation and downregulation. There were also qualitative differences in the genes which were undergoing DGE. Examples can be seen marked by the asterisks.

### *6.2.2 Differential Gene Expression in Haem Synthesis in Pre-Natal and Young $Fech^{m1PAS/m1PAS}$ Mice.*

In the later time points discussed in chapter 5, haem synthesis was shown to be upregulated in the $Fech^{m1PAS/m1PAS}$ mouse. It is possible that this occured to meet the haem demands of increased transcription of the phase I biotransformation cytochrome P450 genes.

At 18 days gestation the components of the haem biosynthesis pathway show a global decrease in transcription (figure 6.2) in particular the *Fech* gene and *Cpox*.

The global down regulation of haem synthesis genes pre-natal was seen to become less pronounced over time until by 4 weeks over expression was detected in several genes; This effect complements the expression profile of *Alas1*, the rate limiting step in haem synthesis, which was found to have a 20% reduction in transcription rate

against the wild type at 18 days gestation but by 1 week post-natal was being over expressed at a rate of 160% of the wild type (figure 6.2).

**Figure 6.2**

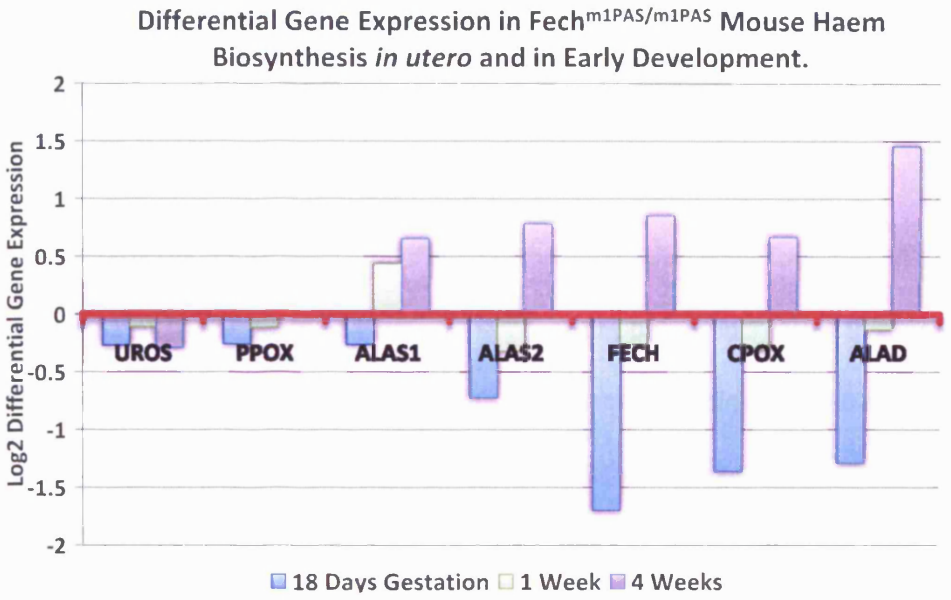


Figure 6.2) **Differential Gene Expression in the Regulation of Haem Synthesis in the Fech$^{m1Pas/m1PAS}$ Neonate Compared with the Wild Type.** The graph shows DGE in Fech$^{m1PAS/m1PAS}$ mice from 18 days gestation to 4 weeks after birth. n≥3. All changes significant to p≤0.05.

### *6.2.3 Differential Gene Expression in the Prenatal Fech$^{m1PAS/m1PAS}$ of Genes Relating to EPP Phenotypes.*

To understand the initial stages of the disease progression in the Fech$^{m1PAS/m1PAS}$ mouse, genes associated with the changing phenotypes were analysed at 18 days gestation and 1 week post-natal; these data were then compared against the gene expression changes found at the later stages (table 6.1.) discussed in chapter 5.

Genes involved in glutathione mediated biotransformation were found to be downregulated in the prenatal Fech$^{m1PAS/m1PAS}$ mouse before increasing in expression after birth. The key glutathione gene transcription factors *Gclc* and *Gclm* showed a ≈2 fold downregulation prior to birth, raising to a ≈1.6 fold upregulation by 4 weeks of age.

The cytochrome P450 genes showed a different pattern of DGE compared with the glutathione genes with an over expression in many *Cyp* genes prior to birth and an oscillation through lowered expression at 1 weeks to overexpression at 4 weeks post-natal.

Members of the *period* family responsible for maintenance of the circadian rhythm showed very mild differential gene expression prenatal, unlike at later time points. Prior to birth some up regulation was observed in *Per2* and the transcription factor *Clock* but not the large down regulation observed in the Fech$^{m1PAS/m1PAS}$ after 4 weeks.

The results suggest that after birth there is a trend towards lowered expression in genes associated with the circadian rhythm.

The other major class of genes observed to have DGE in the Fech$^{m1PAS/m1PAS}$ mouse prenatally compared with later time points was the epigenetic regulation by methylation. At 18 days gestation there was a significant decrease in the expression of *Dnmt1* which propagates throughout the timecourse (section 5.2.5.1). Prior to 4 weeks of age this was the only major change in gene expression in genes associated with methylation.

A marked change in gene expression was seen in genes associated with ATP requirement where, by 4 weeks of age the expression of mitochondrial ATP synthase genes (*Atp5*) were greatly increased in the Fech$^{m1PAS/m1PAS}$ mice. However, prior to birth and to a lesser extent by the 1$^{st}$ week, expression was significantly lower compared to that seen in the wild type.

The genes associated with bile synthesis showed upregulation of the last step in bile synthesis (*Baat*) and the bile acid transporter *Abcb11* which was consistent with the DGE found in later time points. However, contrasting with the later time points, expression of the retinoid X-receptor *Rxra* at 18 days gestation was reduced to 40% of wild type whilst post-natal the expression of *Rxra* rises to upregulation.

Table 6.1

| Gene | 0 Week Mean Expression | p-value | 1 Week Mean Expression | p-value | 4 Week Mean Expression | p-value |
|---|---|---|---|---|---|---|
| Gsta1 | | | -0.070 | 0.159 | | |
| Gsta3 | 0.238 | 0.040 | -0.655 | 0.000 | 1.637 | 0.019 |
| Gsta4 | 0.192 | 0.071 | -0.015 | 0.882 | 1.127 | 0.037 |
| Gstm1 | -0.298 | 0.089 | 0.775 | 0.000 | 1.680 | 0.074 |
| Gstm5 | -0.304 | 0.005 | 0.548 | 0.003 | 1.195 | 0.090 |
| Gstm6 | -0.498 | 0.031 | | | 1.357 | 0.023 |
| Gstm7 | | | 0.085 | 0.690 | | |
| Gsto1 | 0.376 | 0.001 | -0.198 | 0.063 | 0.773 | 0.006 |
| Gstp1 | -0.234 | 0.033 | 0.245 | 0.000 | | |
| Gstt1 | 0.119 | 0.662 | 0.114 | 0.172 | 1.222 | 0.043 |
| Gstt2 | -0.014 | 0.800 | -0.208 | 0.005 | 0.927 | 0.025 |
| Gstz1 | -0.483 | 0.049 | -0.426 | 0.000 | 1.035 | 0.066 |
| Gclc | -0.767 | 0.000 | 0.095 | 0.130 | 0.716 | 0.070 |
| Gclm | -1.050 | 0.000 | 0.002 | 0.974 | 0.588 | 0.001 |
| | | | | | | |
| Per1 | | | -0.003286 | 0.961 | -0.414531 | 0.026 |
| Per2 | 0.307215 | 0.031 | 0.0180512 | 0.604 | 0.233117 | 0.043 |
| Per3 | -0.126467 | 0.283 | -0.0758132 | 0.154 | | |
| Clock | 0.349021 | 0.084 | 0.00690933 | 0.918 | -0.261715 | 0.131 |
| Npas2 | | | 0.007955 | 0.843 | -0.230922 | 0.392 |
| | | | | | | |
| Atp5b | -0.479737 | 0.024 | -0.226775 | 0.097 | 1.6134 | 0.012 |
| Atp5c1 | -0.48447 | 0.105 | -0.11972 | 0.283 | 1.74806 | 0.026 |
| Atp5d | -0.544163 | 0.030 | 0.0124133 | 0.829 | | |
| Atp5h | -0.392532 | 0.012 | -0.33169 | 0.175 | | |
| Atp5j | -0.276292 | 0.325 | -0.191588 | 0.008 | 1.49531 | 0.008 |
| Atp5k | 0.0305302 | 0.810 | -0.220688 | 0.014 | 1.37857 | 0.007 |
| | | | | | | |
| Dnmt1 | -0.706447 | 0.000 | -0.0392421 | 0.295 | -0.493207 | 0.006 |
| Dnmt3b | 0.186597 | 0.110 | -0.215283 | 0.123 | | |
| Mbd1 | -0.129855 | 0.214 | 0.229835 | 0.004 | -0.25354 | 0.052 |
| Mbd3 | 0.0105502 | 0.865 | -0.0824153 | 0.387 | 0.7252 | 0.102 |
| Mbd4 | -0.046609 | 0.254 | -0.057344 | 0.638 | 0.741964 | 0.024 |

| Gene | 0 Week Mean Expression | p-value | 1 Week Mean Expression | p-value | 4 Week Mean Expression | p-value |
|---|---|---|---|---|---|---|
| Cyp11a1 | 0.145 | 0.259 | -0.122 | 0.003 | -0.978 | 0.006 |
| Cyp1a2 | -0.338 | 0.109 | -0.397 | 0.004 | 0.872 | 0.023 |
| Cyp20a1 | -0.247 | 0.077 | 0.071 | 0.055 | | |
| Cyp21a1 | 0.470 | 0.018 | | | -0.251 | 0.242 |
| Cyp27a1 | 0.453 | 0.272 | 0.004 | 0.718 | 0.576 | 0.016 |
| Cyp2a12 | 0.650 | 0.006 | 0.028 | 0.155 | 1.567 | 0.023 |
| Cyp2a4 | 0.509 | 0.000 | -0.055 | 0.060 | 0.945 | 0.020 |
| Cyp2b20 | 0.027 | 0.658 | | | 0.214 | 0.131 |
| Cyp2b9 | 0.299 | 0.423 | 0.297 | 0.012 | 0.161 | 0.304 |
| Cyp2c29 | 0.757 | 0.000 | 0.007 | 0.593 | 1.501 | 0.067 |
| Cyp2d10 | 0.000 | 0.000 | -0.072 | 0.373 | 0.018 | 0.906 |
| Cyp2d26 | 0.267 | 0.122 | | | 0.776 | 0.168 |
| Cyp2e1 | 1.456 | 0.000 | -0.718 | 0.000 | 1.591 | 0.074 |
| Cyp2f2 | 0.157 | 0.688 | -0.271 | 0.013 | 1.381 | 0.010 |
| Cyp2j5 | | | -0.413 | 0.000 | 1.002 | 0.103 |
| Cyp2j6 | | | -0.140 | 0.049 | -0.062 | 0.902 |
| Cyp2s1 | 0.017 | 0.801 | -0.157 | 0.193 | 0.405 | 0.137 |
| Cyp39a1 | -0.024 | 0.691 | -0.242 | 0.017 | 0.471 | 0.316 |
| Cyp3a11 | -0.035 | 0.680 | -0.181 | 0.000 | | |
| Cyp3a13 | 0.411 | 0.046 | -0.230 | 0.020 | | |
| Cyp3a25 | 0.135 | 0.368 | -0.084 | 0.000 | 0.615 | 0.260 |
| Cyp4a10 | 0.695 | 0.147 | -0.336 | 0.025 | 0.448 | 0.027 |
| Cyp4a14 | 0.935 | 0.000 | -0.515 | 0.000 | 0.040 | 0.670 |
| | | | | | | |
| Baat | 0.514758 | 0.050 | 0.400043 | 0.088 | 1.04568 | 0.029 |
| Cyp39a1 | -0.0244425 | 0.691 | -0.241946 | 0.017 | 0.471469 | 0.032 |
| Nr5a1 | -0.18546 | 0.026 | -0.231706 | 0.197 | -1.0833 | 0.061 |
| Abcb11 | 0.762443 | 0.038 | -0.0614799 | 0.469 | 0.638203 | 0.041 |
| Rxra | -1.40069 | 0.004 | 0.188256 | 0.217 | 0.828991 | 0.005 |
| Rxrb | -0.25911 | 0.209 | -0.129952 | 0.190 | 0.210393 | 0.119 |
| Rxrg | 0.0780973 | 0.105 | 0.158254 | 0.265 | 0.840518 | 0.057 |

Table 6.1) **Differential Gene Expression in Fech$^{m1PAS/m1PAS}$ Mice at 18 Days Gestation, 1 Week and 4 Weeks.** The table shows differential gene expression in the Fech$^{m1PAS/m1PAS}$ mouse before birth (18 days gestation), 1 week of age and 4 weeks of age. The 4 week data was previously shown in chapter 5. Genes were selected based on biological function and differential gene expression in the later time points.

The data presented in this table is displayed using the same gradient to denote fold change as chapter 5 to ease comparison (legend shown on the right).

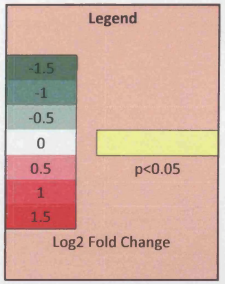

Table 6.1

| Gene | 0 Week Mean Expression | p-value | 1 Week Mean Expression | p-value | 4 Week Mean Expression | p-value |
|---|---|---|---|---|---|---|
| Gsta1 | | | -0.070 | 0.159 | | |
| Gsta3 | 0.238 | 0.040 | -0.655 | 0.000 | 1.637 | 0.019 |
| Gsta4 | 0.192 | 0.071 | -0.015 | 0.882 | 1.127 | 0.037 |
| Gstm1 | -0.298 | 0.089 | 0.775 | 0.000 | 1.680 | 0.074 |

| Gene | 0 Week Mean Expression | p-value | 1 Week Mean Expression | p-value | 4 Week Mean Expression | p-value |
|---|---|---|---|---|---|---|
| Cyp11a1 | 0.145 | 0.259 | -0.122 | 0.003 | -0.978 | 0.006 |
| Cyp1a2 | -0.338 | 0.109 | -0.397 | 0.004 | 0.872 | 0.023 |
| Cyp20a1 | -0.247 | 0.077 | 0.071 | 0.055 | | |
| Cyp21a1 | 0.470 | 0.018 | | | -0.251 | 0.242 |

### *6.2.4 Gene Expression in the Griseofulvin Mouse*

In the previous chapters comparisons have been drawn between the $Fech^{m1PAS/m1PAS}$ mouse and Balb/C mice with griseofulvin induced EPP. Figure 6.3 demonstrates the similarity in differential gene expression between these two models of EPP, validating their comparison in the previous chapters; Mice were fed a diet treated with griseofulvin for a period of 22 days, during which time the mice develop an acute porphyria leading to adenoma(Gant, Baus et al. 2003). In the liver this is similar pathologically to that seen in the $Fech^{m1PAS/m1PAS}$ mice.

The genes shown in figure 6.3 are related to the key processes identified in chapter 5; *Gstm2* is a glutathione S-transferase involved in phase II biotransformation (section 1.4.2.2. *Gstm2* expression was shown to be induced in both the $Fech^{m1PAS/m1PAS}$ mice and those fed griseofulvin.

*Clock* is the transcription factor responsible for maintenance of the circadian rhythm and circadian calibration by the SCN. *Clock* was found to be down-regulated in both models of EPP.

Increased cytochrome oxidase (*Por*) expression was discussed in chapter 5 as a potential protective response against ROS attack. In the griseofulvin mice a progressive induction of *Por* was observed at a similar level of induction to the $Fech^{m1PAS/m1PAS}$ mice.

**Figure 6.3**

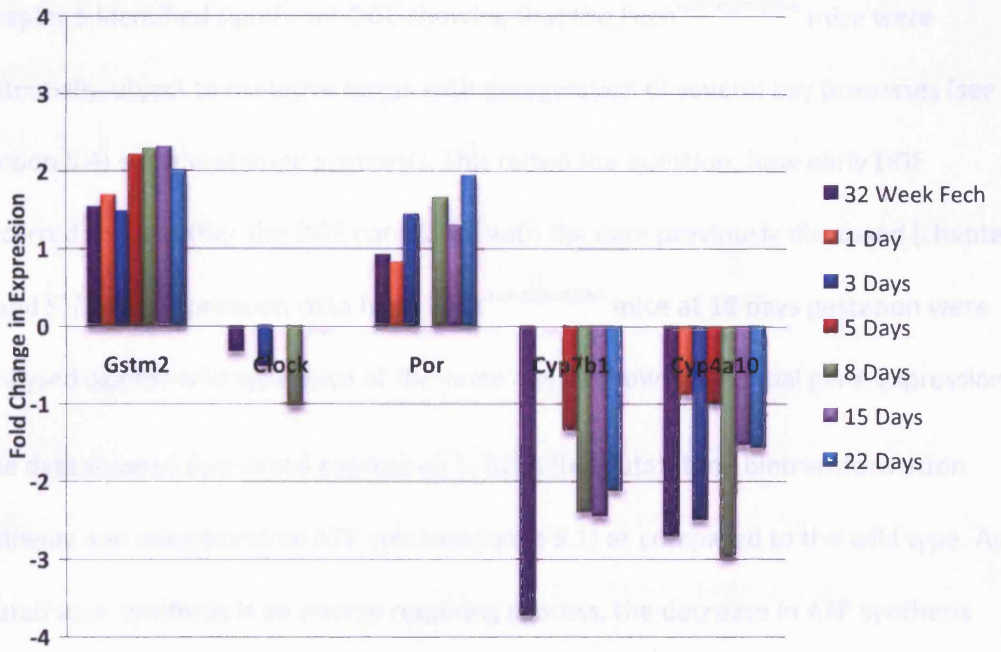


Figure 6.3) **Figure showing the similarity between Gene Expression Changes in the Fech$^{m1PAS/m1PAS}$ and Griseofulvin Mice.** Balb/C mice were fed a diet containing griseofulvin for a period of 22 days. The figure above shows differential gene expression in the griseofulvin mice over the time period and data from the 32 week Fech$^{m1PAS/m1PAS}$ mice. n≥3, all data significant to p≤0.05.

## 6.3 Discussion

### *6.3.1 Differential Gene Expression in Prenatal Fech$^{m1PAS/m1PAS}$ Mice.*

Chapter 5 identified significant DGE showing that the Fech$^{m1PAS/m1PAS}$ mice were potentiallysubject to oxidative stress with deregulation of several key processes (see section 5.4) e.g. glutathione synthesis. This raised the question, how early DGE occurred and whether the DGE correlated with the data previously discussed (chapters 4 and 5)? Gene expression data from Fech$^{m1PAS/m1PAS}$ mice at 18 days gestation were analysed against wild type mice of the same age to show differential gene expression.

The data showed decreased expression in both the glutathione biotransformation pathway and mitochondrial ATP synthase(table 6.1) as compared to the wild type. As glutathione synthesis is an energy requiring process, the decrease in ATP synthesis may be due to a lowered ATP requirement.

The cause of the down regulation in phase II biotransformation may be effect of the glutathione pathway regulatory genes *Gclc* and *Gclm*; Gclc and Gclm form a dimer which regulates the transcription of the glutathione S-transferases. The cause of aberrant gene expression of *Gclc* and *Gclm* is not clear, however glutathione pathways have been linked to circadian rhythm(Gachon 2006) which is also subject to mild DGE in the prenatal Fech$^{m1PAS/m1PAS}$ mice. Although the DGE in the *period* genes is not the same magnitude as the postnatal mice it has been reported that prenatal mice may be more susceptible to oxidative damage. Gallagher and Gardner (Gallagher and Gardner 2002) reported that the prenatal livers defence against oxidative stress was less efficient relative to postnatal, due to elements of the glutathione pathway were

subject to developmental regulation. They showed that members of the *Gsta* subfamily were expressed in preference to other glutathione S-transferases; this finding is consistent with the increased expression of *Gsta3* and *Gsta4* in the 18 day gestation Fech$^{m1PAS/m1PAS}$ mice. Other indications of oxidative stress were shown through activation of the cytochrome P450 genes associated with phase I biotransformation both prenatal and postnatal in the Fech$^{m1PAS/m1PAS}$ mice (section 1.4.1 and 5.4.2).

It is unclear as to whether the source of oxidative stress is protoporphyrin accumulation in the prenatal mouse or in the highly porphyric mother. However, oxidative stress in the prenatal Fech$^{m1PAS/m1PAS}$ is likely to be high as pregnancy itself causes production of ROS due to the increased activity of mitochondria in the placenta(Myatt and Cui 2004). This increased oxidative stress may underlie an increased susceptibility to any ROS generated. In addition to ROS generated from the accumulated protoporphyrin in either the mother or pup, another source of oxidative stress and deregulation of mitochondrial processes is the alteration of bile composition. Altered bile composition was identified in the griseofulvin fed mice (section 4.7.6 and 5.4.3)(Meerman, Koopen et al. 1999). Differential gene expression in the Fech$^{m1PAS/m1PAS}$ mouse at 18 days gestation showed a reduction in expression of the transcription factors *Rxra* and *Rxrb* involved in regulation of bile synthesis as well as upregulation of *Baat* and *Abcb11*. The contrast between the expression of the transcription factors involved in bile synthesis and the increase in the expression of *Baat*, the gene responsible for the last step in bile acid synthesis suggest that there

was decoupling of the bile synthesis regulatory mechanisms in the Fech$^{m1PAS/m1PAS}$ prenatal mouse. The increase in expression of *Abcb11* implies that an increase in bile acid concentration in the bile canaliculi occurred which may have led to the initiation of cholestatic liver disease.

### *6.3.2 Gene Expression Data from Mice Fed Griseofulvin Correlates with Differential Gene Expression in the Fech$^{m1PAS/m1PAS}$ Mice.*

The inhibition of ferrochelatase activity by griseofulvin provides a useful model to study the progression of EPP which has been used in conjunction with the Fech$^{m1PAS/m1PAS}$ mouse in both this thesis and the literature(Gant, Baus et al. 2003). Previously the griseofulvin mouse has been shown to exhibit the same phenotypic changes as seen in the Fech$^{m1PAS/m1PAS}$ mouse(Davies, Schuurman et al. 2005) and severe human EPP(Knasmuller 1997). The results in section 6.2.4 demonstrate that in addition to presenting with the same hepatic symptoms as the Fech$^{m1PAS/m1PAS}$ mouse, the gene expression changes observed in griseofulvin induced EPP correlate with DGE in the Fech$^{m1PAS/m1PAS}$ mouse. This demonstrates that the comparison of the two models in the elucidation of the disease mechanisms in EPP is valid supporting the conclusions in this thesis that have used data from both the Fech$^{m1PAS/m1PAS}$ mouse and the griseofulvin induced model of EPP.

# Chapter 7) General Discussion

## 7.1) General Discussion

The aim of this thesis was to apply genomic technology to gain information on the progression of disease in the $Fech^{m1PAS}$ model of EPP. EPP is a complex human disease with both genetic and environmental components (chapter 1); the elucidation of interactions between the genetic and environmental components and their relationship with pathological change, has furthered our insight into mechanisms of disease.

### *7.1.1 Environmental and Genetic Components in the $Fech^{m1PAS/m1PAS}$ Mouse Lead to Differential Gene Expression Prior to the Detection of Pathological Change.*

One of the major unknowns surrounding the progression of EPP in the $Fech^{m1PAS/m1PAS}$ mouse was the point at which physiological and genetic change occurred. The results presented here in chapters 4 and 5 showed phenotypic changes and differential gene expression shortly after birth. This prompted further investigation of differential gene expression in prenatal $Fech^{m1PAS/m1PAS}$ mice showing that aberrant genetic regulation occurred prior to birth (chapter 6). These data raised the hypothesis that disease in the $Fech^{m1PAS/m1PAS}$ mice is not attributable to extrahepatic cholestasis caused by protoporphyrin accumulation in the bile canaliculi but by a series of targeted gene expression changes and modification of cellular processes.

After birth the disease progresses with the formation of pathological change (chapter 4). By correlation to differential gene expression in the $Fech^{m1PAS/m1PAS}$ mouse

compared to the wild type over the time course (chapters 5 and 6), the increase in the severity of phenotypes detected in chapter 4 were found to have genetic determinants associated with several key cellular processes (Figure 7.1)

The differentially expressed genes found to correlate with the progression of phenotypic severity in the $Fech^{m1PAS/m1PAS}$ mice were involved in bile metabolism (section 5.4.3), oxidative stress (section 5.4.2), haem metabolism (section 5.4.1), cellular respiration (section 5.4.4) and temporal and epigenetic control mechanisms (sections 5.4.5 and 5.4.6).

**Figure 7.1**

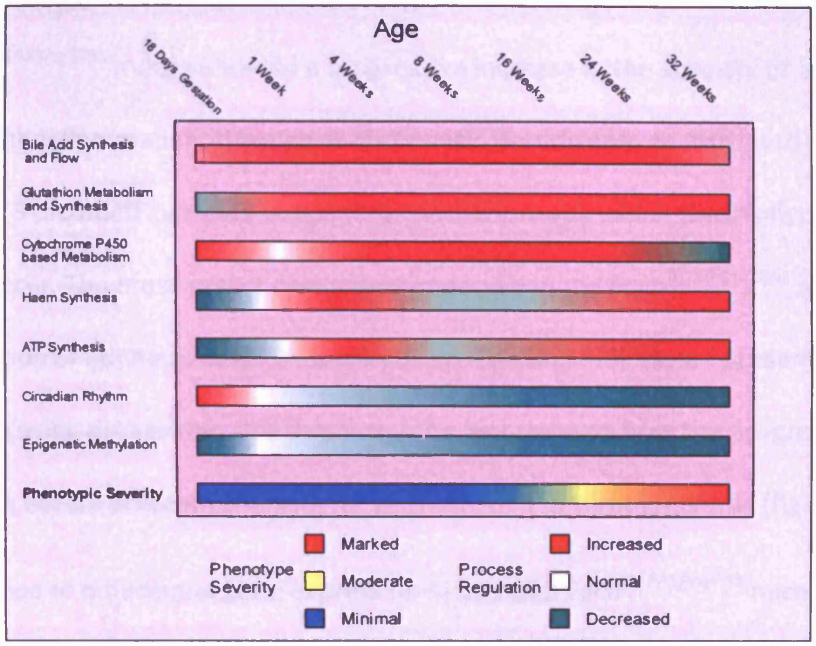


Figure 7.1) **Differential Expression and Activity of Cellular Processes Associated with Phenotypic Change in the Fech$^{m1PAS/m1PAS}$ Mouse compared to the Wild Type.** The figure shows how differential gene expression in key processes related to the progressive increase in severity of the disease phenotype. The phenotypic severity is shown in the bottom row and was graded on the same schema as used in section 4.6 with blue showing minimal severity through to red, showing marked severity. The legend at the base of the figure shows the relationships between colour an differential gene expression.

### *7.1.2 A Cascade of ROS Generation coupled with Loss of Temporal and Epigenetic Regulation Leads to Tumourgenesis in the Fech$^{m1PAS/m1PAS}$ Mouse.*

The Fech$^{m1PAS/m1PAS}$ mouse showed a progressive increase in the severity of symptoms, starting with inflammation, through to cholestatic liver disease as discussed in chapter 4. Chapter 5 provided evidence supporting mechanisms by which these phenotypic changes occur. The most severe phenotype observed in the Fech$^{m1PAS/m1PAS}$ mouse was the formation of adenoma after 24 weeks of age (section 4.6). Here I present a hypothesis using data within this thesis and the literature on how the progression of the disease occurs and a mechanism for the induction of tumourgenesis (figure 7.2).

The presence of differential gene expression in prenatal Fech$^{m1PAS/m1PAS}$ mice (chapter 6) demonstrated that the initial stages of the disease occurred *in utero*. At 18 days gestation the Fech$^{m1PAS/m1PAS}$ mice showed evidence of oxidative stress through the induction of genes involved in glutathione biotransformation and cytochrome P450 mediated biotransformation (figure 6.1). The source of the oxidative stress was unclear as haem biosynthesis was down regulated at this stage, reducing the likelihood of the prenatal Fech$^{m1PAS/m1PAS}$ mouse haem synthesis causing an accumulation of protoporphyrin. However, the mother was highly porhyric and as pregnancy induces increased ROS production across the placenta(Myatt and Cui 2004), the combined effect of maternal protoporphyrin, prenatal protoporphyrin and the increased oxidative damage from the placenta may have caused the initial response.

**Figure 7.2**

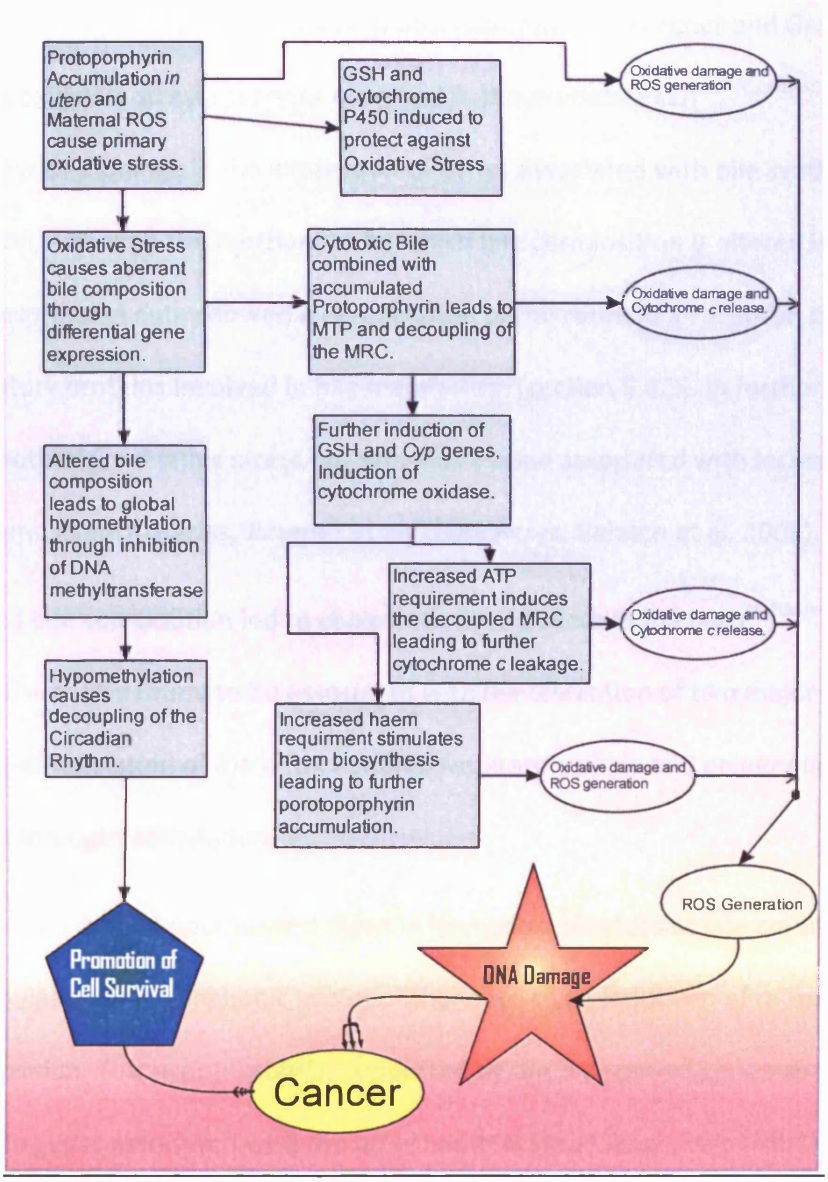


Figure 7.2) **Hypothesised Progression of Disease in the Fech$^{m1PAS/m1PAS}$ Mouse Model of EPP.** The diagram shows the hypothesised progression of disease in the Fech$^{m1PAS/m1PAS}$ mouse through to the formation of adenoma.

The initial response to oxidative stress would have been exacerbated further by the known inefficiency of foetal glutathione biotransformation(Gallagher and Gardner 2002). The oxidative stress response observed in the prenatal Fech$^{m1PAS/m1PAS}$ correlated with a change in the expression of genes associated with bile synthesis and composition. Although the mechanism by which bile composition is altered is not clear, the gene expression data showed a deregulation of the retinoid X-receptor, one of the key regulatory proteins involved in bile metabolism (section 5.4.3). In further support of this hypothesis, oxidative stress has previously been associated with increased bile synthesis and export(Macias, Jimenez et al. 2006; Perez, Velasco et al. 2006).

The altered bile composition led to cholestatic liver disease in the Fech$^{m1PAS/m1PAS}$ mouse and was also found to be associated with the disruption of two major cellular processes; deregulation of the mitochondrial respiratory chain and epigenetic regulation through methylation.

In section 5.4.4 it was hypothesised that the formation of cytotoxic bile coupled with the accumulation of hydrophobic protoporphyrin led to an induction of mitochondrial phase transition. This hypothesis was supported by the differential gene expression observed in genes associated with the mitochondrial respiratory chain (MRC) and previous findings by Palmeira and Rolo(Palmeira and Rolo 2004) who showed that modified bile composition led to a decoupling of the MRC and leakage of cytochrome *c* allowing further ROS generation and oxidative damage. Further evidence for impaired mitochondrial function was drawn from the work of Schoenfeld and Thierbach(Schoenfeld, Napoli et al. 2005; Thierbach, Schulz et al. 2005) who showed a

similar disruption in frataxin deficient mice (section 5.4.4) which led to hepatic tumour formation.

The presence of oxidative damage and ROS in the Fech$^{m1PAS/m1PAS}$ led to the induction of protective processes. GSH, cytochrome P450s and cytochrome oxidase genes all showed an increase in expression compared with the wild type. The induction of these genes are known responses to oxidative damage(Itoh, Chiba et al. 1997; Tan, Shi et al. 2006) and were also seen to be induced in the griseofulvin model(Gant, Baus et al. 2003). Although these processes form a protective role in the cell their induction may have also exacerbated the oxidative damage by increasing ATP requirements to further induce the MRC allowing further production of free cytochrome *c*. This was shown by an increase in the expression of genes forming the mitochondrial ATP synthase (section 5.4.4) and observations made in the griseofulvin model of EPP(Navarro, del Hoyo et al. 2005).

The increased transcription of cytochrome P450s may also have modulated haem synthesis to further the accumulation of protoporhyrin due to the requirement of haem in the cytochrome P450 proteins. Genes involved with haem biosynthesis showed differential gene expression in the Fech$^{m1PAS/m1PAS}$ compared to the wild type across the time course of this study (section 5.2.1); their increased expression at 32 weeks coincides with a decrease in *Cyp* gene transcription which may be a response due to a haem deficit.

As discussed above and in chapter 5, in the Fech$^{m1PAS/m1PAS}$ mouse altered bile composition led to a state of global hypomethylation. Evidence for this was presented

in section 5.4.6 and supported by comparison with the choline deficient mice(Bachman, Kamendulis et al. 2006).

A reduced expression in DNA methyltransferase (*Dnmt*) genes responsible for both semi-conservative and *de novo* methylation were found to be decreased in their expression with genes responsible for active demethylation (Mbd) increased in their expression relative to the wild type from 4 weeks of age. *Dnmt1* was also found to be greatly reduced in expression in the $Fech^{m1PAS/m1PAS}$ at 18 days gestation compared to the wild type indicating that the state of hypomethylation arose during early development. Dnmt1 is responsible for methylation during DNA replication; it's repression *in utero* implies that as the liver develops in the pup methylation states were not reaffirmed in the dividing cells leading to a state of global hypomethylation from early development.

The presence of hypomethylation had several consequences in the $Fech^{m1PAS/m1PAS}$ mouse. Abberent methylation has been associated with tumour formation in states of both hyper- and hypomethylation through an increased rate of DNA damage and promotion of genome instability(Chen, Pettersson et al. 1998; Eden, Gaudet et al. 2003; Gaudet, Hodgson et al. 2003; Yamada, Jackson-Grusby et al. 2005; Pogribny, Ross et al. 2006). Increased DNA damage through loss of methylation in the $Fech^{m1PAS/m1PAS}$ mouse would have compounded the effect of oxidative damage caused by the accumulation of protoporphyrin and cytochrome *c* leakage. Secondly, the loss of epigenetic regulation in the $Fech^{m1PAS/m1PAS}$ mouse led to deregulation of the cells circadian rhythm (section 5.4.5) as deregulation of *Period* genes, had previously been

associated with aberrant methylation found in breast carcinoma(Chen, Choo et al. 2005).

The *Period* genes (*per1, per2* and *per3*) are responsible for the maintenance of the circadian rhythm, the cells method of temporal organisation(Reppert and Weaver 2002; Reddy 2006). As shown in section 5.4.5 the expression of these genes in the $Fech^{m1PAS/m1PAS}$ mice were decreased relative to the wild type. Further evidence of temporal deregulation was shown by the down regulation of the circadian transcription factors *Clock* and *NPas2* which are effectors regulating temporal expression of processes including GSH metabolism and haem biosynthesis(Lavery, Lopez-Molina et al. 1999; Kaasik and Lee 2004; Kondratov, Kondratova et al. 2006). The loss of circadian regulation of the GSH pathway may have resulted in a decrease in the efficiency of the biotransformation pathway furthering the effects of oxidative stress(Gachon 2006).

Another process which is directly controlled by the circadian rhythm is the cell cycle(Matsuo, Yamaguchi et al. 2003). The loss of temporal organisation in the $Fech^{m1PAS/m1PAS}$ mouse would have benefited the cancer phenotype as the deregulation of the cell cycle allows the increased cell proliferation observed across the time course (section 4.6) as well as promoting cell survival(Matsuo, Yamaguchi et al. 2003).

## 7.2 Summary

The study of the $Fech^{m1PAS}$ model of erythropoietic protoporphyria presented here has led to a greater understanding of the mechanisms by which environmental and genetic

factors contribute to progression in disease. The application of genomic analysis, bioinformatics and reverse genetics has allowed the association of disease phenotypes to the underlying genetic and epigenetic processes.

The combination of the data presented in this thesis with previous data seen in both the $Fech^{m1PAS/m1PAS}$ mice and mice fed griseofulvin led to the hypothesis that the induction of adenoma in the $Fech^{m1PAS/m1PAS}$ mouse is a result of a cascade of increasing ROS generation and oxidative stress combined with the reduced efficiency of protective mechanisms and cell cycle control.

This project has also identified the importance of epigenetic regulation in disease progression. As the tools to study the epigenome advance, it is likely that further knowledge of the progression of cancers and other serious diseases will be obtained.

This thesis has furthered our understanding of the progression of EPP in the $Fech^{m1PAS/m1PAS}$ model. There are however several unknowns that require further study.

Directly relating to the $Fech^{m1PAS}$ model, chapter 7 hypothesised that tumourgenesis was the result of a cascade of ROS generation and oxidative stress. This requires further investigation to elucidate the levels and localisation of ROS generation.

Due to a lack of biological material the biochemical assays carried out in chapter 4 were limited. Further insight into the level of liver damage attributable directly to cholestasis could be obtained by further analysis by assaying alkaline phosphatise levels. Additionally the differential gene expression data presented here suggests that key epigenetic regulatory mechanisms are impaired, in particular the methylation

state due to the impaired transcription of DNA methyltransferases. Further work on the Fech$^{m1PAS}$ mouse should include assays to determine the level of methylation and to study the methylation states of promoter regions for tumour suppressor genes as aberrant methylation of their promoters have been associated with multiple cancers.

The study of the Fech$^{m1PAS/m1PAS}$ mouse model gives us some insight into the progression of severe phenotypes associated with EPP, however it is limited in its comparison to the human condition as in humans the penetrance of the condition is variable. Further insight into the mechanism of EPP in humans could be gained by further study of other less severe models of EPP such as the exon 10 deletion mutant discussed in section 4.7.3.

Data presented within this thesis led to the following publication:

Davies, R., Schuurman, A., Barker, C. R. *et al.*

Hepatic gene expression in protoporphyic Fech mice is associated with cholestatic injury but not a marked depletion of the heme regulatory pool.

**American Journal of Pathology** **166**(4): 1041-1053. (2005)

## References.


Abitbol, M., F. Bernex, et al. (2005). "A mouse model provides evidence that genetic background modulates anemia and liver injury in erythropoietic protoporphyria." American Journal of Physiology-Gastrointestinal and Liver Physiology **288**(6): G1208-G1216.

Akhtar, R. A., A. B. Reddy, et al. (2002). "Circadian cycling of the mouse liver transcriptome, as revealed by cDNA microarray, is driven by the suprachiasmatic nucleus." Current Biology **12**(7): 540-550.

Allain, L. R., D. N. Stratis-Cullum, et al. (2004). "Investigation of microfabrication of biological sample arrays using piezoelectric and bubble-jet printing technologies." Analytica Chimica Acta **518**(1-2): 77-85.

Arthur, J. R. (2000). "The glutathione peroxidases." Cellular and Molecular Life Sciences (CMLS) **57**(13 - 14): 1825-1835.

Bachman, A. N., G. M. Curtin, et al. (2006). "Altered methylation in gene-specific and GC-Rich regions of DNA is progressive and nonrandom during promotion of skin tumorigenesis." Toxicological Sciences **91**(2): 406-418.

Bachman, A. N., L. M. Kamendulis, et al. (2006). "Diethanolamine and phenobarbital produce an altered pattern of methylation in GC-Rich regions of DNA in B6C3F1 mouse hepatocytes similar to that resulting from choline deficiency." Toxicological Sciences **90**(2): 317-325.

Bachman, A. N., J. M. Phillips, et al. (2006). "Phenobarbital induces progressive patterns of GC-rich and gene-specific altered DNA methylation in the liver of tumor-prone B6C3F1 mice." Toxicological Sciences **91**(2): 393-405.

Badminton, M. N. and G. H. Elder (2005). "Molecular mechanisms of dominant expression in porphyria." Journal of Inherited Metabolic Disease **28**(3): 277-286.

Bakker, J., X. Lin, et al. (2002). "Methyl-CpG Binding Domain Protein 2 Represses Transcription from Hypermethylated pi -Class Glutathione S-Transferase Gene Promoters in Hepatocellular Carcinoma Cells." J. Biol. Chem. %R 10.1074/jbc.M203009200 **277**(25): 22573-22580.

Benjamini, Y. and Y. Hochberg (1995). "Controlling the False Discovery Rate - a Practical and Powerful Approach to Multiple Testing." Journal of the Royal Statistical Society Series B-Methodological **57**(1): 289-300.

Bentz, M., A. Plesch, et al. (1998). "Minimal sizes of deletions detected by comparative genomic hybridization." Genes Chromosomes & Cancer **21**(2): 172-175.

Bloomer, J. R., Y. M. Wang, et al. (2006). "Biochemical abnormality in erythropoietic protoporphyria: Cause and consequences." Journal of Pediatric Gastroenterology and Nutrition **43**: S36-S40.

Boulechfar, S., J. Lamoril, et al. (1993). "Ferrochelatase Structural Mutant (Fech(M1pas)) in the House Mouse." Genomics **16**(3): 645-648.

Broome, R. L., L. Feng, et al. (1999). "Non-invasive transgenic mouse genotyping using stool analysis." Febs Letters **462**(1-2): 159-160.

Casarett, L. J., C. D. Klaassen, et al. (2003). Casarett and Doull's essentials of toxicology. New York ; London, McGraw-Hill.

Chanas, S. (2002). "Loss of the Nrf2 transcription factor causes a marked reduction in constitutive and inducible expression of the glutathione S-transferase Gsta1, Gsta2, Gstm1, Gstm2, Gstm3 and Gstm4 genes in the livers of male and female mice." BIOCHEMICAL JOURNAL **365**: 405-416.

Chen, R. Z., U. Pettersson, et al. (1998). "DNA hypomethylation leads to elevated mutation rates." Nature **395**(6697): 89-93.

Chen, S.-T., K.-B. Choo, et al. (2005). Deregulated expression of the PER1, PER2 and PER3 genes in breast cancers. **26:** 1241-1246.

Chen, Z. M. E., K. G. Crone, et al. (2005). "Identification of a unique gene expression signature that differentiates hepatocellular adenoma from well-differentiated hepatocellular carcinoma." American Journal of Surgical Pathology **29**(12): 1600-1608.

Chiang, A. P., J. S. Beck, et al. (2006). "Homozygosity mapping with SNP arrays identifies TRIM32 an E3 ubiquitin ligase, as a Bardet-Biedl syndrome gene (BBS11)." Proceedings of the National Academy of Sciences of the United States of America **103**(16): 6287-6292.

Choi, J. K., J. Y. Choi, et al. (2004). "Integrative analysis of multiple gene expression profiles applied to liver cancer study." Febs Letters **565**(1-3): 93-100.

Cui, Z. J., Y. D. Zhou, et al. (2003). A physiological role for protoporphyrin IX photodynamic action in the rat Harderian gland? **179:** 149-154.

Davies, R., A. Schuurman, et al. (2005). "Hepatic gene expression in protoporphyic Fech mice is associated with cholestatic injury but not a marked depletion of the heme regulatory pool." American Journal of Pathology **166**(4): 1041-1053.

DeRisi, J., L. Penland, et al. (1996). "Use of a cDNA microarray to analyse gene expression patterns in human cancer." Nature Genetics **14**(4): 457-460.

Dhami, P., A. J. Coffey, et al. (2005). "Exon array CGH: Detection of copy-number changes at the resolution of individual exons in the human genome." American Journal of Human Genetics **76**(5): 750-762.

Dietel, M. and C. Sers (2006). "Personalized medicine and development of targeted therapies: the upcoming challenge for diagnostic molecular pathology. A review." Virchows Archiv **448**(6): 744-755.

Dsnick, R. J. and K. H. Astrin (2002). "Congenital erythropoietic porphyria: Advances in pathogenesis and treatment." British Journal of Haematology **117**(4): 779-795.

Eden, A., F. Gaudet, et al. (2003). "Chromosomal instability and tumors promoted by DNA hypomethylation. (Brevia)." **300**(5618): 455(1).

Fodor, S. P. A., J. L. Read, et al. (1991). "Light-Directed, Spatially Addressable Parallel Chemical Synthesis." Science **251**(4995): 767-773.

Gachon, F. (2006). "The circadian PAR-domain basic leucine zipper transcription factors DBP, TEF, and HLF modulate basal and inducible xenobiotic detoxification." CELL METABOLISM **4**(1): 25-36.

Gallagher, E. P. and J. L. Gardner (2002). "Comparative expression of two alpha class glutathione S-transferases in human adult and prenatal liver tissues." Biochemical Pharmacology **63**(11): 2025-2036.
Gamberoni, G., S. Storari, et al. (2006). "Finding biological process modifications in cancer tissues by mining gene expression correlations." Bmc Bioinformatics **7**.
Gant, T. W., P. R. Baus, et al. (2003). "Gene expression profiles associated with inflammation, fibrosis, and cholestasis in mouse liver after griseofulvin." Environmental Health Perspectives **111**(6): 847-853.
Gant, T. W. and S. D. Zhang (2005). "In pursuit of effective toxicogenomics." Mutation Research-Fundamental and Molecular Mechanisms of Mutagenesis **575**(1-2): 4-16.
Gaudet, F., J. G. Hodgson, et al. (2003). "Induction of tumors in mice by genomic hypomethylation. (Reports)." **300**(5618): 489(4).
Goldstein, J. A. and M. B. Faletto (1993). "Advances in Mechanisms of Activation and Deactivation of Environmental Chemicals." Environmental Health Perspectives **100**: 169-176.
Gouya, L., H. Puy, et al. (2002). "The penetrance of dominant erythropoietic protoporphyria is modulated by expression of wildtype FECH." Nature Genetics **30**(1): 27-28.
Gouya, L., H. Puy, et al. (2004). "Modulation of penetrance by the wild-type allele in dominantly inherited erythropoietic protoporphyria and acute hepatic porphyrias." Human Genetics **114**(3): 256-262.
Grandchamp, B., J. C. Deybach, et al. (1980). "Studies of Porphyrin Synthesis in Fibroblasts of Patients with Congenital Erythropoietic Porphyria and One Patient with Homozygous Coproporphyria." Biochimica Et Biophysica Acta **629**(3): 577-586.
Hacia, J. G. (1999). "Resequencing and mutational analysis using oligonucleotide microarrays." Nature Genetics **21**: 42-47.
Hansch, C. and W. J. Dunn (1972). "Linear Relationships between Lipophilic Character and Biological-Activity of Drugs." Journal of Pharmaceutical Sciences **61**(1): 1-&.
Itoh, K., T. Chiba, et al. (1997). "An Nrf2/Small Maf Heterodimer Mediates the Induction of Phase II Detoxifying Enzyme Genes through Antioxidant Response Elements." Biochemical and Biophysical Research Communications **236**(2): 313-322.
Jansen, P. L. M. and E. Sturm (2003). "Genetic cholestasis, causes and consequences for hepatobiliary transport." Liver International **23**(5): 315-322.
Jendrassik, L. and P. Grof (1938). "Vereinfachte photmetrische Methode zur Bestimmung des Blutbilurubins." Biochem. Z. **297**: 81.
Ji, M. J., P. Hou, et al. (2004). "Microarray-based method for genotyping of functional single nucleotide polymorphisms using dual-color fluorescence hybridization." Mutation Research-Fundamental and Molecular Mechanisms of Mutagenesis **548**(1-2): 97-105.

Jiang, J. F., B. F. Serinkan, et al. (2003). "Peroxidation and externalization of phosphatidylserine associated with release of cytochrome c from mitochondria." Free Radical Biology and Medicine **35**(7): 814-825.
Kaasik, K. (2004). "Reciprocal regulation of haem biosynthesis and the circadian clock in mammals." NATURE **430**(6998): 467-471.
Kaasik, K. and C. C. Lee (2004). "Reciprocal regulation of haem biosynthesis and the circadian clock in mammals." Nature **430**(6998): 467-471.
Kallioniemi, A., O. P. Kallioniemi, et al. (1992). "Comparative Genomic Hybridization for Molecular Cytogenetic Analysis of Solid Tumors." Science **258**(5083): 818-821.
Kamdem, L. K., I. Meineke, et al. (2006). "Dominant contribution of P450 3A4 to the hepatic carcinogenic activation of aflatoxin B-1." Chemical Research in Toxicology **19**(4): 577-586.
Kaplan, M. M. (2002). "Alanine Aminotransferase Levels: What's Normal?" Ann Intern Med **137**(1): 49-51.
Kauppinen, R. (2004). "Porphyrias." Lancet **365**(9455): 241-252.
Kim, N. H. and J. H. Kang (2006). "Oxidative damage of DNA induced by the cytochrome c and hydrogen peroxide system." Journal of Biochemistry and Molecular Biology **39**(4): 452-456.
Knasmuller, S. (1997). "Toxic effects of griseofulvin: disease models, mechanisms, and risk assessment." Crit Rev Toxicol **27**(5): 495-537.
Kojima, T., W. Mukai, et al. (2006). "Determination of genomic breakpoints in an epileptic patient using genotyping array." Biochemical and Biophysical Research Communications **341**(3): 792-796.
Kondratov, R. V., A. A. Kondratova, et al. (2006). "Post-translational regulation of circadian transcriptional CLOCK(NPAS2)/BMAL1 complex by CRYPTOCHROMES." Cell Cycle **5**(8): 890-895.
Korsching, E., K. Agelopolous, et al. (2006). "Improvements in the analysis strategy make single nucleotide polymorphism analysis a powerful tool in the detection and characterization of amplified chromosomal regions in human tumors." Pathobiology **73**(1): 18-25.
Krishnamurthy, P., D. D. Ross, et al. (2004). "The stem cell marker Bcrp/ABCG2 enhances hypoxic cell survival through interactions with heme." Journal of Biological Chemistry **279**(23): 24218-24225.
Kullak-Ublick, G. A., B. Stieger, et al. (2004). "Enterohepatic bile salt transporters in normal physiology and liver disease." Gastroenterology **126**(1): 322-342.
LaFramboise, W. A., K. L. Bombach, et al. (2006). "Hepatic gene expression response to acute indomethacin exposure." Molecular Diagnosis & Therapy **10**(3): 187-196.
Lander, E. S., L. M. Linton, et al. (2001). "Initial sequencing and analysis of the human genome." Nature **409**(6822): 860-921.
Larsen, J., A. M. Ottesen, et al. (2001). "High resolution comparative genomic hybridization detects 7-8 megabasepair deletion in PCR amplified DNA." Analytical Cellular Pathology **23**(2): 61-64.
Lavery, D. J., L. Lopez-Molina, et al. (1999). Circadian Expression of the Steroid 15 alpha -Hydroxylase (Cyp2a4) and Coumarin 7-Hydroxylase (Cyp2a5) Genes in

Mouse Liver Is Regulated by the PAR Leucine Zipper Transcription Factor DBP. **19:** 6488-6499.
Lertratanangkoon, K., C. J. Wu, et al. (1997). "Alterations of DNA methylation by glutathione depletion." Cancer Letters **120**(2): 149-156.
Li-Hawkins, J., M. Gafvels, et al. (2002). "Cholic acid mediates negative feedback regulation of bile acid synthesis in mice
10.1172/JCI200216309." J. Clin. Invest. **110**(8): 1191-1200.
Li, Z. and C. Chan (2004). "Integrating gene expression and metabolic profiles." Journal of Biological Chemistry **279**(26): 27124-27137.
Libbrecht, L., L. Meerman, et al. (2003). "Liver pathology and hepatocarcinogenesis in a long-term mouse model of erythropoietic protoporphyria." Journal of Pathology **199**(2): 191-200.
Lock, E. A. and C. J. Reed (2006). "Trichloroethylene: Mechanisms of Renal Toxicity and Renal Cancer and Relevance to Risk Assessment." Toxicol. Sci. %R 10.1093/toxsci/kfj107 **91**(2): 313-331.
Lockhart, D. J. and E. A. Winzeler (2000). "Genomics, gene expression and DNA arrays." Nature **405**(6788): 827-836.
Lowe, G. (2000). "Structure, spectra, and function of heme sites." International Journal of Quantum Chemistry **77**(1): 54-70.
Luo, J. and C. K. Lim (1995). "Isolation and characterization of new porphyrin metabolites in human porphyria cutanea tarda and in rats treated with hexachlorobenzene by HPTLC, HPLC and liquid secondary ion mass spectrometry." Biomedical Chromatography **9**(3): 113-122.
Macias, R. I. R., S. Jimenez, et al. (2006). "Effect of maternal cholestasis and treatment with ursodeoxycholic acid on the expression of genes involved in the secretion of biliary lipids by the neonatal rat liver." Life Sciences **79**(10): 1014-1019.
Magness, S. T. and D. A. Brenner (1999). "Targeted disruption of the mouse ferrochelatase gene producing an exon 10 deletion." Biochimica Et Biophysica Acta-Molecular Basis of Disease **1453**(1): 161-174.
Magness, S. T., N. Maeda, et al. (2002). "An exon 10 deletion in the mouse ferrochelatase gene has a dominant-negative effect and causes mild protoporphyria." Blood **100**(4): 1470-1477.
Magnus, I. A., A. Jarett, et al. (1961). "ERYTHROPOIETIC PROTOPORPHYRIA A NEW PORPHYRIA SYNDROME WITH SOLAR URTICARIA DUE TO PROTOPORPHYRINÆMIA." The Lancet **278**(7200): 448-451.
Matsuo, T., S. Yamaguchi, et al. (2003). "Control Mechanism of the Circadian Clock for Timing of Cell Division in Vivo." Science %R 10.1126/science.1086271 **302**(5643): 255-259.
McMahon, M., K. Itoh, et al. (2001). "The Cap 'n' Collar Basic Leucine Zipper Transcription Factor Nrf2 (NF-E2 p45-related Factor 2) Controls Both Constitutive and Inducible Expression of Intestinal Detoxification and Glutathione Biosynthetic Enzymes." Cancer Res **61**(8): 3299-3307.
Meeks, R. G., S. D. Harrison, et al. (1991). Hepatotoxicology. Boca Raton, Fla., CRC Press.

Meerman, L., N. R. Koopen, et al. (1999). "Biliary fibrosis associated with altered bile composition in a mouse model of erythropoietic protoporphyria." Gastroenterology **117**(3): 696-705.
Milgrom, L. R. (1997). The colours of life : an introduction to the chemistry of porphyrins and related compounds. Oxford, Oxford University Press.
Mills, G. C. (1957). "HEMOGLOBIN CATABOLISM. I. GLUTATHIONE PEROXIDASE, AN ERYTHROCYTE ENZYME WHICH PROTECTS HEMOGLOBIN FROM OXIDATIVE BREAKDOWN." J. Biol. Chem. **229**(1): 189-197.
Molnar, A., R. Dedic, et al. (2005). "Protoporphyrin IX and hematoporphyrin derivatives interactions with oxygen studied by time and spectral resolved phosphorescence." Journal of Molecular Structure **744**: 723-726.
Montgomery, B. L. and J. C. Lagarias (2002). "Phytochrome ancestry: sensors of bilins and light." Trends in Plant Science **7**(8): 357-366.
Myatt, L. and X. L. Cui (2004). "Oxidative stress in the placenta." Histochemistry and Cell Biology **122**(4): 369-382.
Nagai, M., A. Nakamura, et al. (2003). "Expression of DNA (5-cytosin)-methyltransferases (DNMTs) in hepatocellular carcinomas." Hepatology Research **26**(3): 191.
Navarro, S., P. del Hoyo, et al. (2005). "Increased mitochondrial respiratory chain enzyme activities correlate with minor extent of liver damage in mice suffering from erythropoietic protoporphyria." Experimental Dermatology **14**(1): 26-33.
Nebert, D. W. and D. W. Russell (2002). "Clinical importance of the cytochromes P450." The Lancet **360**(9340): 1155-1162.
Nelson (2004). "Comparison of cytochrome P450 (CYP) genes from the mouse and human genomes, including nomenclature recommendations for genes, pseudogenes and alternative-splice variants." Pharmacogenetics **14**(1): 1.
Njalssson, R. and S. Norgren (2005). "Physiological and pathological aspects of GSH metabolism." Acta Paediatrica **94**(2): 132-137.
Nordmann, Y., D. Amram, et al. (1990). "Coexistent Hereditary Coproporphyria and Congenital Erythropoietic Porphyria (Gunther Disease)." Journal of Inherited Metabolic Disease **13**(5): 687-691.
Norlin, M., S. von Bahr, et al. (2003). "On the substrate specificity of human CYP27A1: implications for bile acid and cholestanol formation." J. Lipid Res. %R 10.1194/jlr.M300047-JLR200 **44**(8): 1515-1522.
Palmeira, C. M. and A. P. Rolo (2004). "Mitochondrially-mediated toxicity of bile acids." Toxicology **203**(1-3): 1-15.
Patil, M. A., M. S. Chua, et al. (2005). "An integrated data analysis approach to characterize genes highly expressed in hepatocellular carcinoma." Oncogene **24**(23): 3737-3747.
Pawliuk, R., R. Tighe, et al. (2005). "Prevention of murine erythropoietic protoporphyria-associated skin photosensitivity and liver disease by dermal and hepatic ferrochelatase." Journal of Investigative Dermatology **124**(1): 256-262.

Pelicano, H., D. Carney, et al. (2004). "ROS stress in cancer cells and therapeutic implications." Drug Resistance Updates **7**(2): 97-110.
Perez, M. J., E. Velasco, et al. (2006). "Maternal ethanol consumption during pregnancy enhances bile acid-induced oxidative stress and apoptosis in fetal rat liver." Toxicology **225**(2-3): 183-194.
Pikuleva, I. A. (2006). "Cholesterol-metabolizing cytochromes P450." Drug Metabolism and Disposition **34**(4): 513-520.
Piper, J., D. Rutovitz, et al. (1995). "Computer Image-Analysis of Comparative Genomic Hybridization." Cytometry **19**(1): 10-26.
Plant, N. (2003). Molecular toxicology. Oxford, BIOS Scientific.
Plasilova, M., I. Stoilov, et al. (1999). "Identification of a single ancestral CYP1B1 mutation in Slovak Gypsies (Roms) affected with primary congenital glaucoma." J Med Genet **36**(4): 290-294.
Poblete-Gutierrez, P., S. Badeloe, et al. (2006). "Dual porphyrias revisited." Experimental Dermatology **15**(9): 685-691.
Pogribny, I. P., S. A. Ross, et al. (2006). "Irreversible global DNA hypomethylation as a key step in hepatocarcinogenesis induced by dietary methyl deficiency." Mutation Research-Fundamental and Molecular Mechanisms of Mutagenesis **593**(1-2): 80-87.
Reddy, A. (2006). "Circadian orchestration of the hepatic Proteome." CURRENT BIOLOGY **16**(11): 1107-1115.
Redinger, R. N. (2003). "The coming of age of our understanding of the enterohepatic circulation of bile salts." American Journal of Surgery **185**(2): 168-172.
Repa, J. J., S. D. Turley, et al. (2000). "Regulation of Absorption and ABC1-Mediated Efflux of Cholesterol by RXR Heterodimers
10.1126/science.289.5484.1524." Science **289**(5484): 1524-1529.
Reppert, S. M. and D. R. Weaver (2002). "Coordination of circadian timing in mammals." Nature **418**(6901): 935-941.
Rolo, A. P., P. J. Oliveira, et al. (2000). "Bile acids affect liver mitochondrial bioenergetics: Possible relevance for cholestasis therapy." Toxicological Sciences **57**(1): 177-185.
Russell, D. W. (2003). "THE ENZYMES, REGULATION, AND GENETICS OF BILE ACID SYNTHESIS." Annual Review of Biochemistry **72**(1): 137-174.
Sambrook, J. and D. W. Russell (2001). Molecular cloning : a laboratory manual. Cold Spring Harbor, N.Y., Cold Spring Harbor Laboratory Press.
Schena, M., D. Shalon, et al. (1995). "Quantitative Monitoring of Gene-Expression Patterns with a Complementary-DNA Microarray." Science **270**(5235): 467-470.
Schoenfeld, R. A., E. Napoli, et al. (2005). "Frataxin deficiency alters heme pathway transcripts and decreases mitochondrial heme metabolites in mammalian cells." Human Molecular Genetics **14**(24): 3787-3799.
Schulz, T. J., R. Thierbach, et al. (2006). "Induction of oxidative metabolism by mitochondrial frataxin inhibits cancer growth - Otto Warburg revisited." Journal of Biological Chemistry **281**(2): 977-981.

Sener, A., D. Ozsavci, et al. (2005). "Do platelet apoptosis, activation, aggregation, lipid peroxidation and platelet-leukocyte aggregate formation occur simultaneously in hyperlipidemia?" Clinical Biochemistry **38**(12): 1081-1087.

Southern, E. M. (1975). "Detection of Specific Sequences among DNA Fragments Separated by Gel-Electrophoresis." Journal of Molecular Biology **98**(3): 503-&.

Splettstoesser, W. D. and P. Schuff-Werner (2002). Oxidative stress in phagocytes - "The enemy within". **57:** 441-455.

Stanca, C., D. Jung, et al. (2001). "Hepatocellular transport proteins and their role in liver disease." World Journal of Gastroenterology **7**(2): 157-169.

Stryer, L. (1995). Biochemistry. New York, W.H. Freeman.

Taketani, S., Y. Nakahashi, et al. (1990). "Molecular-Cloning, Sequencing, and Expression of Mouse Ferrochelatase." Journal of Biological Chemistry **265**(32): 19377-19380.

Tan, Y. X., L. M. Shi, et al. (2006). "Integrating time-course microarray gene expression profiles with cytotoxicity for identification of biomarkers in primary rat hepatocytes exposed to cadmium." Bioinformatics **22**(1): 77-87.

Thierbach, R., T. J. Schulz, et al. (2005). "Targeted disruption of hepatic frataxin expression causes impaired mitochondrial function, decreased life span and tumor growth in mice." Human Molecular Genetics **14**(24): 3857-3864.

Tortora, G. J. and S. R. Grabowski (1993). Principles of anatomy and physiology. New York, HarperCollinsCollege.

Tuchweber, B. (1996). "Nutrition and bile formation." NUTRITION RESEARCH **16**(6): 1041-1080.

Turek, F. W., C. Joshu, et al. (2005). "Obesity and metabolic syndrome in circadian Clock mutant mice." Science **308**(5724): 1043-1045.

Tutois, S., X. Montagutelli, et al. (1991). "Erythropoietic Protoporphyria in the House Mouse - a Recessive Inherited Ferrochelatase Deficiency with Anemia, Photosensitivity, and Liver-Disease." Journal of Clinical Investigation **88**(5): 1730-1736.

Urizar, N. L., D. H. Dowhan, et al. (2000). "The Farnesoid X-activated Receptor Mediates Bile Acid Activation of Phospholipid Transfer Protein Gene Expression 10.1074/jbc.M007998200." J. Biol. Chem. **275**(50): 39313-39317.

Van Veldhoven, P., G. Vanhove, et al. (1992). "Substrate specificities of rat liver peroxisomal acyl-CoA oxidases: palmitoyl-CoA oxidase (inducible acyl-CoA oxidase), pristanoyl-CoA oxidase (non-inducible acyl-CoA oxidase), and trihydroxycoprostanoyl- CoA oxidase." J. Biol. Chem. **267**(28): 20065-20074.

Vaquero, E. C., M. Edderkaoui, et al. (2004). "Reactive oxygen species produced by NAD(P)H oxidase inhibit apoptosis in pancreatic cancer cells." Journal of Biological Chemistry **279**(33): 34643-34654.

Wang, J. H., Y. Qin, et al. (2006). "Detection of aberrant promoter methylation of GSTP1 in the tumor and serum of Chinese human primary hepatocellular carcinoma patients." Clinical Biochemistry **39**(4): 344-348.

Waterston, R. H., K. Lindblad-Toh, et al. (2002). "Initial sequencing and comparative analysis of the mouse genome." Nature **420**(6915): 520-562.

Weiss, M. J. and S. H. Orkin (1995). "Gata Transcription Factors - Key Regulators of Hematopoiesis." Experimental Hematology **23**(2): 99-107.

Weiss, S. L. and R. A. Sunde (1997). "Selenium Regulation of Classical Glutathione Peroxidase Expression Requires the 3' Untranslated Region in Chinese Hamster Ovary Cells." J. Nutr. **127**(7): 1304-1310.

Whatley, S. D., N. G. Mason, et al. (2004). "Autosomal recessive erythropoietic protoporphyria in the United Kingdom: prevalence and relationship to liver disease." Journal of Medical Genetics **41**(8): art. no.-e105.

Williams, P. L., L. H. Bannister, et al. (1995). Gray's anatomy : the anatomical basis of medicine and surgery. New York ; Edinburgh, Churchill Livingstone.

Wolkoff, A. (1978). "Hepatic Accumulation And Intracellular Binding Of Conjugated Bilirubin." Journal of Clinical Investigation **61**(1): 142-149.

Xiong, Y., S. C. Dowdy, et al. (2005). "Opposite alterations of DNA methyltransferase gene expression in endometrioid and serous endometrial cancers." Gynecologic Oncology **96**(3): 609.

Yamada, Y., L. Jackson-Grusby, et al. (2005). "Opposing effects of DNA hypomethylation on intestinal and liver carcinogenesis." Proceedings of the National Academy of Sciences of the United States of America **102**(38): 13580-13585.

Zhang, S. D. and T. W. Gant (2004). "A statistical framework for the design of microarray experiments and effective detection of differential gene expression." Bioinformatics **20**(16): 2821-2828.

Zhou, S., Y. Zong, et al. (2005). "Increased expression of the Abcg2 transporter during erythroid maturation plays a role in decreasing cellular protoporphyrin IX levels." Blood **105**(6): 2571-2576.